Relative Importance of Beta and Gamma Cytoplasmic Actins to Cellular and Organismal Viability

A DISSERTATION

SUBMITTED TO THE FACULTY OF

UNIVERSITY OF MINNESOTA

BY

Xiaobai Patrinostro

IN PARTIAL FULFILLMENT OF THE REQUIREMENTS

FOR THE DEGREE OF

DOCTOR OF PHILOSOPHY

Adviser, James M. Ervasti

May 2018

Acknowledgements

I would like to thank my thesis advisor Dr. James Ervasti for being a wonderful mentor and providing guidance throughout my graduate career. Jim truly created an environment that is both fun to work at and nurtures scientific discovery.

I would like to thank everyone I've had the pleasure of working with while at the Ervasti lab. Thank you, Dana, Jackie, Alli, Tung, JT, Ben, Chris, Joe, Preston, Katrina, D'anna, Lauren and Maria for your scientific advice and general goofiness over the years.

I would like to thank Dr. Diane Slusarski and rest of the Slusarski lab at the University of Iowa for introducing me to the wonders of research. Thank you for being a shining example of a good researcher. I would not be the scientist I am today without the foundational skills you taught me.

I would like to thank Dr. Troy Lund and rest of the Lund & Tolar lab at the University of Minnesota for providing me the opportunity to work as a young scientist and encouraging me to pursue my PhD.

I would like to thank my committee members, Drs. Lincoln Potter, Lishia Chen, Jeonsik Yong, and Scott Dehm for your helpful criticisms and advice on my projects over the years.

I would like to also acknowledge the following for supporting me during my graduate career: The Amstrong-Pothapragada Graduate Student Fellowship, The Frederick J. Bollum Award, The Charles Carr & William Peterson Award, The Bacaner Research Award, and The Huber Warner Fellowship.

I would like to thank my best friends Jennifer and Cassie. Thank you for your humor and your encouragements. We did it girls!

I would like to thank my family, both in the US and in China, thank you for all your support throughout the years. I need to especially thank my parents Jing and Joseph, Lin Xue and Liping Zhou, thank you for everything. I would not have succeeded without your love.

Finally, I am especially grateful to my husband, Bryan. Thank you for being my champion and strongest advocate. It has taken us a long time to achieve this and I could not have done it without you.

Dedication

This dissertation is dedicated to my family.

这篇论文献给我的家人。

Abstract

The highly homologous *Actb* and *Actg1* are ubiquitously expressed and are hypothesized to carry out both redundant and unique functions, but studies using genetic knockout and transcript knockdown have yielded conflicting data. To elucidate the cause of this discrepancy, I characterized actin transcript and protein levels, and cellular phenotypes in both gene- and transcript-targeted primary MEFs. Gene targeting of *Actb*, but not *Actg1*, led to decreased cell proliferation, decreased cellular ATP levels, and increased serum response factor signaling in primary MEFs. However, SV40 largeT antigen transformed MEFs supported proliferation in the absence of *Actb*. Consistent with *in vivo* mouse studies, both gene and transcript targeting approaches demonstrated the loss of *Actb* is more disruptive to primary MEF function than is the loss of *Actg1*.

Previous mouse models showed that *Actb* KOs are embryonically lethal while *Actg1* KOs are viable. To determine whether the four amino acid differences between the cytoplasmic actins are essential for life, we generated a mouse model where the *Actb* gene is edited to encode γ-actin protein instead, an allele referred as $Actb^{c\text{-}g}$. In contrast to the lethal phenotype of *Actb* KOs, homozygous $Actb^{c\text{-}g}$ mice were born at Mendelian ratios, do not exhibit early lethality, and $Actb^{c\text{-}g}$ MEFs displayed proliferation and random migration rates similar to WT. Nonetheless, $Actb^{c\text{-}g}$ mice showed progressive high frequency hearing loss and stereocilia degeneration as previously reported in the hair-cell specific *Actb* knockout mice. Thus β-actin protein is not universally required for normal cellular function, but is necessary for maintenance of auditory stereocilia.

Table of Contents

List of Tables

List of Figures

Chapter 1

Introduction

The Actin family of proteins

Actin is one of the most abundant proteins in eukaryotic cells and its known functions include facilitating cell migration, muscle contraction, endocytosis, maintaining the cell structure, and regulating gene expression. Although actin is often considered a single molecule, in vertebrates, actin actually is expressed from six highly conserved genes, encoded on six separate chromosomes. The actin genes are *Acta1*, *Acta2*, *Actc1*, *Actb*, *Actg1* and *Actg2* which encode for the α_{sk}-actin, α_{sm}-actin, α_{ca}-actin, β_{cyto}-actin, γ_{cyto}-actin, and γ_{sm}-actin proteins respectively. All actin proteins are structurally similar, sharing at least 93% identify at the amino acid level (Perrin and Ervasti, 2010). Additionally, all actins require the chaperonin CCT (Spiess *et al.*, 2004) to fold to its native state, a 42.5 kDa globular protein (G-actin) with four subdomains, and a nucleotide binding cleft between subdomain 2 and 4 which binds ATP (ATP-actin) (Figure 1-1).

Monomeric G-actin can polymerize to form filamentous actin (F-actin), a two stranded helix in a right handed turn where all the subunits are orientated in the same direction (Pollard, 2015). Upon polymerization, actin hydrolyzes ATP into ADP + Pi (ADP-Pi-actin) (Ampe and Troys, 2017). Although G-actin can spontaneously nucleate and form dimers and trimers, these structures are unstable (Pollard, 2015). Instead, actin is dependent on various actin binding proteins (ABPs) to maintain the G-actin pool, and assist in rapid F-actin nucleation and elongation (Pollard, 2015). Organizationally, one end of F-actin is designated as the “plus” or “barbed” end, and the other is designated as the

“minus” or “pointed” end, based on the orientation of myosin head decoration (Figure 1-2a). The two ends of F-actin have different polymerization dynamics. ATP-actin is added onto the barbed end at a 5-fold higher rate than ADP-Pi-actin, while the dissociation rates of both ATP-actin and ADP-P_i-Actin is the same at both ends of the filament (Figure 1-2b) (Pollard, 2015). Because of this difference in filament end dynamic, actin filaments grow at the barbed/plus end and shrinks at the pointed/minus end, simulating a “treadmilling” movement across the cytosol (Pollard, 2015).

Even though all six actin proteins are structurally similar, they have distinct roles within cells. The majority of functional differences can be explained by tissue specific expression. The muscle actins are exclusively expressed in either striated (α_{sk}- and α_{ca}-actins) or smooth (α_{sm}- and γ_{sm}-actins) muscles, where they form the sarcomeric thin-filaments for muscle contraction. The cytoplasmic actins (β- and γ-actins) however, are ubiquitously expressed in all cells. Moreover, β- and γ-actins are 99% identical at the amino acid level, differing by only 4 functionally similar amino acids at the N-terminus (Figure 1-3) (Perrin and Ervasti, 2010). Interestingly, the amino acid variances have been conserved from birds to mammals, indicating an evolutionary pressure to maintain these small differences (Gunning *et al.*, 2015). Numerous cytoplasmic actin functional roles have been revealed since scientists first cloned the genes 3 decades ago (Gunning *et al.*, 1983), but much less is known of how these highly homologous actins are regulated. Recent developments have begun to clarify the tight coordination between transcription factors, transcript regulation, signaling

pathways and translational modifications to ensure correct cytoplasmic actin expression and function.

Cytoplasmic actins can regulate gene expression

Monomeric cytoplasmic actins bind directly to the myocardin related transcription factors (MRTFs), also known as myelin and lymphocyte protein (MAL) or megakryoblastic leukemia-1 (MKL-1), to sequester MRTFs in the cytoplasm. The MRTFs are co-factors to the serum response factor (SRF), a MADs-box transcription factor (Olson and Nordheim, 2010; Small, 2012). Serum stimulation activates Rho signaling, which induces actin polymerization and assembly. The transition of G- to F-actin lowers the cytosolic G-actin concentration, which allows MRTF to dissociate from G-actin and enters the nucleus to stimulate SRF (Posern and Treisman, 2006; Olson and Nordheim, 2010). SRF ultimately activates transcription of growth factor related genes, cytoskeletal proteins, and many muscle specific genes in response to serum stimulation. SRF also is able to bind to the actin promoter via the CArG-Box domains and activate actin transcription, which establishes the negative signaling feedback loop to SRF, which is known as the SRF-MRTF-Actin circuit (Posern and Treisman, 2006; Olson and Nordheim, 2010).

Recent data has shown the SRF-MRTF-Actin autoregulatory circuit is fine-tuned by nuclear actin dynamics. Actin is imported into the nucleus by Importin 9 and exported out by Exportin 6 (Stüven, Hartmann and Görlich, 2003; Dopie *et al.*, 2012) Since nuclear actin concentration is much lower than cytosolic actin concentration, the exact amount of nuclear actin is crucial for proper function. Within the nucleus, actin also exists both as a monomer and as filaments. Cellular signals such as serum stimulation, cell adhesion and DNA damage can

induce actin polymerization within the nucleus (Virtanen and Vartiainen, 2017). mDia, is a member of the formin family of ABPs that aids actin polymerization and prevents G-actin binding to MRTF within the nucleus to maintain activation of SRF for downstream processes (Virtanen and Vartiainen, 2017). Other nuclear proteins, such as Mical-2, lamin A/C, and linker of nucleoskeleton and cytoskeleton (LINC) complex all have been suggested to regulate nuclear actin dynamics, however their exact mechanisms and effects on the actin/MRTF/SRF regulatory circuit are not completely known (Virtanen and Vartiainen, 2017).

Finally, nuclear actin operates in other capacities as well. Cytoplasmic actin is a constituent of all RNA polymerases complexes (Hu, Wu and Hernandez, 2004; Philimonenko *et al.*, 2004; Hofmann *et al.*, 2004; Miralles and Visa, 2006), some chromatin remodeling complexes (Kapoor and Shen, 2013). Nuclear actin is bound to the heterogeneous ribonucleoproteins (hnRNPs) and histone acetyltransferases PCAF during transcription elongation (Percipalle 2003, Obrdlik 2008), is required for DNA replication initiation (Parisis *et al.*, 2017), and can interact with histone deacetylases (HDACs) (Serebryannyy, Cruz and De Lanerolle, 2016). Although it is still uncertain the specific role of actin in these processes, or if these functions depend on specific actin isoforms, it is evident that cytoplasmic actins are central for proper nuclear functions.

Cytoplasmic actin transcript regulation

The *Actb* 3'UTR contains a 54-nucleotide, cis-acting, sequence called the zipcode following directly after the TAG stop codon. The zipcode sequence allows the Zipcode Binding Protein 1 (ZPB1) to bind and regulate both the localization and translation of β-actin at the cell periphery (Doyle and Kiebler, 2012). *Actg1* transcript does not have a zipcode sequence or any other known regulatory element within its 3'UTR.

ZBP1, also known as coding region determinant-binding proteins (CRD-BP) or insulin-like growth factor II mRNA binding proteins (IMPI), is an embryonically expressed protein (Hansen *et al.*, 2004). ZBP1 is a member of the highly conserved family of RNA binding proteins (RBPs) that contain six canonical RNA binding domains (RBDs); two RNA recognition motifs (RRMs) and four hnRNP K homology (KH) domains (Yisraeli, 2005). A sequence of events is proposed to allow proper *Actb* transcript localization. First, zipcode binding protein 2 (ZBP2), a predominantly nuclear protein and a member of the same RBP family, is recruited to the *Actb* transcription site and binds with the *Actb* 3'UTR via a pyrimidine rich sequence in a co-transcriptional manner. (Pan *et al.*, 2007). Then ZBP1 is recruited to the ZBP2 site, binds to the *Actb* 3'UTR via the zipcode and ZBP2 dissociates. The binding of ZBP1 to the *Actb* 3'UTR also inhibits the formation of the 80s ribosomal complex and blocks translation initiation (Hüttelmaier *et al.*, 2005). Therefore, ZBP2 and ZBP1 act in a cooperative manner to regulate *Actb* transcript indicating this co-transcriptional interaction must be assembled in the nucleoplasm and allows for translational

silencing before the mRNA enters the cytoplasm. The ZBP1-*Actb* mRNA ribonucleoprotein complex (RNP) is then exported out of the nucleus and transported to the cell periphery along microtubules using the kinesin-like motor protein Kif11 (Song *et al.*, 2015).

Once the ZPB1-*Actb* mRNA RNP reaches its designated location, Src phosphorylates ZBP1 at residue tyrosine 396 to alleviate the protein-RNA binding and allows β_{cyto}-actin translation (Hüttelmaier *et al.*, 2005). In neurons, brain derived neurotropic factor (BDNF) signals for Src mediated phosphorylation of ZBP1 which regulates local translation of β-actin in growth cones (Sasaki *et al.*, 2010). Phosphorylation of ZBP1 only affect localized translation, not RNA localization, as *Actb* mRNA is still transported to the cell periphery in ZBP1 Y396F mutants (Sasaki *et al.*, 2010).

The *Actb* zipcode contains a bipartite motif of a 5' -CGGAC- sequence and a more promiscuous 3' -C/A-CA-C/U- sequence within the first 30 bases of the zipcode that is required for ZBP1 binding. Mutating either the 5' or the 3' binding sites greatly reduced ZBP1-*Actb* mRNA association analyzed by electrophoretic mobility shift assay (EMSA) (Chao *et al.*, 2010; Patel *et al.*, 2012). The ~20 nucleotide linker region length between the two binding sites is also important as *Actb* mRNA loops around ZBP1 to make contact with two ZBP1 KH domains (Chao *et al.*, 2010). Nucleotide additions or deletions to the linker region disrupts ZBP1-*Actb* mRNA binding, possibly due to improper RNA secondary structure formations. Finally, the *Actb* zipcode bipartite motif is conserved from

birds to mammals (Artman *et al.*, 2014), indicating an evolutionary pressure to both spatially and temporally regulate β-actin translation.

The *Actb* mRNA is also regulated by polyadenylation to control transcript expression and stability. Using rapid amplification of 3'-cDNA ends (3'-RACE) analysis, it was established there are two separate *Actb* transcripts with varying 3'UTR lengths in mice (Ghosh *et al.*, 2008). The first transcript has a short 3'UTR, only comprising the 54-nucleotide zipcode sequence prior to the PolyA signaling sequence. The second 3'UTR is much longer, at over 600 bases, and it encodes a micro-RNA target site for miR-34a/34b-5p. Mutations to this site reduced transcript expression, indicating the microRNA has a positive effect on the long transcript (Ghosh *et al.*, 2008). Since both 3'UTRs contain the zipcode sequence, this suggests proper localization is still a required element for both *Actb* transcripts. The two *Actb* transcripts are also tissue specific, whereas the shorter transcript was enriched in brain tissues and the longer transcript is predominantly enriched in embryonic tissues illustrated by microarray analysis (Ghosh *et al.*, 2008). Much is still unknown on how the different 3'UTR lengths affect specific function, or if ZBP1 truly binds to both transcripts and regulates their localization and translation. Further analysis of polyadenylation in *Actb*, and possibly other actin transcripts, could open a brand-new avenue of research to actin regulation.

Cytoplasmic actins are differentially regulated by arginylation

Cytoplasmic actins can undergo an array post-translational modification such as acetylation, carbonylation, phosphorylation, ubiquitylation and arginylation (Terman and Kashina, 2013). For many of these post-translational modifications (PTMs), their effects on actin stability, binding affinities, and function are similar between β- and γ-actin. However, one PTM, arginylation affects the cytoplasmic actins differently. Arginylation requires prior post-translation modification by Met-aminopeptidation or proteolysis. Subsequently, Ate1, an Arg-transfer RNA protein transferase transfers the Arg residue from the t-RNA and onto the N-terminus via a peptide bond. Three residues can be arginylated; Aspartate, Glutamate and Cysteine (Kai, H 1963, 1968). For cytoplasmic actins, N-terminal Aspartate is arginylated for β_{cyto}-actin while Glutamate is arginylated for γ_{cyto}-actin (Rubenstein, 1990). While both cytoplasmic actins can be arginylated *in vitro*, only arginylated β_{cyto}-actin is detected *in vivo* where 40% of β_{cyto}-actin was arginylated in mouse embryonic fibroblasts (MEFs) (Karakozova *et al.*, 2006). The other percentage of β-actin could be N-terminally acetylated, presumably due to a mutually exclusive modification event (Terman and Kashina, 2013). Cycloheximide chase and immunoprecipitation (IP) experiments revealed that arginylation did not change β_{cyto}-actin metabolic profile or binding to ABPs. However, by comparing rhodamine phalloidin staining in both wild-type and Ate1-/- cells, β_{cyto}-actin in Ate1-/- cells exhibited a decreased rate of polymerization and actin aggregation.

These data suggest that arginylation changes the properties of β_{cyto}-actin important for polymerization (Karakozova *et al.*, 2006).

To assess if *Actb* and *Actg1* coding sequence differences regulated their differential arginylation *in vivo,* chimeric β_{cyto}- and γ_{cyto}-actin cDNAs were produced: β-coded-γ-actin (βc-γ-actin) and γ-coded-β-actin (γc-β-actin) (Zhang *et al.*, 2010). In these chimeric actin constructs, *Actb* nucleotide sequence was changed to produce the γ_{cyto}-actin amino acid sequence and vice versa. When the converted actins are expressed exogenously, it resulted in an inverse of intracellular arginylated β- and γ- actin levels. Non-arginylated actin concentration and degradation dynamics were not changed, indicating the effects of codon switch specifically affected arginylation. *Actb* and *Actg1* coding sequence differences also affected translation speed, as β-actin has higher amino-acid incorporation rate than γ-actin, indicating γ-actin is translated at a lower speed than β-actin (Zhang *et al.*, 2010). Arginylation can expose buried lysine residues that become targeted by ubiquitination mediated degradation. As γ-actin is arginylated, lys18 becomes exposed and is more likely to be degraded via ubiquitination than arginylated β_{cyto}-actin due its slower rate of translation. Once the γ-actin lysine 18 was mutated to leucine, arginylated γ-actin stability increased by 50%. The different translation rate facilitates N-terminal arginylation of both β_{cyto}-actin and γ_{cyto}-actin. However, due to γ_{cyto}-actin slower translation speed, it exposes a normally protected lysine residue ,and is selected for ubiquitination proteolytic degradation (Zhang *et al.*, 2010).

Recent work suggests *Ate1* contains a zipcode like sequence within its 5'UTR (Wang *et al.*, 2017). This in conjunction with *Actb* mRNA localization could work in a synergistic manner to deliver and synthesize arginylated β-actin at the cell periphery for quick and precise cellular functions. The proposed model is that first both *Actb* and *Ate1* mRNAs are transported to the cell periphery via their zipcodes, then localized translation of both Ate1 and β-actin at the cell periphery leads to localized arginylated β-actin. This is further supported by the development of an antibody that specifically recognizes arginylated β-actin (Pavlyk *et al.*, 2018). With this new tool, it has been shown that arginylated β-actin is concentrated at the leading edge of lamellipodia. Additionally, arginylated β-actin level is greatly increased after serum stimulation and greatly decreased in contact inhibited cells, suggesting β-actin arginylation is coupled with cell stimuli and migration. Overall, it suggests β-actin arginylation is tightly regulated and is an integral cell signaling function for cell migration (Pavlyk *et al.*, 2018).

Actb and *Actg1* null mouse models

β- and γ-actin only differ by 4 functionally similar amino acids on their N-terminus and it was assumed both are essential for development and serve similar roles within the cell. To examine specific cytoplasmic actin functions, the Ervasti group generated cre-mediated whole-body knockout (KO) models for both *Actb* and *Actg1* using floxed alleles encompassing exon 2-3 of either *Actb* or *Actg1*. The initiating methionine for both cytoplasmic actins reside in exon 2. *Actb* KO mice were non-viable and only survived until embryonic stage e8.5. Heterozygous *Actb*+/- mice also suffered from high postnatal mortality rate indicating the importance of *Actb* for development (Bunnell *et al.*, 2011). *Actg1* KO mice survived to birth, however two-third of *Actg1* KO mice died by 48 hours post birth due to apparent respiratory failure. *Actg1* KO mice also suffered from progressive hearing loss and stunted growth (Bunnell and Ervasti, 2010). Because whole body *Actb* KO mice are non-viable, the Ervasti group also generated conditional *Actb* KO MEF systems. Mice carrying floxed alleles within *Actb* were crossed to the CAGG-CreER transgenic line. From the conditional KO studies, it was shown that *Actb* KO MEFs suffer from severe migration and growth impairments, which were not seen in *Actg1* KO MEFs (Bunnell and Ervasti, 2010; Bunnell *et al.*, 2011). The data from both whole body and conditional KO MEF studies reveals the specific roles of *Actb* and *Actg1*. *Actb* is required for development, cell growth and migration and *Actg1* is required for cytoskeleton maintenance (Figure 1-4).

Tissue specific KOs of *Actb* and *Actg1* further help elucidate both redundant and unique roles of cytoplasmic actins. *Actb* or *Actg1* muscle specific KOs (msKO) resulted in progressive myopathy leading to increased muscle fiber degeneration/regeneration (Sonnemann *et al.*, 2006; Prins *et al.*, 2011), impaired muscle relaxation and mitochondrial fission (O'Rourke *et al.*, 2017). Central nervous system (CNS) specific *Actb* KO mice resulted in hippocampus and cerebellum malformations in additional to profound hyperactivity and behavior impairments (Thomas R Cheever, Li and Ervasti, 2012). Finally, detailed studies on inner ear mechanotransducing hair cells, called the stereocilia, revealed that ablation of either *Actb* or *Actg1* lead to different patterns of progressive hearing loss and stereocilia degeneration (Belyantseva *et al.*, 2009; Perrin, Sonnemann and Ervasti, 2010; Perrin *et al.*, 2013).

The embryonic lethality of *Actb* KO has been corroborated by other groups (Shawlot *et al.*, 1998; Tondeleir *et al.*, 2012). Both groups have shown that hypomorphic or gene disruption of *Actb* resulted in a non-viable mouse. However, *Actb* ablated immortalized MEFs did not display the migration defect seen in primary MEFs (Bunnell *et al.*, 2011; Tondeleir *et al.*, 2012). Studies using small interfering RNAs (siRNAs) reported that knock down (KD) of *Actg1* more dramatically impaired motility in human subcutaneous fibroblasts, spontaneously immortalized keratinocytes, and neuroblastoma SH-EP cells than did KD of *Actb* (Dugina *et al.*, 2009; Shum *et al.*, 2011). Furthermore, Lechuga *et al.*, 2014 determined specific upregulation of myofibroblast-associated gene products (including *Acta2*) after siRNA KD of *Actg1*, but not *Actb*, in several epithelial cell

lines (Lechuga *et al.*, 2014). Therefore, it is necessary to understand the source of these various results to fully comprehend specific cytoplasmic actin functions.

Human diseases associated with cytoplasmic actin mutations

De novo mutations in the *ACTB* and *ACTG1* genes have been associated with Baraitser-winter syndrome, a rare disease where patients have complex clinical presentations including facial dysmorphism, deafness, brain malformations, intellectual disability and dystonia (Rivière *et al.*, 2012, Troys, 2015). *ACTB* and *ACTG1* mutations associated with Baraitser-Winter syndrome are missense mutations, resulting in a single amino acid change (Rivière *et al.*, 2012). The single amino acid mutations could alter actin function, which is corroborated by biochemical studies using yeast actins with the same mutations seen in the human patient population. K118M and K118N are *Actg1* missense mutations found in human patients that suffer from progressive deafness. These mutations resulted in changes in structure and nucleotide exchange rates. The K118N mutation in particular had a 2-fold increase in polymerization rate and the K118M mutation negatively affected Arp2/3 mediated branching formations (Jepsen *et al.*, 2016). Therefore, the missense mutations most likely resulted in either a gain-of-function or a dominant negative effect. Since both *ACTB* and *ACTG1* mutations led to similar phenotypes, it was hypothesized that both *ACTB* and *ACTG1* serve similar developmental functions (Rivière *et al.*, 2012). However, it was later discovered that the more severe forms of Baraitser-Winter syndrome are caused by *ACTB* mutations rather than *ACTG1* since the same amino acid change, such as Thr120Ile, resulted in worse clinical presentations in the *ACTB* patients (Di Donato *et al.*, 2014).

More recently loss of function mutations such as heterozygous *ACTB*

deletions, nonsense, or frame shift mutations have been discovered in the human population (Cuvertino *et al.*, 2017). Clinical phenotypes presented in these patients are developmental delay, intellectual disability, internal organ malformations and facial malformations distinct from Baraitser-Winter syndrome. Interestingly, the patient phenotypes are similar to those found in chromatin remodeling developmental disorders (Cuvertino *et al.*, 2017). Patient derived cells displayed phenotypes similar to *Actb* KO MEFs, including decreased cell migration, abnormal cell shape, and altered expression of cell-cycle genes which all suggests *ACTB* haploinsufficiency. More intriguingly, patients that were assessed with magnetic resonance imaging (MRI) showed brain malformations such as cortical atrophy, a thinning of the corpus callosum, septum pellucidum cyst, hydrocephalus, and certain patients also reported seizures (Cuvertino *et al.*, 2017). The human patient data coupled with CNS-*Actb* KO mice suggest that *ACTB* is critical for proper brain development. Overall, these loss of function phenotypes indicate that a critical amount of full length β-actin is required for proper human development.

Questions addressed by this thesis

Our lab previously generated whole body, conditional and tissue specific *Actb* and *Actg1* KO mouse models to discover and study unique functional roles of *Actb* and *Actg1*. Since then, other labs using gene-targeting and siRNA mediated KD have both corroborated and contradicted our findings. The first question my thesis seeks to answer is **how do different KO and KD methodologies affect β-actin function and biological findings?**

β- and γ-actin differ by 4 functionally similar amino acids on their N-terminus. Although previous whole body, conditional and tissue specific KO models have begun to clarify the specific functional roles for individual cytoplasmic actin, we do not know what causes their functional differences. Therefore, I used TALEN mediated genome engineering to edit the endogenous *Actb* locus to instead translate for γ-actin, in order to answer the question: **Do the four-amino acid differences between β- and γ-actin contribute to functional differences in cells or tissues?**

Another key difference between *Actb* and *Actg1* is how their mRNAs are regulated. The *Actb* mRNA contains a zipcode sequence that allows ZBP1 to regulate its transcript localization and translation. *Actg1* doesn't have a zipcode and is not spatial or temporally regulated. Hence, I used TALEN mediated genome engineering to edit the *Actb* 3'UTR zipcode sequence disrupting the ZBP1 binding sites in order to answer the question: **How important is the *Actb* zipcode sequence and ZBP1 binding *in vivo*?**

Figures

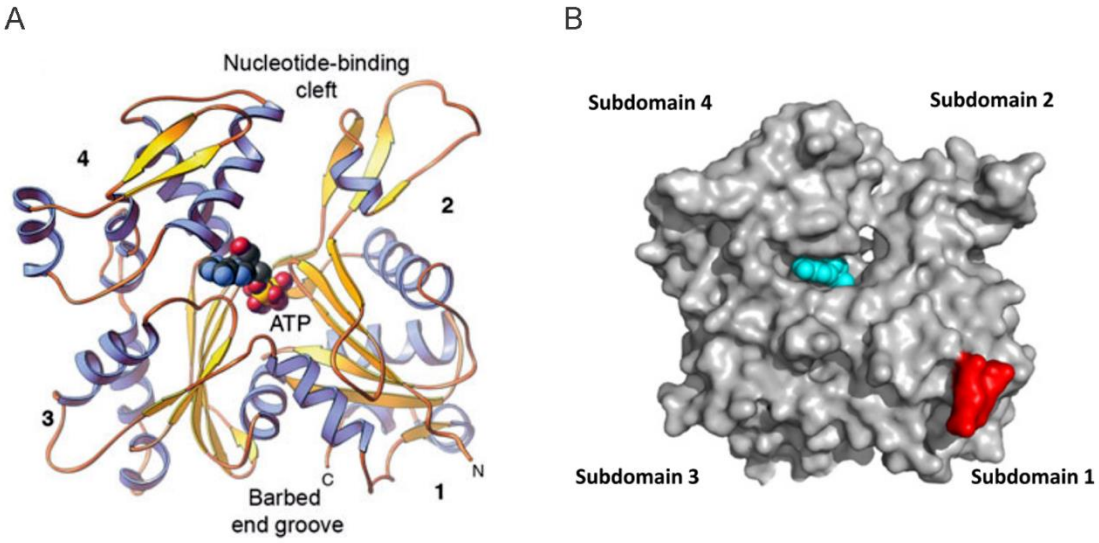

Figure 1-1 G-actin structure. (A) Ribbon diagram of monomeric actin with labeled subdomains and the nucleotide-binding cleft. (B) Crystal structure of β-actin. N-terminal end is labeled in red, ATP is labeled in cyan. PDB ID code 2BTF. Adapted from Pollard, 2015 and Rubenstein and Wen, 2018.

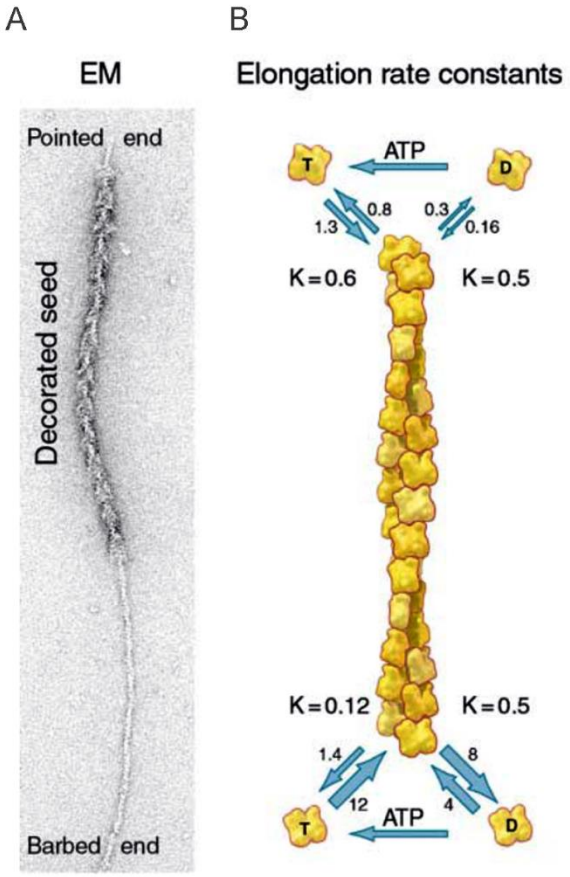

Figure 1-2 Filamentous actin structure. (A) Electron microscopy (EM) image of F-actin with decorated myosin. (B) Elongation rate constants at the pointed and barbed end of F-actin. Adapted from Pollard and Borisy, 2003.

A

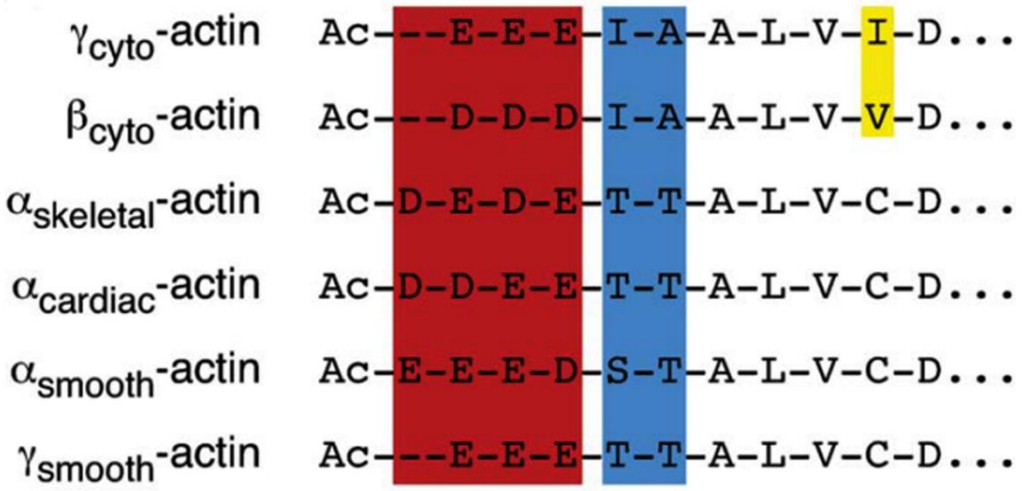

Figure 1-3 Actin isoform sequence differences. (A) Alignment of the N-terminal ends of the six mammalian actin isoforms. Amino acids labeled in red exhibit the most variability within and between the muscle and cytoplasmic actins. Residues in blue primarily vary between cytoplasmic and muscle actins, and residues in yellow only differ between the cytoplasmic actins. Adapted from Perrin and Ervasti, 2010.

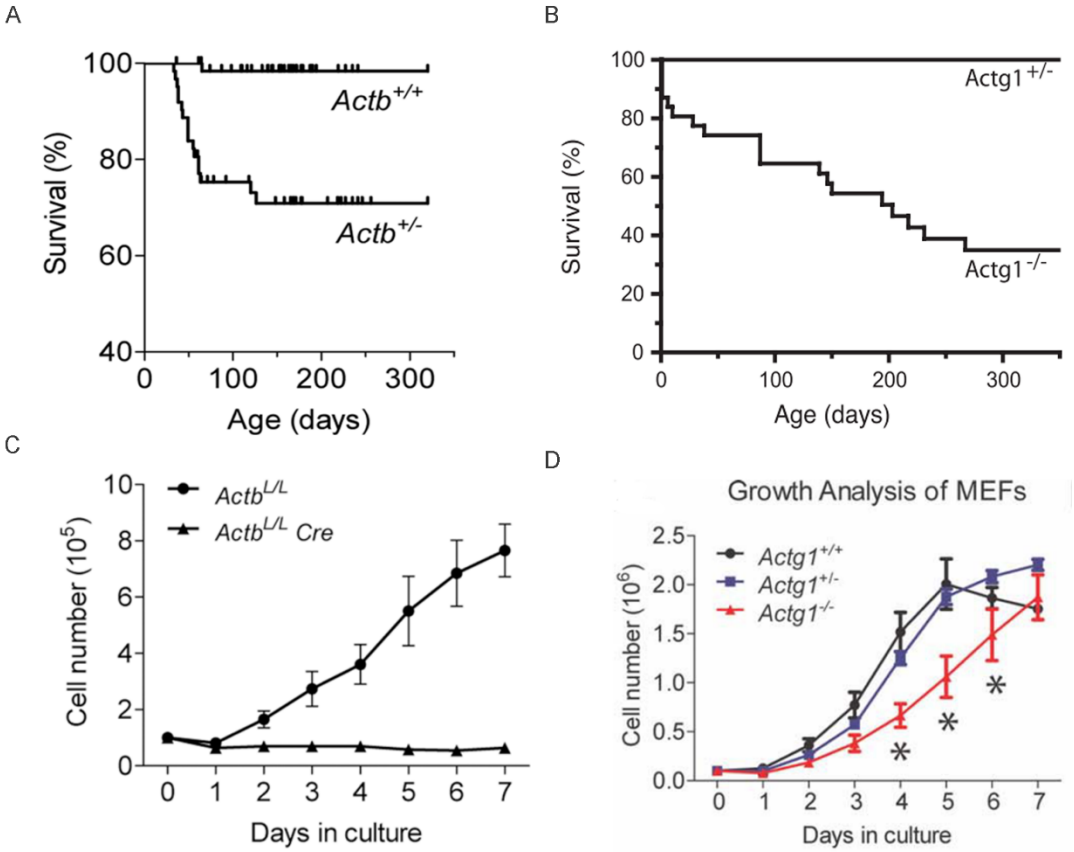

Figure 1-4 *Actb* and *Actg1* KO models. (A) Whole body *Actb* KO Kaplan-Meier survival curve. (B) Whole body *Actg1* KO Kaplan-Meier survival curve. (C) Conditional *Actb* KO MEF cellular proliferation analysis. (D) *Actg1* KO MEF cellular proliferation analysis. Adapted from Belyantseva *et al.*, 2009; Bunnell and Ervasti, 2010; Bunnell *et al.*, 2011.

Chapter 2

Relative importance of β_{cyto}- and γ_{cyto}-actin in primary mouse embryonic fibroblasts

Xiaobai Patrinostro*, Allison R. O'Rourke*, Christopher M. Chamberlain, Branden S. Moriarity, Benjamin J. Perrin, and James M. Ervasti

*Co-authorship

Molecular Biology of the Cell, 2017

Responsibilities:

X. Patrinostro designed experiments, analyzed data, written and edited the manuscript, and was responsible for data in figures 2-1 to 2-2, 2-4 to 2-7, and 2-9 to 2-16.

A.R. O'Rourke designed experiments, analyzed data, written and edited the manuscript, and was responsible for data in figures 2-1, 2-3 and 2-8.

C.M. Chamberlain assisted in mass spectroscopy sample preparation and experimentation.

B.S. Moriarity generated the SV40 LargeT antigen plasmid.

B.J. Perrin and J.M. Ervasti were involved in experimental design and manuscript editing.

Synopsis

The highly homologous beta (β_{cyto}) and gamma (γ_{cyto}) cytoplasmic actins are hypothesized to carry out both redundant and unique essential functions, but studies using targeted gene knockout and siRNA mediated transcript knockdown to examine β_{cyto}- and γ_{cyto}-isoform specific functions in various cell types have yielded conflicting data. Here, we quantitatively characterized actin transcript and protein levels as well as cellular phenotypes in both gene- and transcript-targeted primary mouse embryonic fibroblasts. We found that the smooth muscle α_{sm}-actin isoform was the dominantly expressed actin isoform in WT primary fibroblasts, and was also the most dramatically upregulated in primary β_{cyto}-, or β/γ_{cyto}-actin double knockout fibroblasts. Gene targeting of β_{cyto}-actin, but not γ_{cyto}-actin, led to greatly decreased cell proliferation, decreased levels of cellular ATP, and increased serum response factor signaling in primary fibroblasts while immortalization induced by SV40 largeT antigen supported fibroblast proliferation in the absence of β_{cyto}-actin. Consistent with *in vivo* gene targeting studies in mice, both gene and transcript targeting approaches demonstrate that the loss of β_{cyto}-actin protein is more disruptive to primary fibroblast function than is the loss of γ_{cyto}-actin.

Introduction

Vertebrate actin isoforms, which are encoded by six different genes, share a very high degree of sequence homology and are completely conserved from birds to mammals (Rubenstein, 1990). Four of the actin isoforms are predominately expressed in smooth (α_{sm}- and γ_{sm}-actin), cardiac (α_{ca}-actin) and skeletal muscles (α_{sk}-actin). The two cytoplasmic actins (β_{cyto}- and γ_{cyto}-actin) are ubiquitously expressed in all cell types and differ at only 4 out of 375 amino acids. Despite the remarkable conservation between the β_{cyto}- and γ_{cyto}-actin sequences, purified recombinant β_{cyto}- and γ_{cyto}-actin proteins display marked differences in dynamics *in vitro* (Bergeron *et al.*, 2010). Furthermore, numerous studies of transcript/protein localization, protein overexpression and disease-causing mutations have established a strong argument for unique functions supported by β_{cyto}- or γ_{cyto}-actin (Khaitlina, 2001, Condeelis and Singer, 2005, and Rubenstein and Wen, 2014). More recently, gene targeting studies have been employed to test for non-overlapping functions of actin isoforms (Perrin and Ervasti, 2010). With regard to closely related β_{cyto}- and γ_{cyto}-actins, the embryonic lethality of mice homozygous for severely hypomorphic (Shawlot *et al.*, 1998; Shmerling *et al.*, 2005), or null alleles of *Actb* (Bunnell and Ervasti, 2011) demonstrated that β_{cyto}-actin is an essential gene. In contrast, γ_{cyto}-actin null animals survive to term but display significant perinatal lethality, stunted growth, and decreased survival into adulthood (Belyantseva *et al.*, 2009; Bunnell and Ervasti, 2010). The distinct auditory hair cell and deafness phenotypes in mice in which floxed *Actb* and *Actg1* alleles were selectively ablated also support unique

roles for β_{cyto}- and γ_{cyto}-actin in some tissues (Perrin, Sonnemann and Ervasti, 2010; Perrin *et al.*, 2013). On the other hand, mice with skeletal muscle-specific knockouts of either β_{cyto}-, or γ_{cyto}-actin each develop a similar myopathy with progressive myofiber degeneration/regeneration and muscle weakness (Sonnemann *et al.*, 2006; Prins *et al.*, 2011) supporting that some functions of β_{cyto}- and γ_{cyto}-actins are redundant in some tissues.

We previously investigated the isoform-specific functions of β_{cyto}- and γ_{cyto}-actin in primary mouse embryonic fibroblasts (MEFs) from *Actg1*$^{-/-}$ animals (Bunnell and Ervasti, 2010; Bunnell *et al.*, 2011) and from mice with floxed *Actb* alleles conditionally ablated by tamoxifen-inducible Cre recombinase (Bunnell *et al.*, 2011). γ_{cyto}-Actin null MEFs showed mild growth impairment and a small decrease in cell viability, but were otherwise comparable to control cells in all other parameters tested (Bunnell and Ervasti, 2010; Bunnell *et al.*, 2011). In contrast, β_{cyto}-actin knockout MEFs exhibited a wide range of more severe phenotypes (Bunnell *et al.*, 2011). Ablation of β_{cyto}-actin resulted in severe growth impairment and an increase in the percentage of multinucleate cells, suggesting a specific role for β_{cyto}-actin in cell growth and division (Bunnell *et al.*, 2011) as previously supported by localization of β_{cyto}-actin to the cleavage furrow and contractile ring during cell division (Dugina *et al.*, 2009). Furthermore, β_{cyto}-actin knockout cells exhibited significant migration defects that were not observed in γ_{cyto}-actin null cells. The altered expression of genes that regulate the cell cycle and cell migration observed in β_{cyto}-actin, but not γ_{cyto}-actin knockout MEFs, provided a potential explanation for the more severe phenotypes in β_{cyto}-actin

knockout cells and early lethality in β_{cyto}-actin knockout embryos (Bunnell *et al.*, 2011). Also interesting, β_{cyto}-actin knockout MEFs exhibited some characteristics reminiscent of myofibroblasts, such as an increase in stress fibers and greatly elevated expression of α_{sm}-actin (Bunnell *et al.*, 2011).

In contrast to our results, four studies have reached different conclusions that warrant further investigation. One study of immortalized β_{cyto}-actin knockout MEF lines transformed by SV40 largeT antigen (Tondeleir *et al.*, 2012) reported altered morphology, impaired migration and upregulation of α_{sm}-actin similar to what we observed in primary *Actb* null MEFs (Bunnell *et al.*, 2011), but with no impairment of cell growth. Two studies using small interfering RNA (siRNA) methodologies reported that knock down of γ_{cyto}-actin more dramatically impaired motility in human subcutaneous fibroblasts, spontaneously immortalized keratinocytes, and neuroblastoma SH-EP cells than did knock down of β_{cyto}-actin (Dugina *et al.*, 2009; Shum *et al.*, 2011). Most notably, the fourth study demonstrated specific upregulation of myofibroblast-associated gene products (including α_{sm}-actin) after siRNA knock down of γ_{cyto}-actin, but not β_{cyto}-actin, in several epithelial cell lines (Lechuga *et al.*, 2014). While differences in methodologies and cell types studied are obvious explanations for the different outcomes, Lechuga and colleagues further speculated that the different results could depend on whether the ablated actin isoform was also the most abundant in the cell type under investigation (Lechuga *et al.*, 2014).

To address the bases for differences between ours (Bunnell and Ervasti, 2010; Bunnell *et al.*, 2011) and others (Dugina *et al.*, 2009; Shum *et al.*, 2011;

Tondeleir *et al.*, 2012; Lechuga *et al.*, 2014) studies, we quantitatively profiled actin isoforms at both the transcript and protein level. Because MEFs display extensive developmental and phenotypic heterogeneity (Singhal *et al.*, 2016), we employed adenovirus-5 mediated expression of Cre recombinase (Ad5-Cre) to ablate *Actb* and/or *Actg1* in both primary and Large T antigen immortalized MEFs controlled against the same MEFs infected with Ad5-GFP. α_{sm}-Actin and β_{cyto}-actin transcripts predominated in primary MEFs, while α_{sm}-actin was most abundant at the protein level, with equivalent levels of β_{cyto}- and γ_{cyto}-actin protein expressed despite their marked differences in transcript levels. We also found that immortalization by transformation with SV40 largeT antigen appears to negate the essentiality of *Actb* observed in primary MEFs. Finally, siRNA-mediated transcript knockdown of *Actb* and *Actg1* in the same cells used for gene targeting studies yielded similar results as those observed after gene targeting. We conclude that the genetic reprogramming associated with immortalization by transformation with SV40 largeT antigen can markedly influence the cellular response to β_{cyto}- and γ_{cyto}-actin protein ablation.

Results

Adenoviral Cre mediated knock-out of *Actb* and *Actg1*.

Because primary MEFs display extensive developmental and phenotypic heterogeneity (Singhal *et al.*, 2016), each of our biological replicates consisted of E13.5 primary MEFs obtained from a single mouse embryo carrying floxed alleles of either *Actb* (*Actb*$^{L/L}$, Bunnell *et al.*, 2011), *Actg1* (*Actg1*$^{L/L}$, Sonnemann *et al.*, 2006), or both *Actb* and *Actg1* (*Actb*$^{L/L}$ *Actg1*$^{L/L}$). MEFs from each animal were split into two pools that were treated with Ad5-GFP (Figure 2-1A) as a negative control, or with Ad5-Cre (Figure 2-1B) to conditionally knock out *Actb* (β_{cyto}-actin KO), *Actg1* (γ_{cyto}-actin KO), or both *Actb* and *Actg1* (dKO). Quantitative reverse transcription polymerase chain reaction (qRT-PCR) analysis showed that *Actb* and *Actg1* transcripts were reduced 95% by 3dpi in β_{cyto}-actin KO, γ_{cyto}-actin KO and dKO MEFs compared to controls (Figure 2-1C-F). Western blot analysis revealed that β_{cyto}- and γ_{cyto}-actin were each undetectable at 5dpi in single β_{cyto}-actin KO or γ_{cyto}-actin KO cells, respectively (Figure 2-1G, H). In contrast, complete loss of β_{cyto}- and γ_{cyto}-actin in dKO cells was observed at 9dpi (Figure 2-1I). Thus, Ad5-Cre was an efficient and robust method to eliminate both β_{cyto}-and γ_{cyto}-actin transcripts and proteins in primary MEFs.

β-Actin KO MEFs are growth impaired with reduced ATP levels.

We previously showed that tamoxifen-induced, cre-mediated ablation of β_{cyto}-actin caused significant growth impairment in primary MEFs while only a modest decrease in cell growth was observed in *Actg1-/-* MEFs (Bunnell and

Ervasti, 2010; Bunnell *et al.*, 2011). However, our previous experiments involved different methods of gene ablation for *Actb* and *Actg1* and compared knockout MEFs with controls derived from different embryos (Bunnell and Ervasti, 2010; Bunnell *et al.*, 2011). Therefore, we more directly compared the effects of β_{cyto}- versus γ_{cyto}-actin gene ablation on cell growth using β_{cyto}-actin KO and γ_{cyto}-actin KO MEFs. Under these more controlled conditions, γ_{cyto}-actin KO MEFs exhibited a normal growth rate, while both β_{cyto}-actin KO and dKO MEFs displayed growth impairment by 3dpi that became significantly different from controls at 7dpi (Figure 2-2). Because growth deficiency was not previously observed in MEFs ablated for β_{cyto}-actin expression after transformation by SV40 largeT antigen (Tondeleir *et al.*, 2012), we immortalized *Actb*$^{L/L}$, *Actg1*$^{L/L}$ and double *Actb*$^{L/L}$ *Actg1*$^{L/L}$ MEFs by transformation with SV40 largeT antigen and measured cell growth after infection with either Ad5-Cre or Ad5-GFP. Both SV40 largeT antigen immortalized β_{cyto}-actin KO and γ_{cyto}-actin KO MEFs exhibited growth rates not different from controls (Figure 2-11A-B), suggesting that β_{cyto}-actin is important for cell growth in primary MEFs, but not in MEFs transformed by SV40 largeT antigen. In contrast, SV40 largeT antigen immortalized dKO MEFs displayed growth impairment that was significantly different from control at 8-10dpi (Figure 2-11C), but less severe than in primary MEFs, suggesting that MEFs immortalized by SV40 largeT antigen transformation are able to circumvent the essential function supported by β_{cyto}-actin in primary cells and during embryonic development.

To assess whether growth deficiencies seen in β_{cyto}-actin KO and dKO MEFs could potentially be due to decreases in energy availability, we utilized a luciferase-based assay to measure the relative levels of cellular ATP in β_{cyto}-actin KO, γ_{cyto}-actin KO and dKO MEFs. Correlating with the deficiencies seen in growth, ATP levels were significantly decreased in β_{cyto}-actin KO and dKO MEFs compared to controls, but not in γ_{cyto}-actin KO MEFs (Figure 2-3A). However, western blot analysis demonstrated that a number of proteins in the mitochondrial electron transport chain complexes were equivalent across the MEF lines tested (Figure 2-3B-C), as were basal and maximal oxygen consumption rates measured in β_{cyto}-actin KO and γ_{cyto}-actin KO MEFs using a Seahorse XF24 extracellular flux analyzer (Figure 2-3D). Therefore, we conclude that the measured decreases in cellular ATP are not due to impaired mitochondrial function in β_{cyto}-actin KO and dKO MEFs.

Quantitation of actin isoform transcript and protein levels in primary MEFs.

qRT-PCR was used to measure transcript levels for all six actin isoforms in control, β_{cyto}-actin KO, γ_{cyto}-actin KO and dKO MEFs after 5dpi. The amount of transcript for each actin isoform in MEFs was calculated from standard curves that were amplified in parallel (Figure 2-12A-F). In all control MEFs, α_{sm}- and β_{cyto}-actins were the dominant transcripts (Figure 2-4A-C), in contrast to NIH3T3s fibroblasts cultured under the same conditions, where β_{cyto}-and γ_{cyto}-actins were the predominant transcripts (Figure 2-13A). α_{sm}-Actin was the only actin transcript significantly upregulated in β_{cyto}-actin KO MEFs (Figure 2-4A) while

both α_{sm}- and β_{cyto}-actins transcripts were upregulated in γ_{cyto}-actin KO MEFs (Figure 2-4B). Similar to β_{cyto}-actin KO MEFs (Figure 2-4A), α_{sm}-actin was the only transcript significantly upregulated in dKO MEFs (Figure 2-4C). The high levels of α_{sm}-actin transcript suggest a myofibroblast-like phenotype in the primary MEFs that was enhanced to a greater extent by ablation of *Actb* over *Actg1*.

Since α_{sm}-, β_{cyto}- and γ_{cyto}- were the most abundant actin transcripts in primary MEFs, we measured α_{sm}-, β_{cyto}- and γ_{cyto}-actin protein levels in both control and KO MEFs via quantitative Western blot analysis at 5dpi in each single KO and at 9dpi in the dKO using purified α_{sm}-, β_{cyto}- and γ_{cyto}-actin proteins as standards. α_{sm}-Actin was the most abundant actin isoform protein expressed, while β_{cyto}- and γ_{cyto}-actin proteins were expressed to similar levels in all control MEFs (Figure 2-5B-D). Consistent with transcript analysis (Figure 2-13A), β_{cyto}- and γ_{cyto}-actin were the dominant actin proteins expressed in NIH3T3 fibroblasts cultured under the same conditions (Figure 2-13B). In β_{cyto}-actin KO MEFs, α_{sm}-actin protein was dramatically increased by 6 fold over controls, but γ_{cyto}-actin protein was not significantly increased (Figure 2-5A-B). In γ_{cyto}-actin KO MEFs, α_{sm}-actin protein was upregulated by 1.7 fold while β_{cyto}-actin protein was not significantly increased (Figure 2-5A, C). α_{sm}-Actin protein was also significantly upregulated by 7 fold in dKO MEFs (Figure 2-5A, D). Thus, α_{sm}-actin was prominently expressed in all control primary MEFs and more dramatically upregulated upon ablation of *Actb* compared to *Actg1*, suggesting that primary MEFs may be predisposed to a myofibroblast-like phenotype that can be most

enhanced by selective perturbation of *Actb*. Also, interesting, β_{cyto}-actin transcript was expressed six-fold higher than γ_{cyto}-actin transcript in all control MEFs, yet the ratio of β_{cyto}-actin protein to γ_{cyto}-actin protein was 1:1 (Figure 2-6A-C). The unequal transcript-to-protein ratio supports other studies concluding that *Actb* and *Actg1* gene expression are differentially regulated post-transcriptionally (Hüttelmaier *et al.*, 2005; Zhang *et al.*, 2010).

siRNA mediated knockdown of *Actb* and*Actg1*.

Since other studies reporting results different from ours used siRNA approaches to knock down (KD) *Actb* and *Actg1* transcripts and proteins (Dugina *et al.*, 2009; Shum *et al.*, 2011; Lechuga *et al.*, 2014), we assessed how siRNA-mediated KD of β_{cyto}- and/or γ_{cyto}-actin in *Actb*$^{L/L}$ (β_{cyto}-actin KD), *Actg1*$^{L/L}$ (γ_{cyto}-actin KD), and *Actb*$^{L/L}$ *Actg1*$^{L/L}$ (β/γ_{cyto}-actin dKD) primary MEFs impacted cell phenotype. On average, we were able to specifically KD β_{cyto}-actin protein by 70% and γ_{cyto}-actin protein by 55% when compared to controls. In dKD MEFs, β_{cyto}-actin protein was reduced by 65% and γ_{cyto}-actin protein was reduced by 55% (Figure 2-7A). Quantitative Western blot analysis showed that α_{sm}-actin protein was dramatically increased 9-fold in β_{cyto}-actin KD cells, over controls, but γ_{cyto}-actin protein was not significantly increased (Figure 2-7A-B). In γ_{cyto}-actin KD cells, neither α_{sm}-actin protein nor β_{cyto}-actin protein was significantly increased (Figure 2-7A, C). α_{sm}-Actin protein was also significantly upregulated 4-fold in β/γ_{cyto}-actin dKD cells (Figure 2-7A, D). Thus, both siRNA mediated transcript KD and cre mediated gene KO gave similar results in primary MEFs.

Actb gene ablation enhances some myofibroblast-like phenotypes of primary MEFs

In response to a variety of perturbations (Small, 2012; Davis and Molkentin, 2013), fibroblasts often differentiate into smooth muscle-like cells called myofibroblasts via a process called the fibroblast to myofibroblast transition (FMT). In addition to increased α_{sm}-actin expression, another hallmark of myofibroblasts is increased stress fiber formation (Small, 2012; Davis and Molkentin, 2013), which we observed in β_{cyto}-actin KO, γ_{cyto}-actin KO and dKO MEFs, compared to controls (Figure 2-8A-F). To quantify the change in the stress fibers of KO MEFs, line scans across the cell width were made (Figure 2-8G). Peak-to-valley ratios were taken as an average measure of the fluorescence intensity of the stress fibers (Figure 2-8H). All KO cell types displayed significant elevation in the average peak-to-valley ratios, indicating increased stress fiber formation (Figure 2-8A-F). Because caldesmon, calponin and transgelin proteins have been shown to be upregulated during epithelial to myofibroblast transition (Lechuga *et al.*, 2014), we measured their protein levels in addition to myosin light chain 2 and phosphorylated myosin light chain 2 protein levels in control and knock out MEFs. Caldesmon expresses a higher molecular weight isoform in smooth muscle cells ($Cald1_{sm}$) than in non-smooth muscle cells (Ueki *et al.*, 1987; Frid *et al.*, 1992). In agreement with our previously published data (Bunnell *et al.*, 2011), $Cald1_{sm}$ was upregulated in β_{cyto}-actin KO, γ_{cyto}-actin KO and dKO primary MEFs, though more so in β_{cyto}-actin KO MEFs than γ_{cyto}-actin KO MEFs (Figure 2-9A-D). In contrast, none of the other myofibroblast marker proteins

interrogated were significantly upregulated (Figure 2-9A-D). siRNA-treated primary MEFs showed similar upregulation of $Cald_{sm}$ in KD MEFs (Figure 2-14A-D). Thus, increased stress fiber formation and expression of $Cald1_{sm}$ suggests that ablation of *Actb* enhances a partial myofibroblast-like phenotype in primary MEFs.

Finally, actin dynamics are known to play a role in myofibroblast differentiation via the serum response factor (SRF)/myocardin-related transcription factor (MRTF) gene regulatory pathway (Small, 2012). Therefore, we investigated whether either SRF or MRTF-A protein expression, and SRF activity, was perturbed when cytoplasmic actins were ablated. In all knockout MEFs, SRF protein levels were not significantly altered compared to controls (Figure 2-10A, C). MRTF-A protein level was downregulated in all gene knockout MEFs, which was significant in dKO MEFs (Figure 2-10A-B). Similar results were observed in siRNA KD MEFs (Figure 2-15A-B). Although no drastic changes in protein expression were observed, SRF activity was significantly increased by 6-fold in both β_{cyto}-actin KO and dKO MEFs compared to controls. SRF activity increased by 2-fold in γ_{cyto}-actin KO MEFs, although this increase was not significantly different from controls. Our data suggest that *Actb* knockout more significantly and specifically impacts the SRF/MRTF gene regulatory pathway than does the loss of *Actg1*.

Discussion

β_{cyto}-actin is thought to be an essential protein based on the early embryonic lethality observed in *Actb* gene-targeted mice (Shawlot *et al.*, 1998; Shmerling *et al.*, 2005; Bunnell *et al.*, 2011). In addition, many cell biological studies provide further compelling support to the essentiality of β_{cyto}-actin in a wide array of cellular processes (Zhao *et al.*, 1998; Hofmann *et al.*, 2004; Hu, Wu and Hernandez, 2004; Karakozova *et al.*, 2006; Leung *et al.*, 2006; Yao *et al.*, 2006). While γ_{cyto}-actin is clearly important *in vivo*, it is not essential given that *Actg1* null mice can survive up to 2 years (Belyantseva *et al.*, 2009). Here we attempted to resolve the different results reported across a group of cell-based studies all seeking to elucidate the respective roles of β_{cyto}- and γ_{cyto}-actin through ablation of protein expression using different targeting approaches in different cell types. Most vexing, β_{cyto}-actin gene knockout in two studies caused essentially the same effects on cell motility and α_{sm}-actin expression (Bunnell *et al.*, 2011; Tondeleir *et al.*, 2012) as those caused by γ_{cyto}-actin knockdown in three other studies (Dugina *et al.*, 2009; Shum *et al.*, 2011; Lechuga *et al.*, 2014). Because gene and transcript targeting have been shown to cause strikingly different *in vivo* phenotypes for a number of loci (Rossi *et al.*, 2015), we anticipated that actin gene knockout and transcript knockdown experiments carried out in the same cells would explain the discrepant results. Instead, we observed the same experimental outcomes whether siRNA-mediated transcript knockdown or Cre-mediated gene knockout were employed. As an alternative explanation for the discrepant

results across studies (Dugina *et al.*, 2009; Bunnell *et al.*, 2011; Shum *et al.*, 2011; Tondeleir *et al.*, 2012; Lechuga *et al.*, 2014), Lechuga and colleagues hypothesized that loss of the most abundantly expressed actin isoform may dictate a given cell type's response to actin gene ablation (Lechuga *et al.*, 2014). However, our quantitative western blot analysis demonstrated that β_{cyto}- and γ_{cyto}-actin proteins were present in equal abundance in the primary MEFs studied here. We conclude that neither differences in actin isoform targeting method or endogenous protein levels can explain the dramatically different and often opposite results reported in the six studies from five different groups.

Here (Figure 2-2) and previously (Bunnell *et al.*, 2011), we measured dramatic cell proliferation defects with ablation of β_{cyto}-actin in primary MEFs that could account for the embryonic lethality associated with *Actb* gene deletion (Shawlot *et al.*, 1998; Shmerling *et al.*, 2005; Bunnell *et al.*, 2011). We measured significantly decreased levels of cellular ATP associated with knockout of β_{cyto}-actin in the presence of apparently unaffected mitochondrial function (Figure 2-3). While the basis for decreased ATP levels in β_{cyto}-actin knockout MEFs remains an interesting question for future studies, it will be challenging to answer given that ablation of functionally disparate genes in MEFs has been shown to impact cellular ATP levels independent of corresponding defects in mitochondrial respiration (Gautier, Kitada and Shen, 2008; Giaime *et al.*, 2012). We also found that immortalization induced by transformation with SV40 largeT antigen rendered *Actb* nonessential for proliferation (Figure 2-11). Although Tondelair et al., 2012 previously noted that cell survival was not impaired in their *Actb* null

MEFs immortalized by transformation with SV40 largeT antigen, a more recent study reported a general delay in cell cycle progression, impaired colony growth and reduced proliferation rate in the same cell line (Almuzzaini *et al.*, 2016). While we cannot exclude other effects of transformation with SV40 largeT antigen, cell immortalization has been associated with substantial changes in gene expression (Kuo, Burl and Hu, 2012; Gordon *et al.*, 2014). A recent comparison of primary and spontaneously immortalized MEFs reported almost 2,000 transcripts that were up- or down-regulated by 3-fold (Kuo, Burl and Hu, 2012). Other studies have demonstrated that immortalization can significantly impact cell behavior both in the absence (Vasioukhin *et al.*, 2000), or presence of subsequent perturbations (Wade *et al.*, 2002), and even after reversal (Wang *et al.*, 2014). In one highly cited study, primary epithelial cells form prominent "adhesion zippers" that become challenging to detect after immortalization (Vasioukhin *et al.*, 2000). Moreover, the essential role for p27 in mediating the growth-inhibitory effects of vitamin D in mouse knockout models and primary MEFs was not recapitulated in immortalized MEFs (Wade *et al.*, 2002). Given the unpredictable effects of immortalization and transformation on cell biological function, we suggest that primary MEFs more appropriately model the embryonic lethality associated with *Actb* gene ablation in mice.

We measured striking differences between the ratios of β_{cyto} to γ_{cyto}-actin transcript versus protein in primary MEFs: β_{cyto}-actin transcript was 6-fold greater than γ_{cyto}-actin transcript, yet β_{cyto}- and γ_{cyto}-actin protein levels were equivalent (Figure 6). β_{cyto}-actin translation is more rapid than γ_{cyto}-actin (Zhang *et al.*, 2010)

and also tightly regulated via an RNA regulatory sequence in its 3'UTR named the "zipcode" (Kislauskis *et al.*, 1993; Ross *et al.*, 1997; Hüttelmaier *et al.*, 2005). Because β_{cyto}-actin protein is the more dynamic of the two cytoplasmic actin isoforms (Bergeron *et al.*, 2010), it is tempting to speculate that the greater abundance of the β_{cyto}-actin transcript is maintained for rapid translation and dynamic cytoskeletal rearrangement. However, the similar levels of β_{cyto}- and γ_{cyto}-actin protein (Figure 6) and similar rates of decay after gene ablation in primary MEFs (Figure 1) suggest that β_{cyto}-actin transcript may play some additional function in cells independent of its role as a template for translation. As one possibility, the large pool of *Actb* transcript may serve to buffer miRNAs important in regulating the expression of other genes important for cell proliferation, motility, and/or differentiation. Of the more than 20 different miRNA binding sites collectively predicted by TargetScan, microRNA.Org, and PicTar to be present in the 3' UTR of the *Actb* transcript but absent from *Actg1* (Table 2-1), only mir-205 was identified by all three programs while mir-1 and mir206 were identified by two of three algorithms. Interestingly, mir-1, mir-205 and mir-206 have all been previously hypothesized to function as tumor suppressors based on experiments demonstrating a correlation between growth inhibition with miRNA overexpression (Hudson *et al.*, 2012; Jalali *et al.*, 2012; Liu *et al.*, 2012; Koshizuka *et al.*, 2016), or increased proliferation after miRNA inhibition (Jalali *et al.*, 2012). Of further relevance to our study, overexpression of mir-1, mir-205 and mir-206 also was associated with significantly decreased cell motility, increased expression of α_{sm}-actin and calponin, and perturbations in actin cytoskeletal

dynamics (Hudson *et al.*, 2012; Jalali *et al.*, 2012; Liu *et al.*, 2012). We speculate that ablation of *Actb* transcript could indirectly drive similar phenotypic changes by freeing up normally sequestered miRNAs. Finally, differential miRNA binding may not be required to explain different phenotypic outcomes for *Actb* versus *Actg1* transcript ablation. The miRNA mir-145 is predicted to bind both *Actb* and *Actg1* and is important in smooth muscle cell proliferation and differentiation (Cordes *et al.*, 2009) so it is possible that more abundant *Actb* transcript could play the dominant role in sequestering mir-145 during development.

Finally, the differentiation status and/or tissue origin of cells utilized may also account for some of the differences between studies (Dugina *et al.*, 2009; Bunnell *et al.*, 2011; Shum *et al.*, 2011; Tondeleir *et al.*, 2012; Lechuga *et al.*, 2014). While *Actb* and/or β_{cyto}-actin are essential during relatively early stages of embryonic development (Shawlot *et al.*, 1998; Shmerling *et al.*, 2005; Bunnell *et al.*, 2011), neither is specifically required for later stage development of more differentiated auditory hair cells (Perrin, Sonnemann and Ervasti, 2010), neurons of the peripheral (Cheever, Olson and Ervasti, 2011) or central (Thomas R. Cheever, Li and Ervasti, 2012) nervous systems, or skeletal muscle (Sonnemann *et al.*, 2006; Prins *et al.*, 2011). These data suggest that cells transition from an *Actb*-essential state to an *Actb*-important state as development and differentiation progress *in vivo*. Clearly, the challenge remains to define the *in vivo* biological process modeled by any particular cell in culture.

Methods

Cell Culture: Primary MEFs were cultured from E13.5 *Actb* $^{L/L}$, *Actg1*$^{L/L}$ and double *Actb*$^{L/L}$/*Actg1*$^{L/L}$ mouse embryos as described previously (Bunnell and Ervasti, 2010). Cells were grown to 80% confluency on 10-cm plates and frozen down at passage 1 at 1x10^{6} cells/mL in MEF freezing media (DMEM supplemented with 10% FBS, 1% Pen/Strep, 0.5ug/mL Fungizone and 5% dimethyl sulfoxide). Primary MEFs were immortalized by transformation with SV40 largeT antigen expression, which was incorporated into the genome via the piggyBac transposase system, a generous gift from Dr. Brandon Moriarity. MEFs from individual embryos were thawed, cultured in MEF media (DMEM supplemented with 10% FBS, 1% Pen/Strep, 0.5ug/mL Fungizone), grown to 80% confluency, split into two culture dishes and treated with either Ad5-GFP control virus (Ad5CMV-hrGFP) or Ad5-Cre (Ad5CMV-Cre-eGFP) virus purchased from The University of Iowa Viral Vector Core following their Adenovirus Adfection Protocol (http://www.medicine.uiowa.edu/vectorcore).

SiRNA transfection: MEFs from individual embryos were thawed, grown to 80% confluency, split into two culture dishes and treated with either control or β_{cyto}- and/or γ_{cyto}-actin ONTARGET*plus* siRNAs purchased from Dharmacon following their protocol. (http://dharmacon.gelifesciences.com/uploadedFiles/Resources/basic-dharmafect-protocol.pdf) See supplemental methods for siRNA sequences.

SRF Luciferase Activity Assay: *Actb*$^{L/L}$, *Actg1*$^{L/L}$ and double *Actb*$^{L/L}$*Actg1*$^{L/L}$ MEFs from individual embryos were treated with either Ad5-GFP or Ad5-Cre. sKO at 3dpi and dKO at 7dpi were nucleofected (Amaxa® Nucleofector® II) with PGL3-Basic-luc (control) or PGL3-FHL2_145-luc (Four and a half LIM domain protein-2) promoter (SRF reporter) constructs (Schmidt *et al.*, 2012), generously provided by Dr. Hannelore V. Heemers. Two days post nucleofection, at 5dpi for sKO and 9dpi for dKO, cells were lifted and hand counted using a hematocytometer. Equal numbers of cells between Ad5-GFP and Ad5-Cre treated MEFs were washed with PBS and processed based on manufacture protocols (Dual-Luciferase® Reporter Assay, Promega). Aliquots (20µL) of cleared processed lysates were used to determine SRF luciferase activity (BioTek Synergy 4 spectrometer with Gen5 2.07 software).

Quantitative Reverse Transcription Polymerase Chain Reaction (qRT-PCR): Mouse actin isoform cDNAs were amplified from WT MEFs by PCR using the primers listed in the supplemental methods and cloned into pENTR™/D-TOPO vector (Life Technologies) to generate a control construct for each actin isoform. Each actin isoform qRT-PCR primer set, listed in the supplemental methods, was tested for amplification of all control constructs to assess primer specificity. Total RNA was extracted from *Actb* $^{L/L}$, *Actg1*$^{L/L}$ and double *Actb*$^{L/L}$/*Actg1*$^{L/L}$ MEF samples using the Biorad-Aurum ™ Total RNA Mini Kit following the manufacturer's instructions. RNA concentration and purity (260/280 ratio) were determined using a NanoDrop spectrophotometer (Wilmington, DE). First-strand

cDNA was synthesized with a Biorad-iScript Advanced cDNA Synthesis Kit for qRT-PCR using the same initial RNA amount (1ug) for all samples. Individual control constructs, were used in a 10-fold dilution to generate a standard curve, and MEF samples were amplified in parallel with each specific qRT-PCR primer set using Biorad -SsoAdvanced Universal SYBR polymerase on the Biorad-CFX96 Real Time System C1000 Touch Thermal Cycler to profile each actin isoform transcript amount (pmol).

Actin Isoforms: Platelet non-muscle actin (β_{cyto}- and γ_{cyto}-actin) was purchased from Cytoskeleton, Inc. (Denver, CO). Recombinant γ_{cyto}- and α_{sm}-actin were expressed in the Bacto-Bac insect cell-expression system and purified as previously described (Perrin *et al.*, 2013). Protein concentrations were determined using a NanoDrop spectrophotometer (Wilmington, DE). Contamination of recombinant γ_{cyto}- and α_{sm}-actins by insect cell actin was measured by ESI mass spectrometry acquired using a QSTAR Pulsar i (Applied Biosystems, Inc., Foster City, CA) quadrupole-TOF (time-of-flight) mass spectrometer equipped with a turbo-ESI source. Protein samples were loaded directly in 50% Acetonitrile and 0.1% formic acid. The ion spray voltage was 1000 V, the TOF region acceleration voltage was 4 kV, and the injection pulse repetition rate was 7.0 kHz. External calibration was performed using renin (monoisotopic mass [MH3+] 586.9830 and [MH2+] 879.9705; Sigma-Aldrich, St. Louis, MO). Mass spectra were summed and averaged over the injection peak.

Deconvolution of the charge envelope was performed with the Bioanalyst, AnalystQS software package (ABI).

Western Blotting: For western blot quantitation of actin isoforms against a standard curve, Total MEF protein was extracted with 1%SDS buffer in 1xPBS and a cocktail of protease inhibitors (Aprotinin 100uM, Benzamide 0.79mg/mL, E-64 10nM, Leupeptin 10uM, Pepstatin 0.1mg/mL, PMSF 1mM), sonicated (Model 150V/T Ultrasonic homogenizer, BioLogics, Inc.), boiled and centrifuged to remove the insoluble fraction. An increasing amount (25-300ng) of purified actin protein and all MEF samples were run on the same blot to ensure consistency. LiCor fluorescent signal verses purified actin protein amount (ng) was used to generate a standard curve, in order to calculate specific actin isoform concentration (ng protein/µL of total lysate). All samples were western blotted with β-actin (AC-15; Sigma-Aldrich), γ-actin (mAb 117; and α_{sm}-actin (A14; Sigma-Aldrich). For comparisons of relative immunoreactivities, equal amounts of cleared total MEF lysate protein (25µg) were blotted with antibodies to Caldesmon1 (Cat #2980, Cell signaling), SM22 (ab14106; Abcam), Calponin (ab46794; Abcam), SRF (G-20; Santa Cruz), MRTF-A (H-140; Santa Cruz), MTOC1 (ab14705; Abcam), SDHA (ab14715; Abcam), UQCR (ab110252; Abcam), ATP5A (ab14748; Abcam), MLC2 (ab48003; Abcam), MLC2 (phosphor S20) (ab2480; Abcam), and GAPDH (G9545 or G8795; Sigma-Aldrich) was used as loading control.

Cell Fixation and Staining: MEFs cultured for 6 to 8 days post infection (DPI) with either Ad5-GFP or Ad5-CRE were plated on [5ug/ml] fibronectin-coated coverslips at a density of $1x10^4$ cells per coverslip and incubated in MEF culturing media. The following day, cells were fixed with fresh 4% paraformaldehyde in PBS for 15min at room temperature. To stain actin filaments, fixed cells were treated with a 0.2% Triton X-100 and 16.5nM Phalloidin (Life Technologies A22285) in PBS for 30 minutes at room temperature. Coverslips were mounted in Prolong (Life Technologies P36931) mounting media.

Cell Imaging and Quantification: Samples were imaged using a Delta Vision PersonalDV microscope under a 60x1.42 NA objective (GE Technologies). All cells were imaged with the same laser intensity and exposure time. The intensity of the stress fibers was quantified from line scans across the widest part of the cell using ImageJ. The peaks and corresponding valleys were then determined (excluding the first peak which represents the edge of the cell). The average peak to valley ratio per cell was then plotted using GraphPad Prism.

ATP Quantification: At 7 or 9 DPI, cells were lifted and counted. Equal number of CT and KO MEFs were lysed using boiling water (Yang *et al.*, 2002). The lysate was spun at 12,000x*g* for 5 min at 4°C and the supernatant was collected. Following the luciferase based ATP Determination Kit (A22066) protocol, the reaction solution (reaction buffer, DTT, D-luciferin, and firefly luciferase) was added to the cell lysate supernatant. After a 15 min incubation, ATP levels were

determined using a BioTek Synergy 4 spectrometer with Gen5 2.07 software and quantified using an ATP standard ranging from 0nm-1µM.

Analysis of cell growth: $5x10^5$ of MEFs/well were treated with either Ad5-GFP or Ad5-Cre. Samples were counted every other day beginning 1dpi, in duplicate, using a hematocytometer to generate growth curves.

Oxygen Consumption: Cells were plated in triplicate on fibronectin [5ug/µl] coated XF24 cell culture microplates (Seahorse Bioscience) at $5x10^4$ cells per well 24 hours prior to the experiment. Mitochondrial function was examined using the Seahorse XF24 extracellular flux analyzer and the cell mitochondrial stress assay (Seahorse Bioscience). Oligomycin [2ug/ml Final], FCCP [0.5µM Final], and Antimycin A [4µM Final] were injected at time points throughout the experiment according to the company protocol (all compounds from Seahorse Bioscience). Oxygen consumption was measured at multiple points in between each injection and normalized to background controls.

Statistics: For quantitative RT-PCR and quantitative Western blots; two-way ANOVA with a Bonferoni post-test was used on calculated amount of transcript (pmol) and protein (ng/µL of lysate) to determine statistics. For all relative Western blots; immuno-reactivity levels for all samples were normalized to GAPDH and relative to the paired embryo control, which was set at 1, and a One sample t-test was performed to evaluate statistics.

Figures

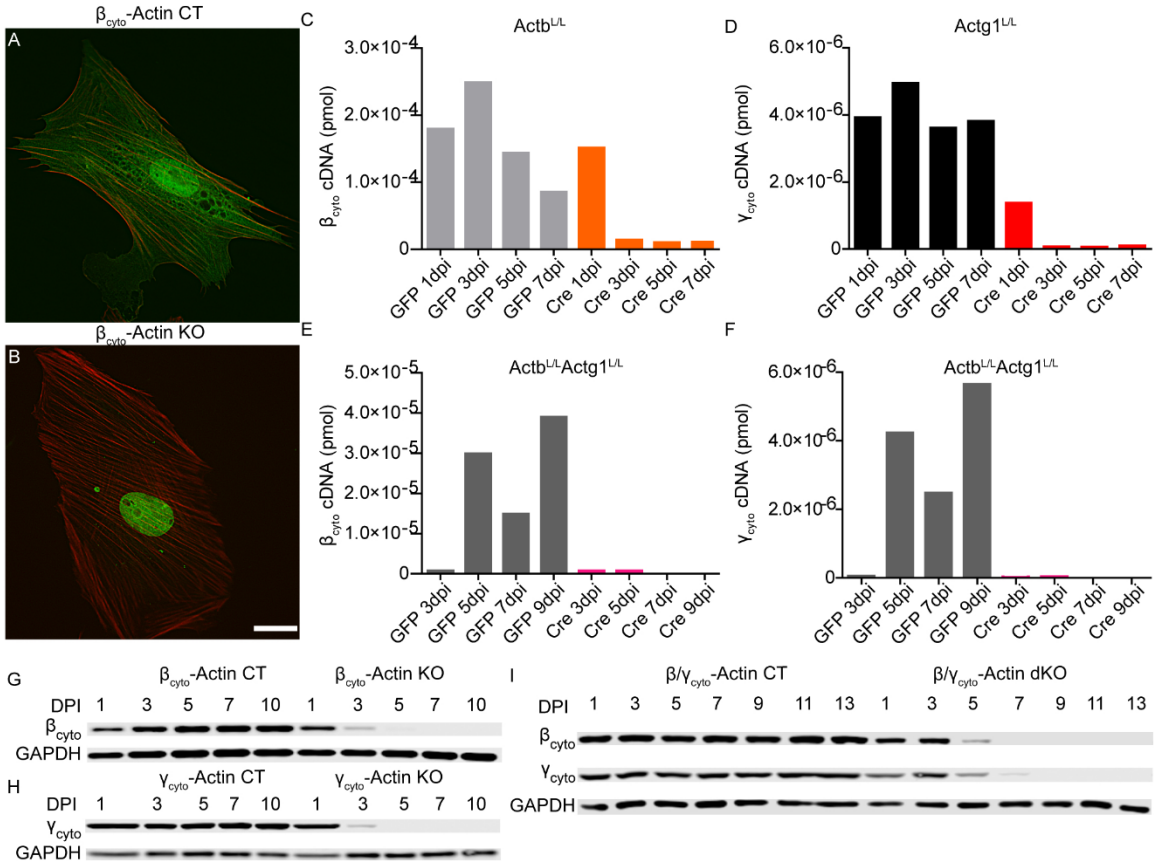

Figure 2-1 Adenoviral Cre efficiently ablated β_{cyto}- and γ_{cyto}-actin in primary mouse embryonic fibroblasts. (A, B) Representative images of β_{cyto}-actin CT and β_{cyto}-actin KO cells at 7dpi. Scale bar is 20 μm. (C-F) Representative qRT-PCR analysis of β_{cyto}- and γ_{cyto}-actin transcript amount (in pmol) in *Actb*$^{L/L}$, *Actg1*$^{L/L}$ and *Actb*$^{L/L}$ *Actg1*$^{L/L}$ MEFs. (G-I) Representative relative Western blot analysis of MEF lysates probed with β_{cyto}-actin and γ_{cyto}-actin antibodies; GAPDH served as loading control.

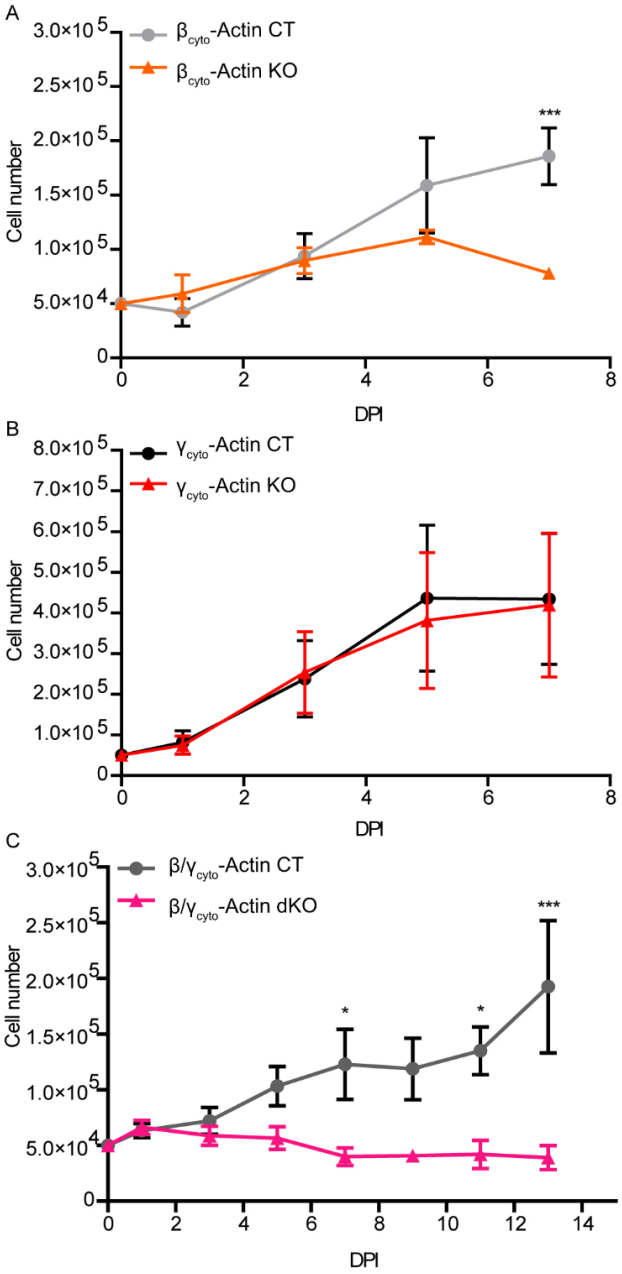

Figure 2-2 β_{cyto}-actin deficient MEFs were growth impaired. (A-C) Growth curve analysis of *Actb*$^{L/L}$, *Actg1*$^{L/L}$ and *Actb*$^{L/L}$*Actg1*$^{L/L}$ MEFs treated with either Ad5-GFP or Ad5-Cre (n=3, hand counted in duplicate). (B). Asterisks denote *P<0.05, *** P<0.001. (Two-way ANOVA with Bonferoni post-test, error bars are S.E.M.).

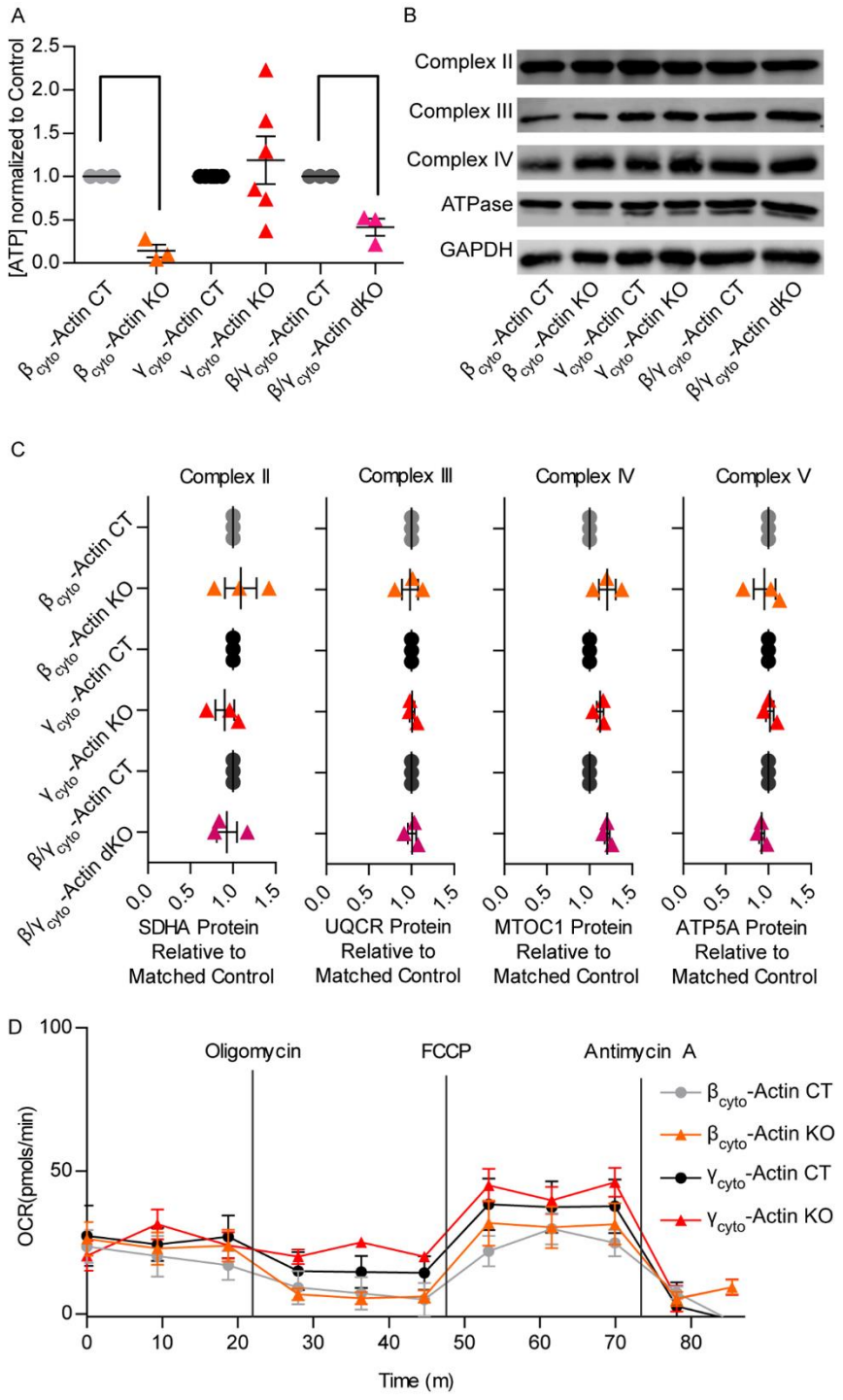

Figure 2-3 β_{cyto}-actin deficient MEFs displayed lower ATP levels but maintained ETC protein abundance. (A) ATP levels for CT and KO MEFs determined through a luciferase assay at 7dpi. Results were normalized to cell

number and relative to the paired embryo control (6≥n≥3). (B-C) Western blot and relative quantification of protein levels of Succinate Dehydrogenase Complex, Subunit A, Flavoprotein (SDHA) for Complex II; Ubiquinol-Cytochrome C Reductase Core Protein I (UQCR) for Complex III; Mitochondrially Encoded Cytochrome C Oxidase I (MTCO1) for Complex IV; and ATP5a ATP synthase, H+ transporting, mitochondrial F1 complex, alpha subunit (ATP5A) for the F1/F0 ATPase; GAPDH served as loading control. Levels were normalized to GAPDH and relative to the paired embryo control which was set at 1 (n=3). Asterisks denote **P<0.01, *** P<0.001. (One sample T-test, error bars are S.E.M.).

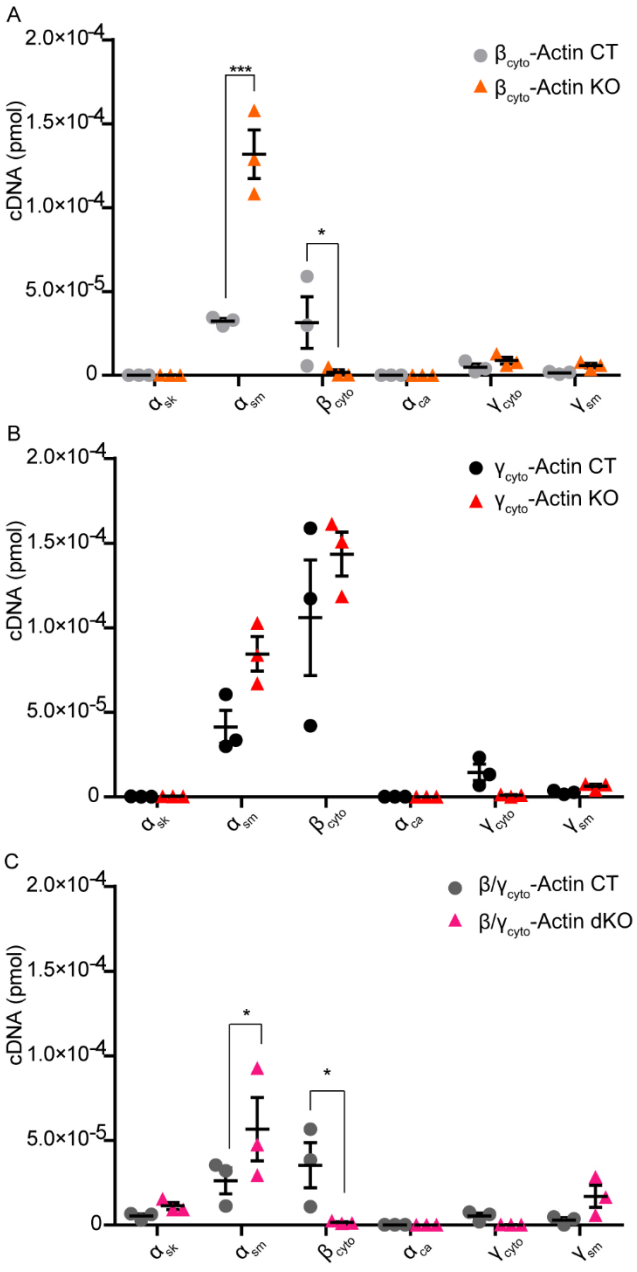

Figure 2-4 α_{sm}-actin transcript was upregulated in β_{cyto}-actin ablated MEFs.

(A-C) qRT-PCR analysis of six mouse actin isoforms in CT and KO MEFs at 5dpi (n=3, in triplicate). Calculated transcript amount (pmol) were calculated based on the standard curve, amplified in parallel. Asterisks denote *P<0.05, *** P<0.001 (Two-way ANOVA with Bonferoni post-test, error bars are s.e.m).

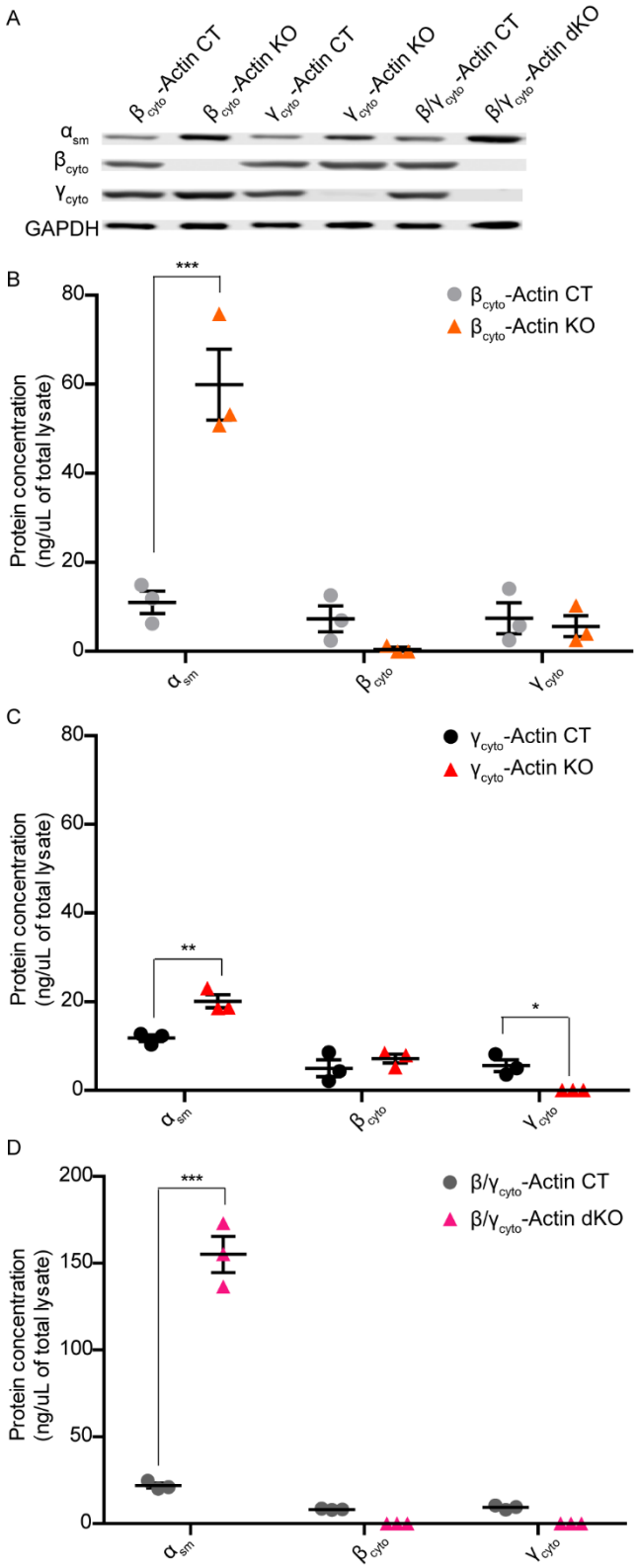
A
βcyto-Actin CT
βcyto-Actin KO
γcyto-Actin CT
γcyto-Actin KO
β/γcyto-Actin CT
β/γcyto-Actin dKO
αsm
βcyto
γcyto
GAPDH
B
***
βcyto-Actin CT
βcyto-Actin KO
Protein concentration (ng/uL of total lysate)
80
60
40
20
0
αsm
βcyto
γcyto
C
γcyto-Actin CT
γcyto-Actin KO
**
*
Protein concentration (ng/uL of total lysate)
80
60
40
20
0
αsm
βcyto
γcyto
D
***
β/γcyto-Actin CT
β/γcyto-Actin dKO
Protein concentration (ng/uL of total lysate)
200
150
100
50
0
αsm
βcyto
γcyto

Figure 2-5 α_{sm}-actin protein was upregulated in cytoplasmic ablated MEFs. (A) Representative Western blot of CT and KO MEF lysates blotted with α_{sm}-actin, β_{cyto}-actin and γ_{cyto}-actin antibodies; GAPDH served as loading control. (B-D) qWB analysis of CT and KO MEF lysates (n=3). Calculated protein concentrations (ng/µL of lysate) were determined based on the standard curve blotted in parallel. Asterisks denote *P<0.05, **P<0.01, and *** P<0.001. (Two-way ANOVA with Bonferoni post-test, error bars are S.E.M.).

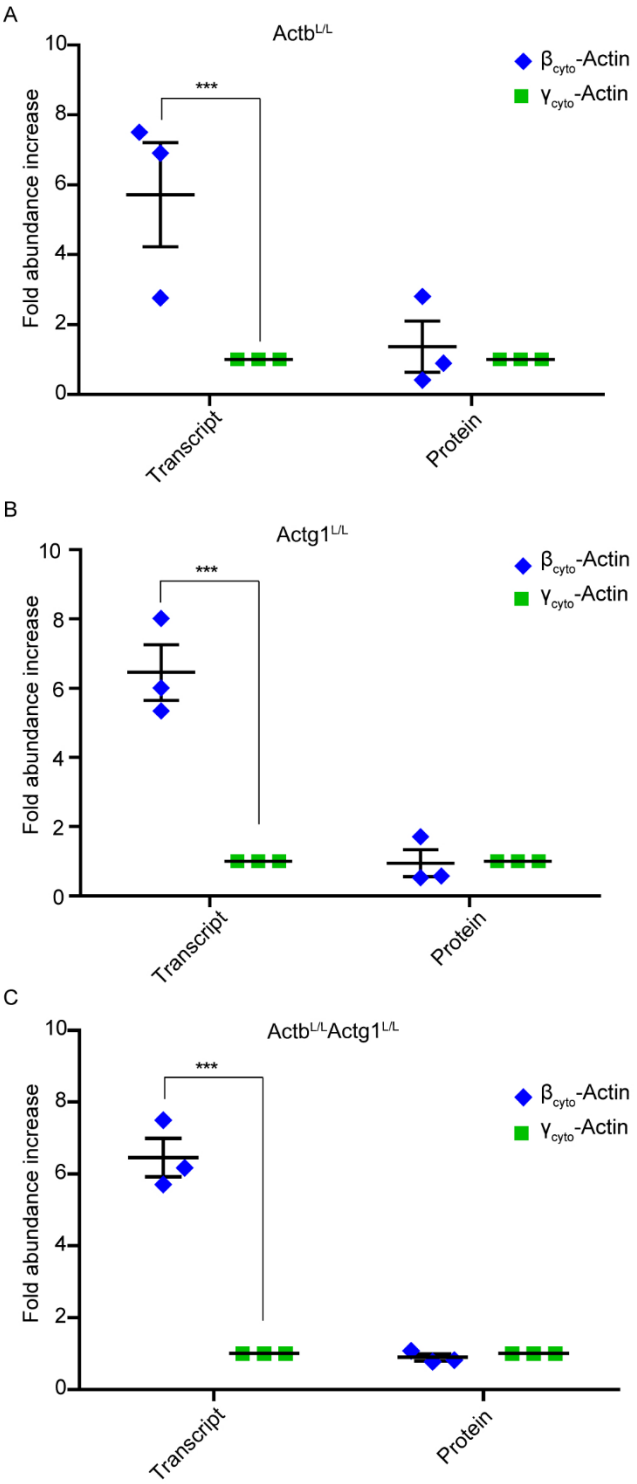
A
Actb$^{L/L}$
β_{cyto}-Actin
γ_{cyto}-Actin
Fold abundance increase
***
Transcript
Protein
B
Actg1$^{L/L}$
C
Actb$^{L/L}$Actg1$^{L/L}$

Figure 2-6 Unequal *Actb/Actg1* transcript and protein ratios in primary MEFs. (A-C) Calculated transcript and protein ratios between β_{cyto}- and γ_{cyto}-actin in CT MEFs (n=3). Calculations were based on the qRT-PCR and qWB data; γ_{cyto}-actin was set at 1. Asterisks denote *** P<0.001 (One sample T-test, error bars are S.E.M.).

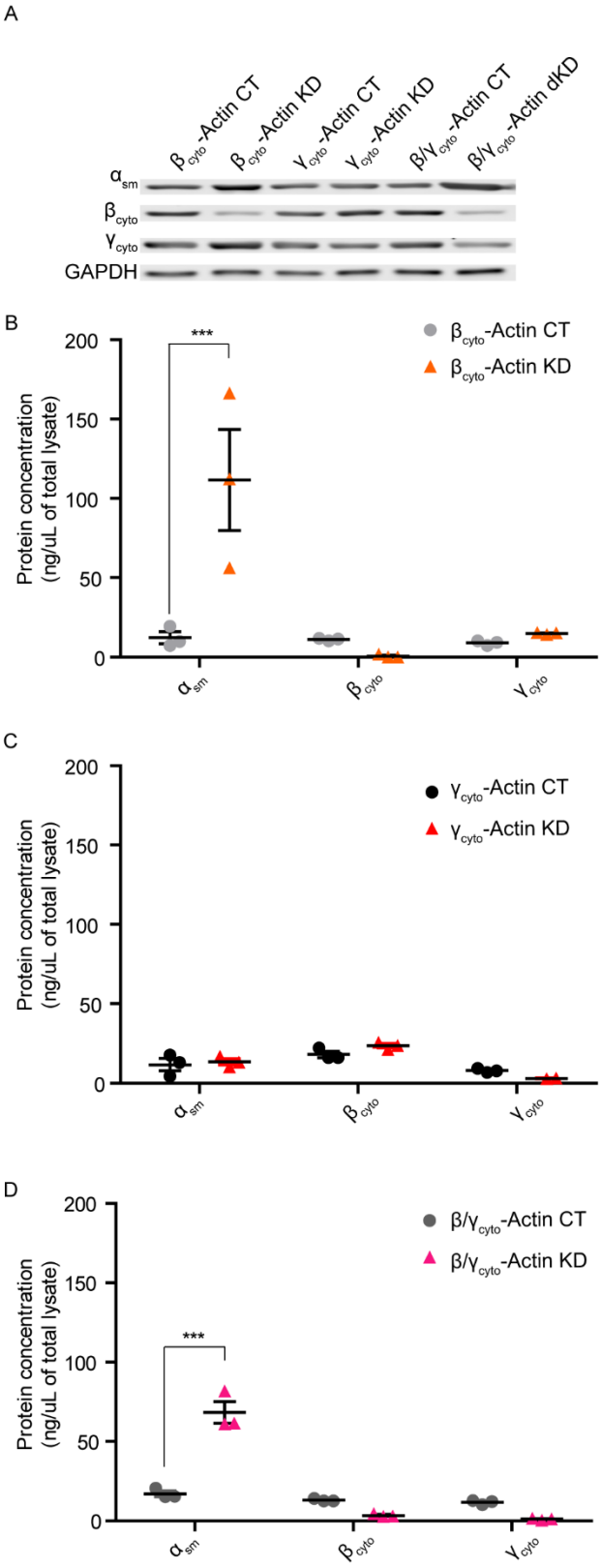
A
βcyto-Actin CT
βcyto-Actin KD
γcyto-Actin CT
γcyto-Actin KD
β/γcyto-Actin CT
β/γcyto-Actin dKD
αsm
βcyto
γcyto
GAPDH
B
βcyto-Actin CT
βcyto-Actin KD
***
Protein concentration (ng/uL of total lysate)
200
150
100
50
0
αsm
βcyto
γcyto
C
γcyto-Actin CT
γcyto-Actin KD
Protein concentration (ng/uL of total lysate)
200
150
100
50
0
αsm
βcyto
γcyto
D
β/γcyto-Actin CT
β/γcyto-Actin KD
***
Protein concentration (ng/uL of total lysate)
200
150
100
50
0
αsm
βcyto
γcyto

Figure 2-7 α_{sm}-actin protein was upregulated in siRNA mediated β_{cyto}-actin knocked-down MEFs. (A) Representative Western blot of CT and β_{cyto}- and/or γ_{cyto}-actin KD MEF lysates 3dpi for sKD and 4dpi for dKD blotted with α_{sm}-actin, β_{cyto}-actin and γ_{cyto}-actin antibodies; GAPDH served as loading control. (B-D) qWB analysis of control and KD MEF lysates (n=3). Calculated protein concentrations (ng/µL of lysate) were determined based on the standard curve, blotted in parallel. Triple asterisks denote $P<0.001$ (Two-way ANOVA with Bonferoni post-test, error bars are s.e.m).

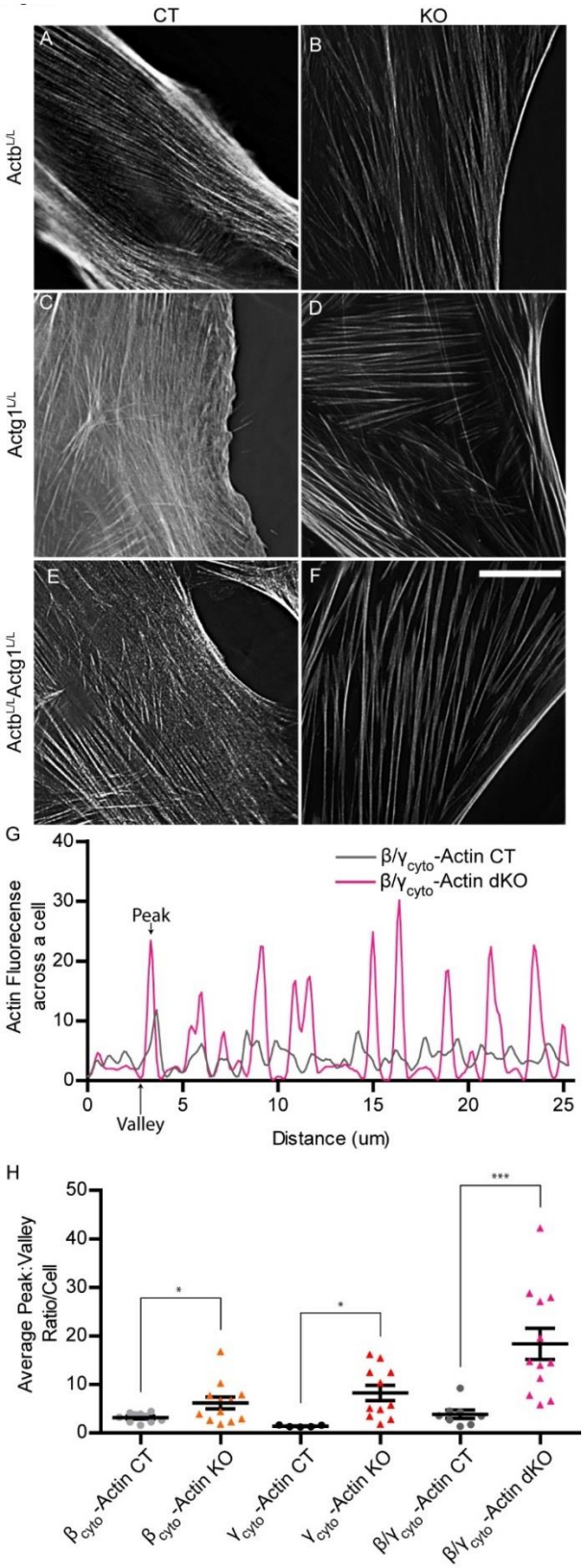
CT
KO
A
B
C
D
E
F
Actb$^{L/L}$
Actg1$^{L/L}$
Actb$^{L/L}$-Actg1$^{L/L}$
G
β/γ$_{cyto}$-Actin CT
β/γ$_{cyto}$-Actin dKO
Peak
Valley
Actin Fluorecense across a cell
Distance (um)
H
Average Peak:Valley Ratio/Cell
β$_{cyto}$-Actin CT
β$_{cyto}$-Actin KO
γ$_{cyto}$-Actin CT
γ$_{cyto}$-Actin KO
β/γ$_{cyto}$-Actin CT
β/γ$_{cyto}$-Actin dKO

Figure 2-8 β_{cyto}- and/or γ_{cyto}-actin ablated MEFs displayed increased stress fiber thickness. (A-F) Representative images of phalloidin stained actin filaments in Ad5-GFP or Ad5-Cre treated primary *Actb* $^{L/L}$, *Actg1* $^{L/L}$, and *Actb*$^{L/L}$*Actg1*$^{L/L}$ MEFs imaged at 7, 7, and 9 DPI respectively. Scale bar is 20 μm. (G) Representative line scans of actin fluorescence across the dKO cells shown in E and F. Arrows denote sample valley and peak. (H) Quantification of differences between valley:peak ratios for all genotypes (n≥8). Asterisks denote *P<0.05, **P<0.01 (Two-way ANOVA, error bars are S.E.M.).

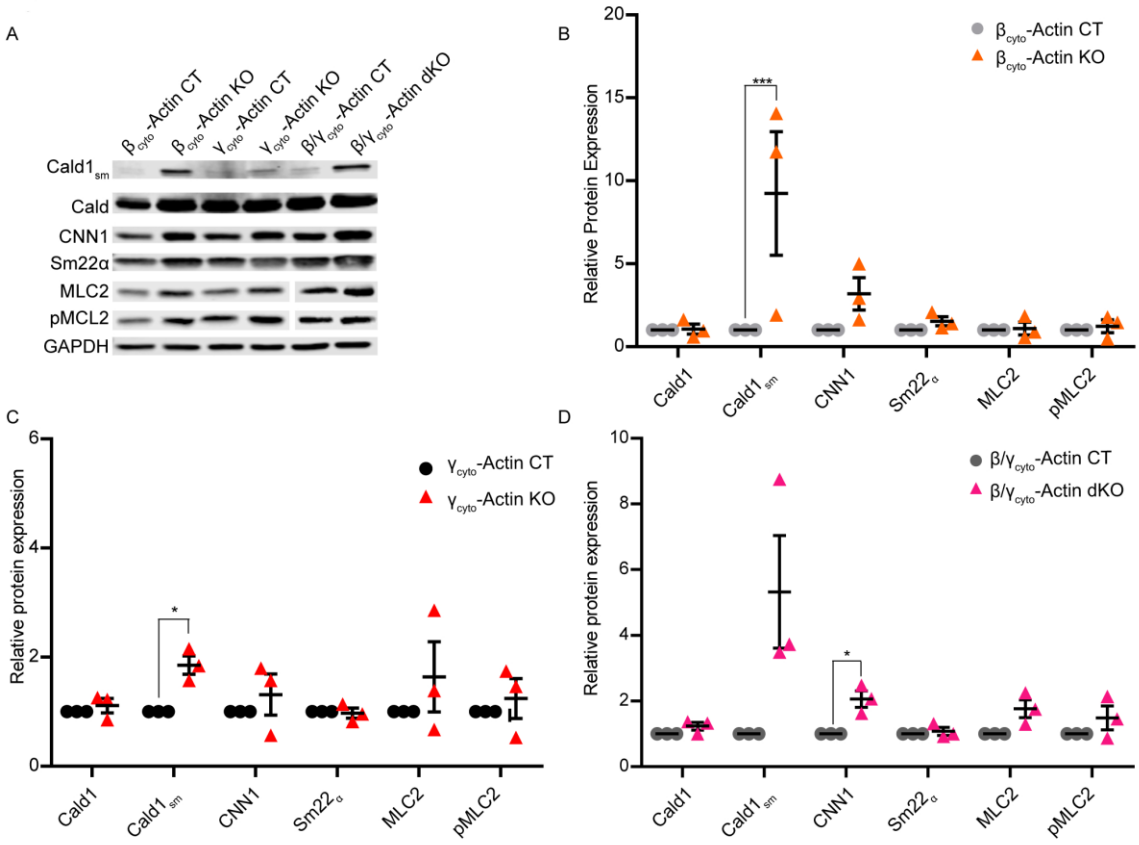

Figure 2-9 Caldesmon smooth muscle isoform protein expression was upregulated in β_{cyto}-actin deficient MEFs. (A) Representative Western blot analysis of CT and KO MEFs blotted with Cald, CNN1, and Sm22α, MLC2 and pMLC2; GAPDH served as loading control. (B-D) Relative protein expression were normalized to GAPDH and relative to the paired embryo control. Asterisks denote **P<0.01, *** P<0.001. (One sample T-test, error bars are S.E.M.).

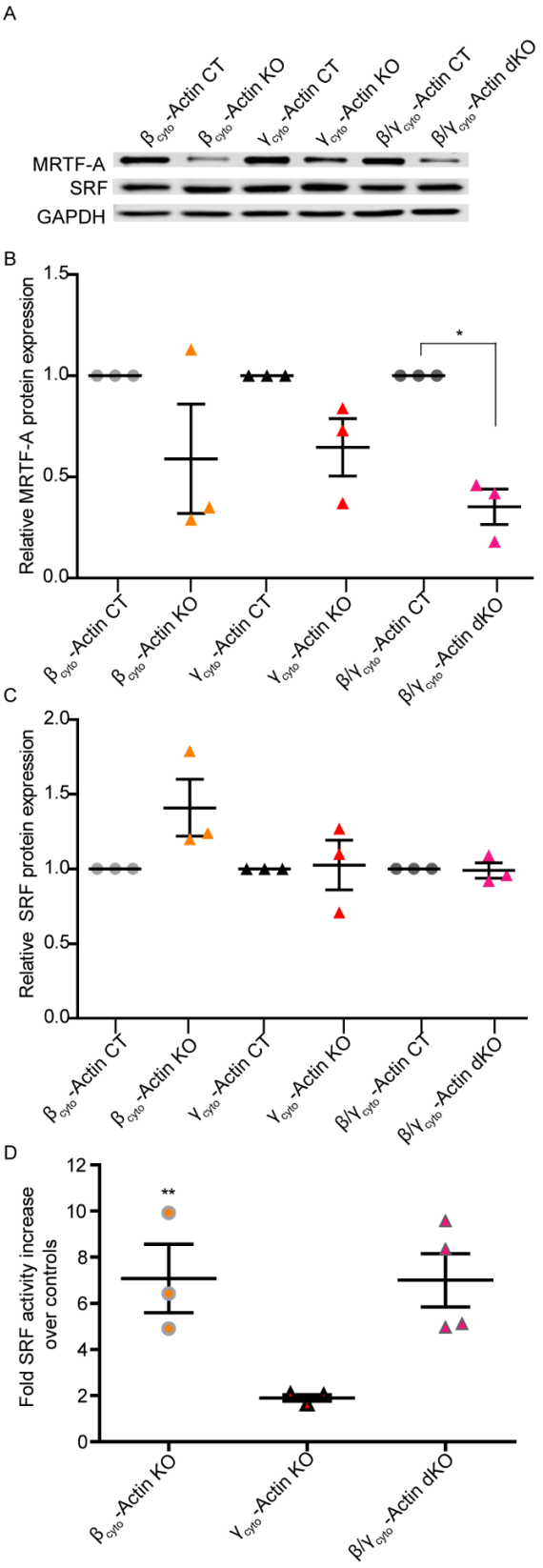
A
βcyto-Actin CT
βcyto-Actin KO
γcyto-Actin CT
γcyto-Actin KO
β/γcyto-Actin CT
β/γcyto-Actin dKO
MRTF-A
SRF
GAPDH
B
Relative MRTF-A protein expression
1.5
1.0
0.5
0.0
*
βcyto-Actin CT
βcyto-Actin KO
γcyto-Actin CT
γcyto-Actin KO
β/γcyto-Actin CT
β/γcyto-Actin dKO
C
Relative SRF protein expression
2.0
1.5
1.0
0.5
0.0
βcyto-Actin CT
βcyto-Actin KO
γcyto-Actin CT
γcyto-Actin KO
β/γcyto-Actin CT
β/γcyto-Actin dKO
D
Fold SRF activity increase over controls
12
10
8
6
4
2
0
**
βcyto-Actin KO
γcyto-Actin KO
β/γcyto-Actin dKO

Figure 2-10 SRF activity but not protein was upregulated in β_{cyto}-actin ablated MEFs. (A) Representative Western blot analysis of CT and KO MEFs blotted with MRTF-A and SRF; GAPDH served as loading control. (B-C) Relative protein expression was normalized to GAPDH and relative to the paired embryo control (n=3). (D) Calculated fold increase in SRF activity, via luciferase assay, in KO over CT MEFs (n=3). Asterisks denote **P<0.01 (One sample T-test, error bars are S.E.M.).

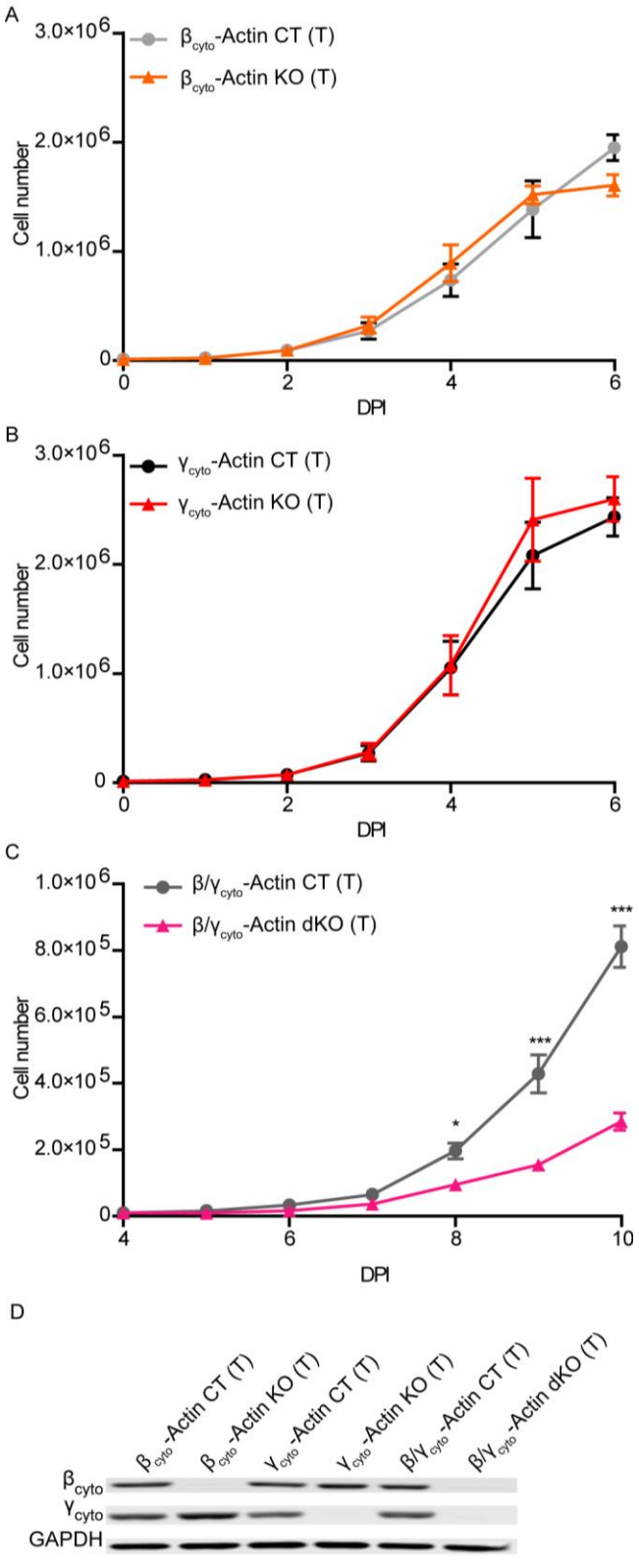
A
3.0×10^6
2.0×10^6
1.0×10^6
0
Cell number
β cyto -Actin CT (T)
β cyto -Actin KO (T)
0
2
4
6
DPI
B
3.0×10^6
2.0×10^6
1.0×10^6
0
Cell number
γ cyto -Actin CT (T)
γ cyto -Actin KO (T)
0
2
4
6
DPI
C
1.0×10^6
8.0×10^5
6.0×10^5
4.0×10^5
2.0×10^5
0
Cell number
β/γ cyto -Actin CT (T)
β/γ cyto -Actin dKO (T)
*
***
***
4
6
8
10
DPI
D
β cyto -Actin CT (T)
β cyto -Actin KO (T)
γ cyto -Actin CT (T)
γ cyto -Actin KO (T)
β/γ cyto -Actin CT (T)
β/γ cyto -Actin dKO (T)
β cyto
γ cyto
GAPDH

Figure 2-11 β_{cyto}-actin sKO SV40 LargeT antigen immortalized MEFs were not growth impaired. (A) Representative Western blot of SV40 LargeT antigen transformed (T) CT and KO MEF lysates blotted with α_{sm}-actin, β_{cyto}-actin and γ_{cyto}-actin antibodies; GAPDH served as loading control. (B-D) Growth curve analysis of SV40 LargeT antigen transformed (T) CT and KO MEFs (n=3, hand counted in duplicate). Asterisks denote *P<0.05, *** P<0.001. (Two-way ANOVA with Bonferoni post-test, error bars are S.E.M.).

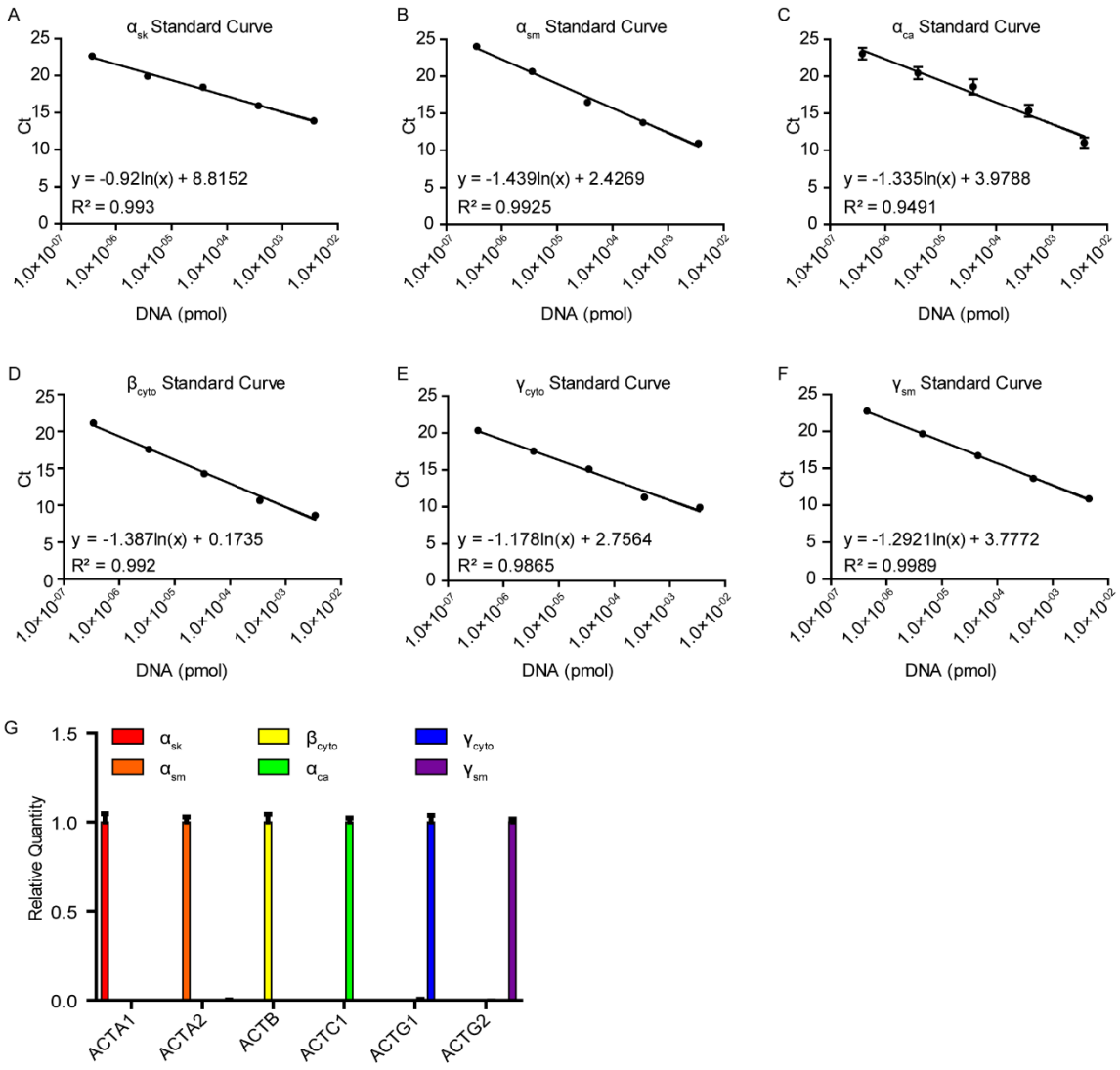

Figure 2-12 Mouse actin isoform standard curves and primer specificity analysis. (A-F) Representative standard curves generated using specific actin isoform primers with the corresponding control actin construct in a ten-fold dilution. (G) Representative graph of qRTPCR primer specificity. Each primer set was used to amplify all actin isoform control constructs to calculate relative quantity. Color bars represent individual actin isoform, y-axis denotes relative quantity, x-axis denotes primer set.

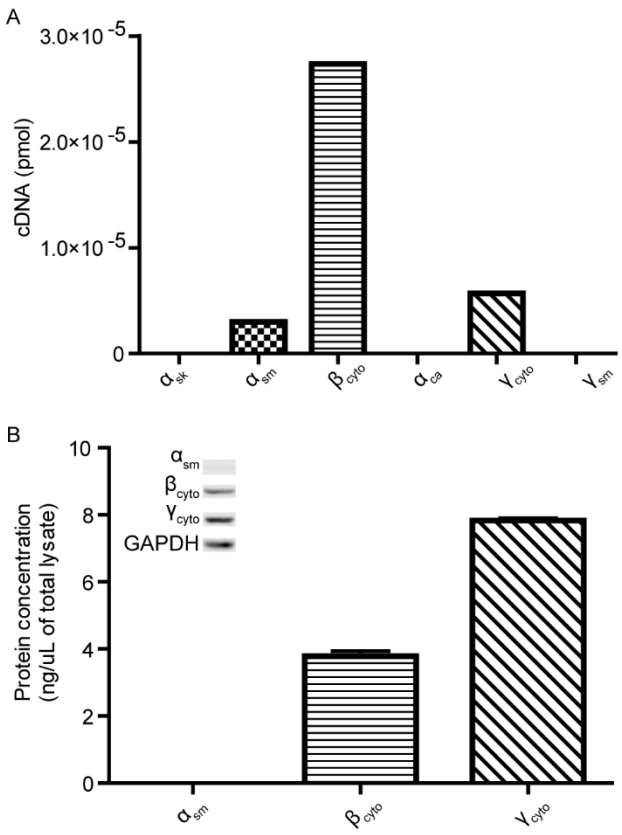

Figure 2-13 β_{cyto}- and γ_{cyto}-actin are the dominant actin isoforms in NIH3T3 fibroblast. (A) Actin isoform transcript profiling in NIH3T3 fibroblasts. Calculated transcript amount (pmol) were calculated based on the standard curve, amplified in parallel (n=1, in triplicate). (B) Representative Western blot of NIH3T3 fibroblast lysates blotted with α_{sm}-actin, β_{cyto}-actin and γ_{cyto}-actin antibodies; GAPDH served as loading control. Calculated protein concentrations (ng/μL of lysate) were determined based on the standard curve, blotted in parallel (n=1, in duplicate).

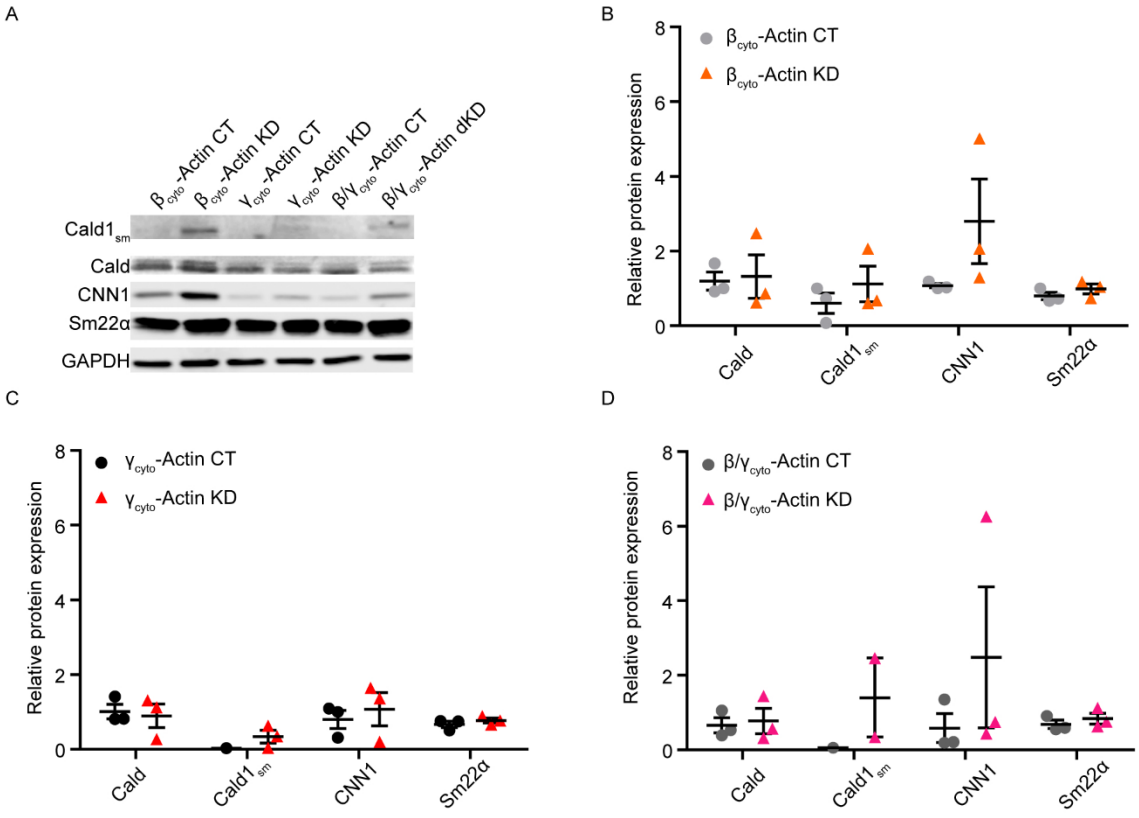

Figure 2-14 Cald1 and CNN1 protein expression are upregulated in β_{cyto}-actin siRNA KD MEFs. (A) Representative Western blot analysis of CT and KD MEFs at 3dpi for sKD and 4dpi for dKD blotted with Cald, CNN1, and Sm22α; GAPDH was used as loading control. (B-D) Relative protein expression were normalized to GAPDH and relative to the paired embryo control (n=3). (One sample T-test, error bars are S.E.M.).

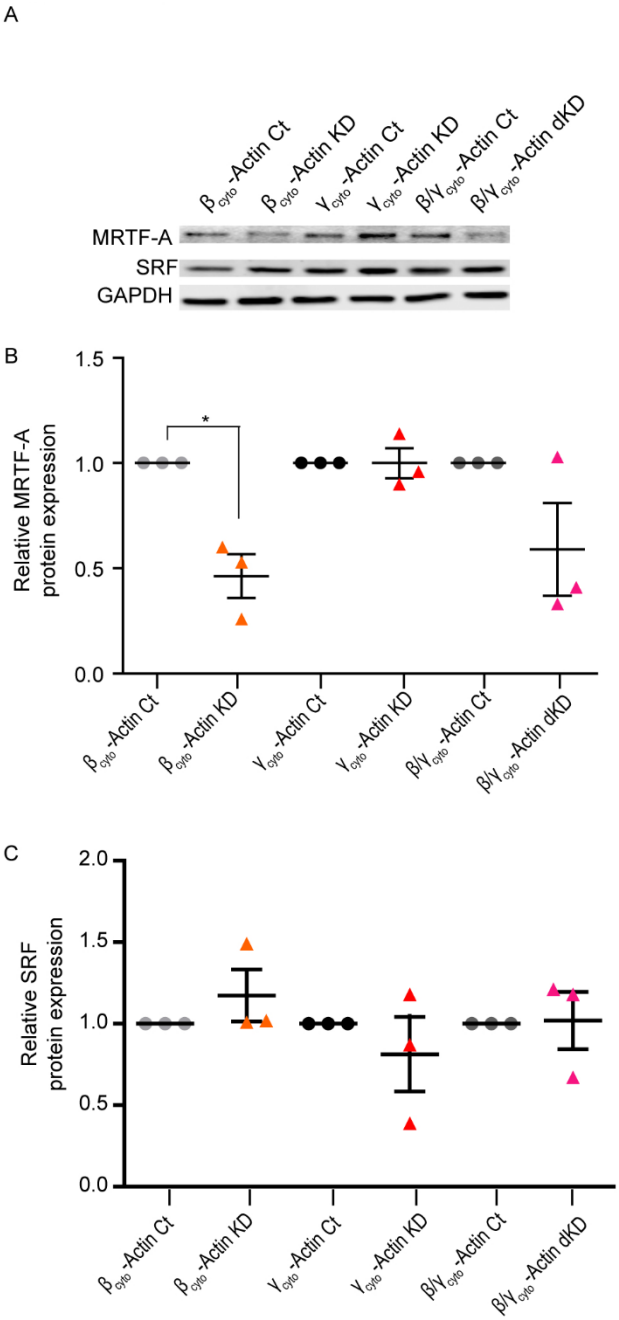

Figure 2-15 MRTF-A protein expression is down regulated ion β_{cyto}-actin KD MEFs. (A) Representative Western blot analysis of CT and KD MEFs at 3dpi for sKD and 4dpi for dKD blotted with MRTF-A and SRF; GAPDH served as loading control. (B) Calculated relative protein expression were normalized to GAPDH

and relative to the paired embryo control (n=3). Asterisk denotes *P<0.05 (One sample T-test, error bars are S.E.M.).

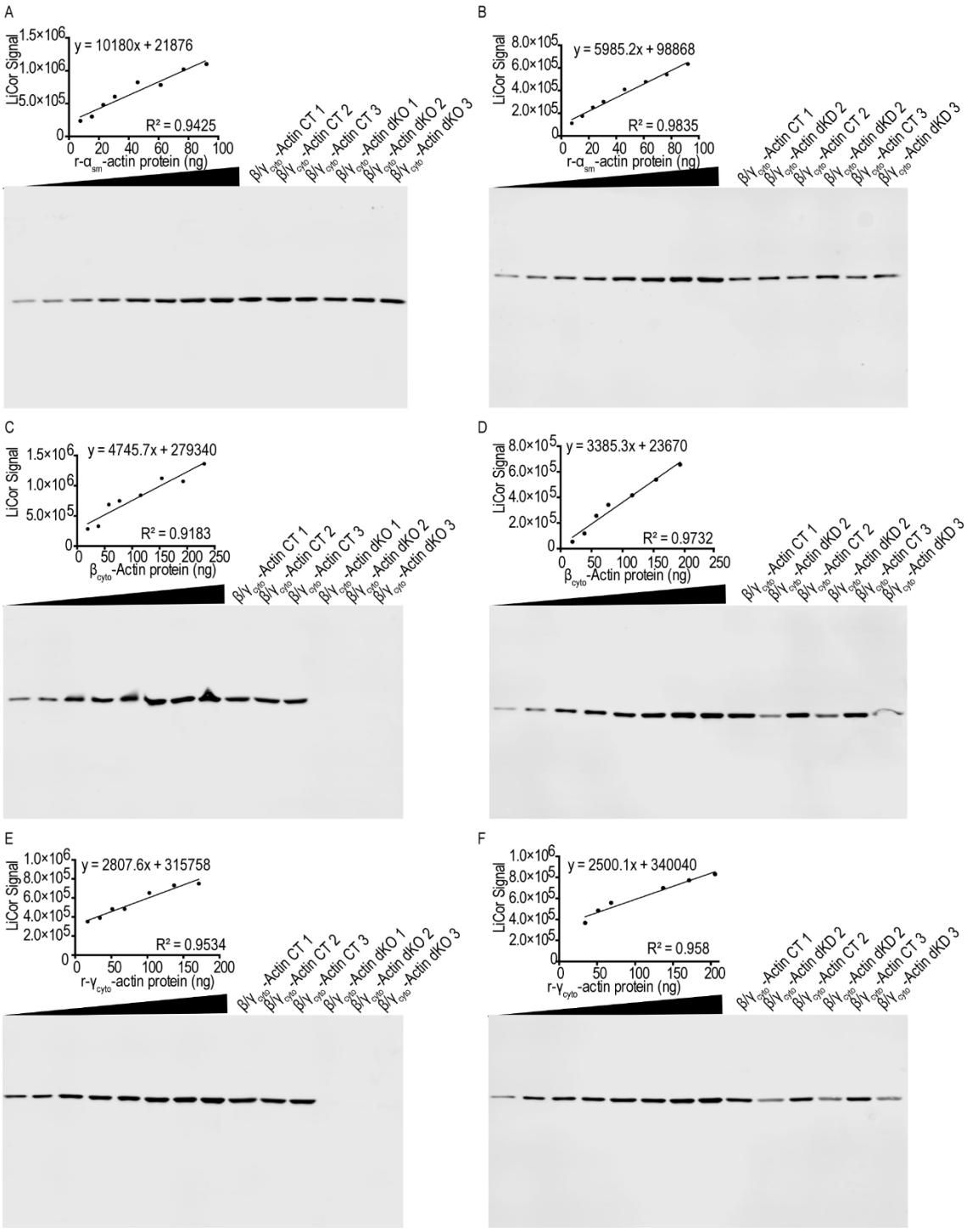

Figure 2-16 Representative quantitative Western blots. (A, C, E) β/γ_{cyto}-Actin CT and β/γ_{cyto}-Actin dKO, at 9dpi, from 3 separate embryos are blotted with α_{sm}-,

β_{cyto}- and γ_{cyto}-actin antibodies. (B, D, F) β/γ_{cyto}-Actin CT - and β/γ_{cyto}-Actin dKD, at 4dpi, from 3 separate embryos blotted with α_{sm}-, β_{cyto}- and γ_{cyto}-actin antibodies. For α_{sm}-actin Western blots, both KO and KD samples were diluted by at least 5-fold in order for the immune activity intensity to fit within the standard curve. An increasing amount of purified α_{sm}-, β_{cyto}- and γ_{cyto}-actins are blotted in parallel to generate a standard curve and used to calculate the amount of individual actin isoform in lysates.

Supplemental Methods

Primers

Gene	Forward Primer (5'→3')	Reverse Primer (5'→3')
mACTA1 Cloning	CACCTCACTTCCTACCCTCGGCA	GCAAAACAGAATGGCTGGCTT
mACTA2 Cloning	CACCGCTGCTCCAGCTATGTGTGA	ATCCATGCACGTGTGTATGCTTTA
mACTB Cloning	CACCGCGAGCACAGCTTCTTTG	AGGTAAGGTGTGCACTTTTATTGGT
mACTC Cloning	CACCCGCCTACAGAACCCACCAAA	TGCAAGTCCTGGTCTGGTTTA
m*ACTG1* Cloning	CACCCCGCCGCCGGCTTACAC	CAGTTACTGCAGCACTTTTATTTC
mACTG2 Cloning	CACCTTGCTCTGGTATTTCTGCCAA	GGTTTTAATGATCTGTGGCTGGTC
Note: CACC is added to all forward cloning primers in order to facilitate directional cloning into pDENTR vector, they are not part of the actin gene sequence.		
mACTA1 qRT	GCCAGCCTCTGAAACTAGACA	CCCACGATGGATGGGAACAC
mACTA2 qRT	TCCAGCTATGTGTGAAGAGGA	CCAACCATTACTCCCTGATGTCT
m*ACTB* qRT	GCGAGCACAGCTTCTTTG	TTTGCACATGCCGGAGCCGTT
mACTC qRT	GATGTGTGACGACGAGGAGA	ATACCCACCATGACACCCTGG
m*ACTG1* qRT	GATTAAGATCATTGCTCCCCCTGA	GCACCTGCTCAGTCCATCTA
mACTG2 qRT	ATGTGTGAAGAAGAGACCACCG	GCCCATTCCCACCATCACAC

ON-TARGET Plus siRNA Sequences

Control ON-TARGETplus Non-targeting Pool Cat# D-001810-10-05	5'-UGGUUUACAUGUCGACUAA-3' 5'-UGGUUUACAUGUUGUGUGA-3' 5'-UGGUUUACAUGUUUUCUGA-3' 5'-UGGUUUACAUGUUUUCUA-3'

βcyto-actin ON-TARGETplus Mouse *Actb* siRNA- SMARTpool Cat# L-057827-01-0005	5’-GCAAGUGCUUCUAGGCGGA-3’ 5’-UUUUAAAUCUUCCGCCUUA-3’ 5’-CCAAGUAUCCAUGAAAUAA-3’ 5’-GCAGUUGGUUGGAGCAAAC-3’
γcyto-actin ON-TARGETplus Mouse *Actg1* siRNA- SMARTpool Cat# L-042869-00-0005	5’-ACGCAGAUAAUGUUUGAAA-3’ 5’-CCUAGCACGAUGAAGAUUA-3’ 5’-AGAGGGAAAUUGUUCGUGA-3’ 5’-GCAUGGAGUCCUGUGGUAU-3’

Table 2-1 Predicted *Actb* and *Actg1* 3'UTR binding microRNAs

Mouse Actin Isoform	Target Scan	microRNA.org	PicTar	Consensus miRNA
ACTB	mir-1 mir-132 mir-145 mir-205 mir-206 mir-212 mir-212-3p mir-34a mir-34b mir-194 mir-613	mir-1 mir-1192 mir-1295p mir-132 mir-145 mir-194 mir-205 mir-206 mir-212 mir-495 mir-544 let-7a let-7b	mir-124a mir-145 mir-18a mir-18b mir-205	mir-145 mir-205
ACTG1	mir-103a mir-107 mir-10a mir-10b mir-10c mir-145 mir-31 mir-485	mir-103 mir-107 mir-10a mir-10b mir-145 mir-186 mir-199a mir-31 mir-361 mir-381 mir-615 mir-873	mir-10a mir-10b mir-145 mir-199a	mir-10a mir-10b mir-145

Supplemental table 1: Predicted *Actb* and *Actg1* 3'UTR binding microRNAs

Three miRNA prediction databases were used to analyzed possible miRNAs that target either/both *Actb* and *Actg1* 3'UTRs. Consensus miRNAs that were predicted in all databases are listed in the right column.

Chapter 3

Essential Nucleotide- and Protein-Dependent Functions of *Actb*/β-Actin

Xiaobai Patrinostro, Pallabi Roy, Angus Lindsey, Christopher M. Chamberlain, Lauren J. Sundby, Colby G. Starker, Daniel F. Voytas, James M. Ervasti and Benjamin J. Perrin

PNAS (Under review), 2018

Responsibilities:

X. Patrinostro designed experiments, analyzed data, written and edited the manuscript, and was responsible for data in figures 3-1 to 3-6, 3-9, and 3-12

P. Roy performed experiments, analyzed data, and was responsible for data in figures 3-7, 3-8, 3-10 and 3-11.

A. Lindsey performed all physiology experiments.

C.M. Chamberlain assisted in the open field activity assay.

L.J. Sundby assisted in gathering live cell imaging data and analyzed data.

C.G. Starker and D.F. Voytas designed and generated the TALENs.

J.M. Ervasti was involved in experimental design and manuscript editing.

B.J. Perrin designed experiments, analyzed data, written and edited the manuscript, and was responsible for data in figures 3-7, 3-8, 3-10 and 3-11.

Synopsis

The highly homologous cytoplasmic β- and γ-actins differ by only 4 functionally similar amino acids yet previous *in vitro* and *in vivo* data suggest they support unique functions due to striking phenotypic differences between *Actb* and *Actg1* null mouse and cell models. To determine if the 4 amino acid variances were responsible for the functional differences between cytoplasmic actin, we gene-edited the endogenous mouse *Actb* locus to translate γ-actin protein. Here we demonstrate that gene-edited mice and primary embryonic fibroblasts completely lacking β-actin proteins are viable and do not present with the most overt and severe cell and organismal phenotypes observed with gene knockout. Nonetheless, the edited mice exhibited progressive high frequency hearing loss and degeneration of actin-based stereocilia as previously reported for hair cell-specific *Actb* knockout mice. Thus β-actin protein is not required for general cellular functions, but is necessary to maintain auditory stereocilia.

Introduction

The actin cytoskeleton contributes to a wide range of cellular functions such as muscle contraction, cytokinesis, migration, chromatin remodeling, transcriptional regulation and regulating cell shape (Pollard and Cooper, 2009). Though often thought of as a single protein, there are actually six actin isoforms encoded by separate genes. Four actins are considered muscle specific while the cytoplasmic β- and γ-actin isoforms are ubiquitously expressed. The cytoplasmic actins are highly similar at the level of both gene and protein: the coding sequences of *Actb and Actg1* are 89% identical and β- and γ-actin differ at just 4 out of 375 amino acid residues. Furthermore, human and mouse *Actb* coding sequences are 90% identical and β- and γ-actin primary sequences are identical across birds and mammals. The fact that selective pressure has maintained these seemingly slight differences for hundreds of millions of years has confounded cell biologists since the cytoplasmic actins were initially cloned four decades ago: why do cells apparently require two such highly similar proteins?

Corresponding to the evolutionary conservation of β- and γ-actin, several lines of evidence demonstrate that both isoforms are required for normal cellular function. In humans, point mutations in *ACTB* and *ACTG1* cause a spectrum of developmental defects as well as progressive hearing loss, demonstrating lack of compensation between the isoforms. In mice, genetic ablation of each isoform results in different phenotypes. Loss of *Actb* results in embryonic lethality and severe cellular proliferation and migration defects in null fibroblasts, while *Actg1*

knockouts survive, though with decreased fitness (Bunnell and Ervasti, 2010; Bunnell *et al.*, 2011; Patrinostro *et al.*, 2017). Finally, ablation of each isoform in auditory sensory hair cells causes different patterns of progressive hearing loss and degeneration of actin-based protrusions (Perrin, Sonnemann and Ervasti, 2010).

The phenotypes arising from conventional gene knockout may result from loss of isoform specific transcript or protein. Most notably, the *Actb* transcript has a 3'UTR "zipcode" sequence not found in *Actg1* transcripts that targets the transcript to subcellular regions and regulates translation (Ross *et al.*, 1997; Zhang *et al.*, 2010). In addition, the transcripts differ in ribosome density and translation rate. On the protein level, purified β- and γ-actin have slightly different polymerization rates and differentially interact with a subset of actin binding proteins (Bergeron *et al.*, 2010). Considering that nucleotide and amino acid sequences are evolutionally maintained, both may contribute to critical cellular functions.

To separate the effects of non-coding regulation from differences in β- and γ-actin protein, we edited the *Actb* gene encoding β-actin to instead encode γ-actin while retaining all the endogenous *Actb* regulatory elements. We found the resulting mice, despite lacking β-protein, were born in Mendelian ratios and that the mice and derived fibroblasts appeared phenotypically normal. These results are in agreement with those of a recent study by Vedula *et al.*, 2017, who independently generated and characterized a nearly identical mouse model. Together these results demonstrate that the nucleotide sequence is a critical

determinant of actin isoform specific function. However, we also found that β-actin protein is required to maintain the shape and function of auditory hair cells, demonstrating that other functions of cytoplasmic actins are defined by their amino acid sequences.

Results

Generation of *Actb*$^{c\text{-}g}$ mice

We used transcription activator-like effector nucleases (TALENs) and a single-stranded oligo (ssOligo) donor template to edit the endogenous *Actb* locus within the mouse genome (Figure 3-1A). Of 11 live-born pups produced, restriction fragment length polymorphism (RFLP) analysis demonstrated that the ssOligo donor template was incorporated into one of the endogenous *Actb* loci of pup #9 (Figure 3-1B). Sanger sequencing confirmed that exon 2 in one allele of *Actb* in pup #9 was edited such that it encodes E2-4 and I10 of γ-actin protein and not D2-4 and V10 of β-actin (Figure 3-1C). We named the edited allele as *Actb*$^{c\text{-}g}$ for *Actb* coding gamma.

Actb$^{c\text{-}g}$ mice are born at Mendelian ratios and do not exhibit early lethality

Cre-mediated knockout of *Actb* results in embryonic lethality for homozygotes and decreased lifespan for heterozygotes (Bunnell *et al.*, 2011). In surprising contrast, both homozygous and heterozygous *Actb*$^{c\text{-}g}$ mice were visibly indistinguishable from WT. Offspring from heterozygous *Actb*$^{c\text{-}g}$ crosses were born at the expected Mendelian ratios and in litter sizes typical of the C57BL/6 strain (Figure 3-2A) (Silver, 2001). Homozygous *Actb*$^{c\text{-}g}$ mice grew at the same rate as WT littermates (Figure 3-2B), and neither heterozygous nor homozygous *Actb*$^{c\text{-}g}$ mice exhibited perinatal or early onset death out to six months of age (Figure 3-2C).

Actb$^{c\text{-}g}$ mice do not express β-actin protein but have a 2-fold increase in γ-actin protein expression

Cre-mediated ablation of β-actin leads to a significant compensatory upregulation of primarily α_{sm}-actin transcript and protein (Bunnell *et al.*, 2011; Tondeleir *et al.*, 2012; Patrinostro *et al.*, 2017). To determine if the edited *Actb*$^{c\text{-}g}$ mice also exhibit this compensatory response, we used qRT-PCR to measure transcript levels for all six WT actin isoforms and the edited *Actb*$^{c\text{-}g}$ transcript. The amount of transcript for each actin isoform in primary MEFs, brain and lung tissues were calculated from standard curves that were amplified in parallel (Patrinostro *et al.*, 2017, Figure 3-9). In all tissues tested, there is a dose response of decreasing WT β-actin transcript from WT, to heterozygous, to homozygous samples and an increasing amount of the edited *Actb*$^{c\text{-}g}$ transcript, indicating that *Actb*$^{c\text{-}g}$ transcript is synthesized from the edited *Actb* locus (Figure 3-3A-C). β-actin protein expression also progressively decreased from WT, to heterozygous and was absent in homozygous *Actb*$^{c\text{-}g}$, which correlated with increasing amounts of γ-actin protein expression (Figure 3-3D-I). α_{sm}-Actin protein expression was not significantly different between all samples tested (Figure 3-3D-I), suggesting the *Actb*$^{c\text{-}g}$ mice, although lacking β-actin protein, do not elicit a compensatory response by other actin isoforms. Interestingly, WT *Actg1* transcript is significantly decreased in the *Actb*$^{c\text{-}g}$ homozygous brain tissue and showed a decreasing trend in *Actb*$^{c\text{-}g}$ homozygous MEFs and lungs (Figure 3-3A-C). Thus, both cells and tissues appear to distinguish β- and γ-actin proteins, and downregulate transcription from the endogenous *Actg1* locus to

compensate for increased expression of γ-actin protein from the edited *Actb*$^{c\text{-}g}$ locus.

Actb$^{c\text{-}g}$ MEF cell proliferation and random migration rates are not different from WT

We immunostained *Actb*$^{c\text{-}g/c\text{-}g}$ and WT MEFs with antibodies that specifically detect β-actin and γ-actin. Consistent with expression of γ-actin from the *Actb*$^{c\text{-}g}$ locus, only γ-actin is detected in homozygous *Actb*$^{c\text{-}g}$ MEFs (Figure 3-4A). Previously we demonstrated that both tamoxifen-induced or adenoviral-cre mediated ablation of β-actin leads to significant cell proliferation defects in primary MEFs (Bunnell *et al.*, 2011; Patrinostro *et al.*, 2017), suggesting *Actb* is essential for cell viability. Here, we directly compared cell growth of WT, *Actb*$^{c\text{-}g}$ heterozygous and homozygous MEFs for 9 days in culture. Both heterozygous and homozygous *Actb*$^{c\text{-}g}$ MEFs displayed cell proliferation rates similar to WT MEFs (Figure 3-4B), indicating γ-actin protein is able to compensate for β-actin function in cell proliferation. β-actin has been suggested to be crucial for membrane protrusions at the leading edge of migratory cells (Pollard and Borisy, 2003; Artman *et al.*, 2014) and gene targeted β-actin null MEFs demonstrated significant migration defects when compared to WT (Bunnell and Ervasti, 2010). Therefore, we tested WT and *Actb*$^{c\text{-}g}$ homozygous MEFs random migration capabilities and found that *Actb*$^{c\text{-}g}$ homozygous MEFs displayed average velocity, linear distance, total distance and directionality persistence comparable to WT

MEFs (Figure 3-4C-F), which further suggests γ-actin is able to substitute for β-actin in cell migration.

Finally, actin exists both as a monomer (G-actin) and as filaments (F-Actin), and the G-to F-actin dynamic plays a key role in the serum response (SRF)/myocardin related transcription factor (MRTF) signaling pathway (Olson and Nordheim, 2010). Previously, cre-mediated β-actin knockout in primary MEFs caused a significant decrease in G-actin which correlated with altered gene expression (Bunnell and Ervasti, 2010). However, we found α_{sm}-, γ- and total actin G- to F-actin ratios were not altered in *Actb*$^{c\text{-}g}$ homozygous MEFs (Figure 3-4G, H). Expression of SRF and MRTF-A proteins were also not altered when compared to WT MEFs (Figure 3-4I, J). Overall, these results suggest that γ-actin and β-actin are functionally redundant for G-actin mediated regulation of gene expression.

Absence of myopathy or hyperactivity in *Actb*$^{c\text{-}g}$ homozygous mice

Because muscle-specific knockout of β-actin was previously associated with a mild quadricep myopathy (Prins *et al.*, 2011), we analyzed *Actb*$^{c\text{-}g}$ mice quadriceps for a skeletal muscle phenotype. At 6 months of age, quadriceps muscles from *Actb*$^{c\text{-}g}$ homozygous mice displayed no evidence of histopathology (Figure 3-5A-C). Furthermore, *Actb*$^{c\text{-}g}$ homozygous mice exhibited no defects in muscle contractile function (Figure 3-5D, Table 1). In contrast to CNS-*Actb* KO mice (Cheever *et al.*, 2012), *Actb*$^{c\text{-}g}$ homozygous mice also exhibited no evidence of hyperactivity in an Open Field assay (Figure 3-5E-F). Overall, these results

suggest γ-actin protein can compensate for the loss of β-actin protein in both skeletal muscle and the central nervous system.

Progressive hearing loss and stereocilia degeneration in *Actb*$^{c-g}$ mice

Auditory sensory hair cells have apical protrusions called stereocilia, which are formed from a core of bundled filamentous β-and γ-actin. Numerous stereocilia are arranged into a bundle with a precise, staircase like morphology such that its deflection by sound triggers mechanotransduction. The heights of stereocilia normally remain constant and their degeneration causes hearing loss. Previously it was shown that cre-mediated knockout of *Actb* resulted in progressive, high-frequency hearing loss (Perrin, Sonnemann and Ervasti, 2010) We therefore measured auditory brainstem responses (ABRs) to assess auditory function in *Actb*$^{c-g}$ mice. Defined frequency tones were played to anesthetized mice and the lowest sound level that elicited an ABR was defined as the threshold. At 6 weeks of age, control and *Actb*$^{c-g}$ mice had comparable thresholds, except at 32 kHz, the highest frequency tested, where *Actb*$^{c-g}$ mice had some hearing loss as demonstrated by their higher ABR threshold (Figure 3-6A). This high frequency hearing loss was more advanced by 6 months of age, with significant elevation of ABR thresholds at and above 16 kHz in *Actb*$^{c-g}$ mice as compared to control mice (Figure 6-6B).

We stained cochlear tissue with dye-conjugated actin isoform specific antibodies to assess the distribution of β-actin in hair cell stereocilia. There are

two types of hair cells in mammalian cochlea, inner hair cells (IHCs) and outer hair cells (OHCs). Both cell types are mechanotransductive, but have different stereocilia morphologies. To better understand the role of β-actin in stereocilia length regulation, we compared its localization in wild type C57Bl/6 hair cells at P7 when bundles are developing and P21-P40 when bundles are mature. β-actin and γ-actin colocalized in developing OHC stereocilia, while in mature OHC stereocilia β-actin was reduced at tips and γ-actin was markedly enriched (Figure 3-7A-B). IHC stereocilia showed a similar trend, although in this cell type β-actin was slightly enriched at tips during development, and this enrichment was reduced in mature stereocilia such that β- and γ-actin colocalized (Figure 3-7C-D). As expected, β-actin was not detected in *Actb*$^{c\text{-}g}$ stereocilia (Figure 3-10). Thus, increased levels of β-actin at stereocilia tips correlates with growth.

The morphology of stereocilia bundles is closely associated with their mechanotransductive function. We used scanning electron microscopy (SEM) to examine OHC stereocilia from the middle turn of the cochlea, which corresponds to the frequency range where ABR thresholds in *Actb*$^{c\text{-}g}$ mice are normal at 6 weeks of age, but elevated at 6 months of age. Six-week-old control and *Actb*$^{c\text{-}g}$ mice had OHC bundles that appeared normal, featuring similar numbers of stereocilia that were of similar height (Figure 3-8A, C-D). In contrast, at 6 months of age, the mechanotransducing stereocilia in *Actb*$^{c\text{-}g}$ mice had started to degenerate and were shorter and fewer in number than in control OHCs. In addition, some OHCs were missing in *Actb*$^{c\text{-}g}$ mice, suggesting an increase in cell

death (Figure 3-8B, C-D). Towards the base of the cochlea where higher pitch sounds are detected, a similar phenotype was observed in *Actb*$^{c\text{-}g}$ OHC stereocilia at 6 weeks of age (Figure 3-11). Together, these data suggest that *Actb*$^{c\text{-}g}$ mechanotransducing OHC stereocilia selectively and progressively degenerate, leading to cell death and hearing loss. Notably, this pattern of hearing loss and stereocilia degeneration is similar to that previously observed in hair cell specific *Actb* knockout mice (Perrin, Sonnemann and Ervasti, 2010; Perrin *et al.*, 2013), demonstrating that this protein isoform is required for stereocilia length maintenance.

Discussion

To distinguish the relative contributions of nucleotide and amino acid sequences to the unique functions of closely-related cytoplasmic actins, we used TALENs to engineer the endogenous *Actb* gene to express γ-actin instead of β-actin. This approach edited only the nucleotides required to substitute the β-actin N-terminal amino acids D2-4, and V10 for γ-actin residues E2-4, and I10. The resulting mice and cells, which produce no β-actin protein, lacked the most severe and overt phenotypes of previously characterized *Actb* knockouts. These findings demonstrate that many functions of the highly conserved and expressed *Actb* gene reside in the nucleotide sequence and do not depend on the protein sequence. However, homozygous $Actb^{c\text{-}g}$ mice did develop progressive hearing loss due to degeneration of actin-rich protrusions on sensory cells. Therefore, β-actin protein has functions in some specialized cell types that cannot be compensated for by γ-actin.

A recent study using clustered regularly interspaced short palindromic repeats (CRISPR)/Cas9 methodology also edited the endogenous *Actb* locus to express γ-actin protein (Vedula *et al.*, 2017), and the resulting mouse line is nearly identical to the one we independently generated and characterized here. Several of the same phenotypes were assessed, and very similar results were obtained. In particular, $Actb^{c\text{-}g}$ mice are viable and appear to develop normally without evidence of premature mortality (Figure 3-2, Vedula *et al.*, 2017). In addition, $Actb^{c\text{-}g}$ MEFs also have proliferation and migration rates similar to WT (Figure 3-4, Vedula *et al.*, 2017). We further show that $Actb^{c\text{-}g}$ muscle viability

and physiology, as well as the activity level of the mice, was comparable to wild type. Overall, these two independent studies are highly consistent and support the major finding that β-actin protein is dispensable for most cellular functions.

The *Actb* gene-edited mice (herein, Vedula *et al.*, 2017) contrast with conventional cre-mediated knockout of a floxed *Actb* allele, where exons 2 and 3 were deleted, and which caused embryonic lethality in mice (Bunnell and Ervasti, 2010). Tissue specific knockout of the same allele also resulted in a variety of phenotypes with muscle showing progressive myofiber degeneration/regeneration, muscle weakness, impaired mitochondrial fission (Prins *et al.*, 2011; O'Rourke *et al.*, 2017), and the CNS showing tissue morphology defects that correlated with hyperactivity and cognitive behavior impairments (Cheever *et al.*, 2012). Additionally, isolated MEFs failed to divide or migrate, suggesting β-actin was required for fundamental cellular processes (Bunnell and Ervasti, 2010; Patrinostro *et al.*, 2017). None of these phenotypes were observed in $Actb^{c\text{-}g}$ mice. It is possible that some of the phenotypes observed following cre-mediated deletion of *Actb* exons 2-3 are independent of normal *Actb* function. For example, there may be an essential element in the intervening intron. It is also possible that recombination produces toxic transcript and/or truncated protein. However, differences between cre-mediated knockouts and $Actb^{c\text{-}g}$ mice most likely suggest that regulatory information embedded in the nucleotide sequence is critical, as this would be altered in the *Actb* floxed knockout but not in the $Actb^{c\text{-}g}$ mice.

A well-established difference between *Actb* and *Actg1* gene and transcript is the *Actb* zipcode, which is conserved from birds to mammals (Artman *et al.*, 2014). ZBP1 binds to this sequence to regulate both transcript localization and translation of β-actin (Ross *et al.*, 1997). Consistent with well-regulated temporal and spatial β-actin protein translation, *Actb* transcript is more abundant than *Actg1* transcript in primary MEFs even when β- and γ- actin protein levels are similarly expressed (Patrinostro *et al.*, 2017). Based on (Vedula *et al.*, 2017) and our findings that the 4 amino acid variances between β- and γ- actin protein are not critical to most cellular functions, it seems likely that transcript targeting and regulated translation via the zipcode is the essential feature of *Actb*. A similar gene-editing approach can potentially address the importance of the *Actb* zipcode *in vivo*.

While β-actin protein is not essential to the function of many cell types, some tissues nonetheless seem to specifically detect and regulate the levels of β- and γ-actin. As $Actb^{c\text{-}g}$ transcript increased in heterozygous and homozygous brain tissue, the level of γ-actin protein increased as it was produced both from the engineered *Actb* locus and the endogenous *Actg1* locus. (Figure 3-3A-C). Interestingly, as γ-actin protein concentration increased, the amount of transcript from the endogenous *Actg1* alleles decreased. In $Actb^{c\text{-}g}$ cells, as well as in most cells and tissues where *Actb* or *Actg1* were knocked out, total actin protein levels remained constant across all genotypes even as transcript levels varied (Bunnell and Ervasti, 2010; Bunnell *et al.*, 2011). Thus, most cell and tissue types appear to maintain actin homeostasis via a protein-based feedback mechanism.

Clinically, spontaneous missense mutations in both *Actb* and *Actg1* have been associated with Baraitser-Winter syndrome, a rare disease with complex phenotypes including facial dysmorphism, learning disabilities and deafness (Troys, 2015). The mutations affect the polymerization properties of actin or interaction with actin binding proteins to cause a gain-of-function or a dominant-negative effect. Interestingly, the more severe forms of Baraitser-Winter syndrome are associated with mutations in *Actb* over *Actg1* (Di Donato *et al.*, 2014). More recently, nonsense and frameshift mutations in *Actb* were identified in the human population (Cuvertino *et al.*, 2017) that caused loss-of-function mutations and resulted in phenotypes such as developmental delay, intellectual disability, internal organ malformations, hearing loss and facial malformations distinct from Baraitser-Winter syndrome (Cuvertino *et al.*, 2017). Patient derived fibroblasts and lymphoblastic cell lines displayed abnormal cell morphology, reduced migration rates and altered expression of cell-cycle genes, suggesting *Actb* haploinsufficiency (Cuvertino *et al.*, 2017). Although it is unclear the exact cause of the phenotypic variations in these patients, it does suggest a full dose of full-length β-actin is important to human health and development.

Although β-actin protein seems to be dispensable for many general cellular functions, we show here that it is clearly required for maintenance of auditory hair cell stereocilia, which may relate to deafness observed in human patients. We observed that β-actin is enriched at the tips of developing stereocilia when they are growing, and that β-actin is displaced from stereocilia tips by γ-actin in mature stereocilia that have achieved their full length. The

preferential localization of β-actin to growing tips suggests that it contributes to stereocilia elongation, which is consistent with the faster polymerization rate of calcium bound β-actin compared to γ-actin (Bergeron *et al.*, 2010).

Actb$^{c\text{-}g}$ hair cells, like cre-mediated *Actb* knockout hair cells characterized previously, have a particular pattern of degeneration where the shorter rows of the bundle shorten irregularly as mice age, but the tallest row of the bundle is largely unaffected (Perrin, Sonnemann and Ervasti, 2010). Interestingly, a similar phenotype is observed when the hair bundle mechanotransduction apparatus is disrupted. During aging, damage to this apparatus seems to result in cycles of stereocilia shortening and regrowth (Narayanan *et al.*, 2015). The progressive degeneration of row 2 and 3 stereocilia in aging *Actb*$^{c\text{-}g}$ mice suggests that β-actin is required to drive efficient stereocilia regrowth, which is necessary to maintain stereocilia length and auditory function.

Beyond the polymerization properties of actin itself, multiple actin binding proteins may also differentially interact with β- and γ-actin. For example, non-muscle myosinIIa and myosinVIIa both exhibit higher ATPase activity with γ-actin filaments (Müller *et al.*, 2013). MyosinVIIa is a particularly interesting candidate for mediating actin isoform specific effects since it is also localized to stereocilia. Finally, based on photoactivation and modeling, β-actin but not γ-actin was shown to depend on the actin filament severing protein cofilin to maintain the concentration of monomeric actin (Kapustina, Read and Vitriol, 2016). Although we did not see a change in G-actin:F-actin ratio in *Actb*$^{c\text{-}g}$ MEF

cell lysates using a biochemical fractionation method, it is possible that a spatially restricted effect may impact stereocilia length. Consistent with this idea, we previously found that mice lacking actin depolymerizing factor (ADF), which is closely related to cofilin (Narayanan *et al.*, 2015), phenocopy the pattern of stereocilia degeneration seen in *Actb*$^{c\text{-}g}$ mice.

Regardless of the mechanism by which β-actin protein contributes to stereocilia maintenance, this isoform has a cellular function that is not met by γ-actin protein. Therefore, it is likely that other cell types also depend on β-actin protein to form or maintain specialized features. However, this scenario is considerably less common than previously appreciated and, in agreement with Vedula *et al.*, 2017, we conclude that the nucleotide sequence rather than amino acid sequence determines the majority of the divergent phenotypes previously associated with *Actb* gene disruption.

Methods

Cell Culture: Primary MEFs were cultured from E13.5 WT, *Actb*$^{c\text{-}g}$ heterozygous and homozygous mouse embryos as described previously (Bunnell and Ervasti, 2010). Cells were grown to 80% confluency on 10-cm plates and frozen down at passage 1 at 1x10^6 cells/mL in MEF freezing media (95% FBS and 5% dimethyl sulfoxide). Primary MEFs from individual embryos were thawed and cultured in MEF media (DMEM supplemented with 10% FBS, 1% Pen/Strep, 0.5ug/mL Fungizone), grown to 80% confluency. NIH3T3 fibroblasts were cultured in 3T3 media (DMEM supplemented with 10% BS, 1% Pen/Strep, 0.5ug/mL Fungizone).

TALEN construction and purification: TALEN constructs were generated using the Golden Gate TALEN assembly method (Cermak *et al.*, 2011) into RCIscript-GoldyTALEN backbone (Addgene #38142, Carlson *et al.*, 2012). TALEN DNA constructs were transformed into DH5α cells, miniprepped with Wizard ® *Plus* SV Minipreps DNA Purification System (Promega, Cat. #A1460), linearized with the BamHI restriction enzyme (New England Biolabs Inc. Cat. #R3136S), and then phenol/chloroform purified. TALEN RNAs were *in-vitro* transcribed from purified linearized DNA using the mMESSAGE mMACHINE® T3 Transcription Kit. (Thermo Fisher Scientific, Cat. #AM1348) and then purified using the MEGAclear™ Kit. (Thermo Fisher Scientific, Cat. #AM1908M) following manufacture protocols. Purified RNAs were stored at -80°C until use. Please see supplemental methods for full TALEN RVDs sequences.

Generating genome engineered mice and validation:

TALEN RNA pairs (25ng/µL) and the corresponding Exon 2 PAGE Ultramer ssOligo donor (15ng/µL) template (Integrated DNA Technologies) were sent to the Murine Genetics Core at The Scripps Research Institute for pronuclear microinjection into fertilized C57BL/6 blastocysts, which were then implanted into pseudo-pregnant female mice. The donor template contained 8 nucleotide alterations to exchange the translation of β-actin D2-4, V10 to the γ-actin E2-4, I10, to disrupt TALEN re-binding to the edited locus, and to insert a BamHI site for restriction fragment length polymorphism (RFLP) analysis. Genomic DNA from all F0 mouse pup tail samples was purified (PureLink® Genomic DNA Mini Kit) and assessed by RFLP assay with the BamHI restriction enzyme (New England Biolabs Inc. Cat. #R3136S) and Sanger sequenced for donor template integration. Primers used for RFLP: *Actb* Exon2 F 5'-GGTAATAATGCGGCCGGTCT-3', *Actb* Exon2 R 5'-TACCCGGGATACTGACCTGG-3'.

Open Field Activity Assay:

Activity was measured using an AccuScan system by Columbus Instruments, Inc. Total horizontal distance (meters) was determined by measuring infrared beam breaks. Mice were placed in the open-field apparatus and horizontal distance was measured for 15 minutes.

Muscle histology and physiology

Quadriceps muscles from each mouse line were cryopreserved in melting isopentane for 30 seconds and 10 µm transverse cryosections were obtained (Leica CM3050 S). For histology, sections were stained with hematoxylin and eosin and imaged on a Leica DM5500 B microscope equipped with a Leica HC PLAN APO 20x objective. Centrally nucleated fibers (CNFs) were counted using the Cell Counter plugin on ImageJ software (NIH) and expressed as a percentage of the total number of myofibers (%CNFs). For *ex-vivo* force analysis, mice were anesthetized with sodium pentobarbital and extensor digitorum longus (EDL) muscles dissected. Silk suture was used to attach the distal tendon to a static structure and the proximal tendon to a force transducer (Model 300B-LR, Aurora Scientific). The EDL was incubated in Krebs-Ringer bicarbonate buffer [120.5 mM NaCl, 4.8 mM KCl, 1.2 mM $MgSO_4$ 1.2 mM Na_2HPO_4, 20.4 mM $NaHCO_3$, 10 mM glucose, 10 mM pyruvate, 1.5 mM $CaCl_2$], oxygenated with 95% O_2/5% CO_2. Muscles were set to their anatomic length (L_o) which was measured from myotendonous junction to myotendonous junction using digital calipers. Muscles remained quiescent for 5 min before passive stiffness was determined by passively stretching the muscles sinusoidally from 97.5% L_o to 102.5% L_o at 0.5 Hz while measuring the resulting force. Isometric tetanic contractions separated by 2 min followed 30s later until a plateau was attained (within 5 mN) and –dP/dt and +dP/dt were measured. EDL muscles were stimulated for 200 ms at 175 Hz. Peak twitch force was then measured 2 min later using a 0.5 ms pulse at 150 V (Grass S48 stimulator delivered through a

SIU5D stimulus isolation unit; Grass Telefactor, Warwick, RI) before active stiffness was calculated using a sinusoidal length oscillation of 0.01% at 500 Hz during a tetanic isometric contraction(Stein and Gordon, 1986; Gordon and Stein, 1988). Two minutes later, the muscle completed 10 eccentric contractions in which muscles were passively shortened to 90 % L_o and then stimulated for 200ms while being simultaneously lengthened to 110 % L_o at 1.0 L_o/s. Each eccentric contraction was separated by 3 min of rest to prevent fatigue. Immediately following the 10^{th} contraction, muscles were readjusted to L_o before a post P_o was measured and compared to pre P_o as a percentage.

Primary MEFs fixation, staining and immunofluorescent imaging

MEFs were plated on 5 µg/ml fibronectin coated coverslips at a density of 1×10^4 cells/coverslip and incubated in MEF culturing media. The next day, cells were fixed with fresh 4% paraformaldehyde in PBS for 15 min at room temperature, washed in phosphate-buffered saline (1xPBS) 3x5min, and blocked in 5% Bovine serum albumin (BSA) for 30min. Coverslips were incubated with 1° antibodies for β-actin (AC15; Sigma-Aldrich) and γ-actin (affinity purified γ-cyto actin rabbit 7577) in 5% BSA at 4°C overnight, washed in 1xPBS 3x5min and incubated with Alexa-488- or 568-conjugated 2° antibodies (Life Technologies). Coverslips were mounted in Prolong (P36931; Life Technologies) mounting medium prior to imaging. All images were obtained were acquired using a 20x/NA0.75 objective on a Delta Vision personalDV microscope using softWoRx 3.7.1 software (GE Technologies).

Cochlea Immunofluorescent microscopy

Dissected cochlea were fixed in 4% paraformaldehyde (PFA) in PBS for 4 hours at room temperature before decalcification in 170 mM EDTA in PBS for 16 hrs at 4°C. Organ of Corti was dissected, incubated in methanol for 10 mins at -20°C, permeabilized with 0.2% triton X-100 for 10 minutes at room temperature and blocked with 5% goat serum in 1xPBS before incubation with Alexa-546 conjugated monoclonal anti γ-actin antibody clone 1-37 and FITC conjugated anti-β-actin antibody clone AC-15 (AbCam, 1:400) overnight at 4°C. Samples were mounted either in Prolong Gold or Prolong Diamond anti-fade reagent (P36930 or P36965, Life Technologies) imaged with a 63X NA 1.4 objective on a Leica SP8 confocal microscope operating in resonant mode. Images were deconvolved using Huygens X11 Essentials software. Fluorescence intensity of actin immunostaining was quantified along the stereocilia length using Leica LasX software.

Scanning electron microscopy:

Dissected cochlea were fixed in 2.5% glutaraldehyde, 0.1 M sodium cacodylate, 2 mM $CaCl_2$ overnight at 4°C and then decalcified in 170 mM EDTA in PBS for 16 hours at 4°C. Dissected organ of Corti was incubated in 2% each of arginine, glutamine, glycine and sucrose in water overnight at room temperature, followed by incubation in 2% tannic acid and guanidine hydrochloride for 2 hours at room temperature and 1% $Os0_4$ in water for 1 hour at room temperature, with

extensive water washes between steps. The samples were transitioned to 100% ethanol, critical point dried from CO_2 and sputter coating with gold. Samples were imaged using a JEOL JSM-7800F field emission scanning electron microscope. The stereocilia length and number measurements were analyzed using Fiji software (National Institutes of health, Bethesda, MD).

Auditory Brainstem Response (ABR):

ABR waveforms were collected for mice using a Tucker Davis Technologies System 3 at frequencies of 4 kHz, 11 kHz, 16 kHz, 22kHz and 32 kHz as described previously (Perrin *et al*, 2013). Mice were anesthetized with Avertin following which scalp potentials were recorded using subdermal electrodes. Waveforms for each frequency were collected starting at 90 dB, decreasing in 5 dB to a sub-threshold level. The collected waveforms were stacked and the lowest level of stimulation that resulted in a definite waveform was considered as the threshold.

Live cell imaging

$10x10^4$ MEFs were plated on a Nunc™ Glass Base Dish (Thermo Scientific) and cultured overnight in regular MEF media. Second day, the dish was sealed with vacuum grease and a glass coverslip. MEF culture media containing 25 mM 4-(2-hydroxyethyl)-1-piperazineethanesulfonic acid (HEPES) was used to stabilize the pH, and the cells were maintained at 37°C by an environmental chamber enclosing the microscope. For random migration assay, images were captured

on a Delta Vision personalDV (GE Technologies) with a 10x/NA0.25 objective with phase contrast illumination. Images were captured at 10-minute intervals for 4 hours, and cells were tracked using the Manual Tracking plugin for ImageJ software (National Institutes of health, Bethesda, MD). Cells that divided or contacted other cells during the experiment were excluded for data analysis. Velocity was calculated as the total track distance divided by the total time (240 min), and directionality (D/T) was calculated as the linear distance (D) divided by the total track distance (T).

qRT-PCR

Generation of WT mouse isoactin control constructs were previously described in Patrinostro *et al.*, 2017. *Actb*$^{c\text{-}g}$ control construct was generated by site-directed mutagenesis using the QuikChange II XL kit (Agilent Technologies, Cat# 200521) according to manufacture protocols from the WT pENTR/D-TOPO-*Actb* vector generated in Patrinostro *et al.*, 2017. Each actin isoform qRT-PCR primer set was tested for amplification of all control constructs to assess primer specificity (Patrinostro *et al.*, 2017, Supplemental Figure 2). Total RNA was extracted from WT, *Actb*$^{c\text{-}g}$ heterozygous and homozygous MEF samples using the Bio-Rad-Aurum Total RNA Mini Kit following the manufacturer's instructions. RNA concentration and purity (260/280 ratio) were determined using a NanoDrop spectrophotometer (Wilmington, DE). First-strand cDNA was synthesized with a Bio-Rad iScript Advanced cDNA Synthesis Kit for qRT-PCR using the same initial RNA amount for all samples. Individual control constructs were used in a

10-fold dilution to generate a standard curve, and MEF samples were amplified in parallel with each specific qRT-PCR primer set using Bio-Rad SsoAdvanced Universal SYBR polymerase on the Bio-Rad CFX96 Real Time System C1000 Touch Thermal Cycler to profile each actin isoform transcript amount (picomoles).

G- to F- Actin ratio

WT and *Actb*$^{c\text{-}g}$ homozygous primary MEFs were counted and equal number of cells from each genotype were pelleted prior to the experiment. G-to F-actin ratio as assed by the commercially available G-Actin/F-Actin In Vivo Assay Biochem Kit (Cytoskeleton, Cat# BK037) according to manufacture protocols and then Westered blotted. Please see Western blotting methods for list of antibodies. LiCor fluorescence intensity for each Western blot fraction band is used to determine the ratio of G-to F-actin in each embryo.

Western blotting

MEF and tissue protein was extracted with 1% SDS buffer in 1x PBS and a cocktail of protease inhibitors (100 μM aprotinin, 0.79 mg/ml benzamide, 10 nM E-64, 10 μM leupeptin, 0.1 mg/ml pepstatin, 1 mM phenylmethylsulfonyl fluoride), sonicated (Model 150V/T Ultrasonic homogenizer; BioLogics), boiled, and centrifuged to remove the insoluble fraction. Equal amounts of cleared total lysate protein (25 μg) were blotted with antibodies β-actin (AC-15; Sigma-Aldrich), γ-actin (mAb 1-17), α_{sm}-actin (A14; Sigma-Aldrich), Pan-actin (C4), SRF

(G-20; Santa Cruz Biotechnology), MRTF-A (H-140; Santa Cruz Biotechnology), with glyceraldehyde 3-phosphate dehydrogenase (GAPDH; G9545 or G8795; Sigma-Aldrich) as loading control.

Animal care:

All mice were tail-clipped and genotyped at weaning (3 weeks) and kept alive until at least 6 months of age for Kaplan-Meier analysis. Heterozygous crosses were used to calculate Mendelian birth ratios. Animals were housed and treated in accordance with the standards set by the University of Minnesota Institutional Animal Care and Use Committee.

Tables

Table 3-1 Physiological parameters of isolated EDL muscles used in *ex vivo* force measurements

Parameter	WT	*Actb*$^{c\text{-}g/c\text{-}g}$	P value
EDL mass (mg)	13.4 ± 0.5	13.8 ± 0.5	0.587
L_o (mm)	13.7 ± 0.1	13.5 ± 0.2	0.397
CSA (mm^2)	2.1 ± 0.1	2.2 ± 0.1	0.500
Passive stiffness (N/m)	13.3 ± 0.4	14.6 ± 1.3	0.367
P_o (mN)	451 ± 30	452 ± 20	0.979
Specific P_o (N/cm^2)	21.6 ± 1.4	20.7 ± 0.8	0.592
ΔP_0 (%)	16.6 ± 2.6	18.4 ± 5.4	0.772
Peak eccentric force (mN)	857 ± 62	834 ± 33	0.752
Specific eccentric force (N/cm^2)	40.9 ± 2.6	38.3 ± 1.0	0.378
Eccentric force loss (%)	27.3 ± 1.5	26.7 ± 1.2	0.763
Active stiffness (N/m)	866 ± 47	844 ± 27	0.696
Peak twitch (mN)	133 ± 9.0	130 ± 4.9	0.777
Twitch Force development time (ms)	16.9 ± 1.1	16.4 ± 0.5	0.690
Twitch ½ relaxation time (ms)	17.1 ± 1.4	16.7 ± 1.4	0.845
Tetanic Maximal rate of contraction (mN/s)	14.4 ± 0.7	14.3 ± 0.5	0.910
Tetanic Maximal rate of relaxation (mN/s)	21.8 ± 1.9	21.9 ± 1.2	0.966

Values are mean ± S.E.M.

L_o = optimal muscle length, CSA = physiological cross-sectional area, P_o = maximal isometric tetanic force. ΔP_o = change in P_o after eccentric contractions.

n = 5 for each line. Statistics were performed using unpaired *t*-test analyses with $p < 0.05$ considered significant.

Supplemental Methods

TALEN sequences:

Target Site	RVD Sequence (N-terminus to C-terminus)
Actb Exon 2, left arm	**RVD:** HD NN HD HD NI NG NN NN NI NG NN NI HD NN NI NG HD NN HD HD NI NG NN NN NI **DNA sequence (5' to 3'):** CTGACCCCGGACCAAGTGGTGGCTATCGCCAGCAACG GTGGCGGCAAGCAAGCGCTCGAAACGGTGCAGCGGCT GTTGCCGGTGCTGTGCCAGGACCATGGCCTGACTCCG GACCAAGTGGTGGCTATCGCCAGCCACGATGGCGGCA AGCAAGCGCTCGAAACGGTGCAGCGGCTGTTGCCGGT GCTGTGCCAGGACCATGGCCTGACCCCGGACCAAGTG GTGGCTATCGCCAGCAACAATGGCGGCAAGCAAGCGC TCGAAACGGTGCAGCGGCTGTTGCCGGTGCTGTGCCA GGACCATGGCCTGACTCCGGACCAAGTGGTGGCTATC GCCAGCCACGATGGCGGCAAGCAAGCGCTCGAAACGG TGCAGCGGCTGTTGCCGGTGCTGTGCCAGGACCATGG CCTGACTCCGGACCAAGTGGTGGCTATCGCCAGCCAC GATGGCGGCAAGCAAGCGCTCGAAACGGTGCAGCGGC TGTTGCCGGTGCTGTGCCAGGACCATGGCCTGACCCC GGACCAAGTGGTGGCTATCGCCAGCAACATTGGCGGC AAGCAAGCGCTCGAAACGGTGCAGCGGCTGTTGCCGG TGCTGTGCCAGGACCATGGCCTGACCCCGGACCAAGT GGTGGCTATCGCCAGCAACGGTGGCGGCAAGCAAGCG CTCGAAACGGTGCAGCGGCTGTTGCCGGTGCTGTGCC AGGACCATGGCCTGACCCCGGACCAAGTGGTGGCTAT CGCCAGCAACAATGGCGGCAAGCAAGCGCTCGAAACG GTGCAGCGGCTGTTGCCGGTGCTGTGCCAGGACCATG GCCTGACCCCGGACCAAGTGGTGGCTATCGCCAGCAA CAATGGCGGCAAGCAAGCGCTCGAAACGGTGCAGCGG CTGTTGCCGGTGCTGTGCCAGGACCATGGCCTGACCC CGGACCAAGTGGTGGCTATCGCCAGCAACATTGGCGG CAAGCAAGCGCTCGAAACGGTGCAGCGGCTGTTGCCG GTGCTGTGCCAGGACCATGGCCTGACCCCGGACCAAG TGGTGGCTATCGCCAGCAACGGTGGCGGCAAGCAAGC GCTCGAAACGGTGCAGCGGCTGTTGCCGGTGCTGTGC CAGGACCATGGCCTGACCCCGGACCAAGTGGTGGCTA TCGCCAGCAACAATGGCGGCAAGCAAGCGCTCGAAAC GGTGCAGCGGCTGTTGCCGGTGCTGTGCCAGGACCAT GGCCTGACCCCGGACCAAGTGGTGGCTATCGCCAGCA ACATTGGCGGCAAGCAAGCGCTCGAAACGGTGCAGCG GCTGTTGCCGGTGCTGTGCCAGGACCATGGCCTGACT CCGGACCAAGTGGTGGCTATCGCCAGCCACGATGGCG

	GCAAGCAAGCGCTCGAAACGGTGCAGCGGCTGTTGCC GGTGCTGTGCCAGGACCATGGC
Actb Exon 2, right arm	**RVD:** NN HD HD NN NN NI NN HD HD NN NG NG NN NG HD NN NI HD NN NI NN HD HD NN NN NI NN HD HD NN **DNA sequence (5' to 3'):** CTGACCCCGGACCAAGTGGTGGCTATCGCCAGCAACAA TGGCGGCAAGCAAGCGCTCGAAACGGTGCAGCGGCTG TTGCCGGTGCTGTGCCAGGACCATGGCCTGACTCCGG ACCAAGTGGTGGCTATCGCCAGCCACGATGGCGGCAA GCAAGCGCTCGAAACGGTGCAGCGGCTGTTGCCGGTG CTGTGCCAGGACCATGGCCTGACTCCGGACCAAGTGG TGGCTATCGCCAGCCACGATGGCGGCAAGCAAGCGCT CGAAACGGTGCAGCGGCTGTTGCCGGTGCTGTGCCAG GACCATGGCCTGACCCCGGACCAAGTGGTGGCTATCG CCAGCAACAATGGCGGCAAGCAAGCGCTCGAAACGGT GCAGCGGCTGTTGCCGGTGCTGTGCCAGGACCATGGC CTGACCCCGGACCAAGTGGTGGCTATCGCCAGCAACAA TGGCGGCAAGCAAGCGCTCGAAACGGTGCAGCGGCTG TTGCCGGTGCTGTGCCAGGACCATGGCCTGACCCCGG ACCAAGTGGTGGCTATCGCCAGCAACATTGGCGGCAAG CAAGCGCTCGAAACGGTGCAGCGGCTGTTGCCGGTGC TGTGCCAGGACCATGGCCTGACCCCGGACCAAGTGGT GGCTATCGCCAGCAACAATGGCGGCAAGCAAGCGCTC GAAACGGTGCAGCGGCTGTTGCCGGTGCTGTGCCAGG ACCATGGCCTGACTCCGGACCAAGTGGTGGCTATCGCC AGCCACGATGGCGGCAAGCAAGCGCTCGAAACGGTGC AGCGGCTGTTGCCGGTGCTGTGCCAGGACCATGGCCT GACTCCGGACCAAGTGGTGGCTATCGCCAGCCACGAT GGCGGCAAGCAAGCGCTCGAAACGGTGCAGCGGCTGT TGCCGGTGCTGTGCCAGGACCATGGCCTGACCCCGGA CCAAGTGGTGGCTATCGCCAGCAACAATGGCGGCAAG CAAGCGCTCGAAACGGTGCAGCGGCTGTTGCCGGTGC TGTGCCAGGACCATGGCCTGACCCCGGACCAAGTGGT GGCTATCGCCAGCAACGGTGGCGGCAAGCAAGCGCTC GAAACGGTGCAGCGGCTGTTGCCGGTGCTGTGCCAGG ACCATGGCCTGACCCCGGACCAAGTGGTGGCTATCGC CAGCAACGGTGGCGGCAAGCAAGCGCTCGAAACGGTG CAGCGGCTGTTGCCGGTGCTGTGCCAGGACCATGGCC TGACCCCGGACCAAGTGGTGGCTATCGCCAGCAACAAT GGCGGCAAGCAAGCGCTCGAAACGGTGCAGCGGCTGT TGCCGGTGCTGTGCCAGGACCATGGCCTGACCCCGGA CCAAGTGGTGGCTATCGCCAGCAACGGTGGCGGCAAG CAAGCGCTCGAAACGGTGCAGCGGCTGTTGCCGGTGC TGTGCCAGGACCATGGCCTGACTCCGGACCAAGTGGT

	GGCTATCGCCAGCCACGATGGCGGCAAGCAAGCGCTC GAAACGGTGCAGCGGCTGTTGCCGGTGCTGTGCCAGG ACCATGGCCTGACCCCGGACCAAGTGGTGGCTATCGC CAGCAACAATGGCGGCAAGCAAGCGCTCGAAACGGTG CAGCGGCTGTTGCCGGTGCTGTGCCAGGACCATGGCC TGACCCCGGACCAAGTGGTGGCTATCGCCAGCAACATT GGCGGCAAGCAAGCGCTCGAAACGGTGCAGCGGCTGT TGCCGGTGCTGTGCCAGGACCATGGCCTGACTCCGGA CCAAGTGGTGGCTATCGCCAGCCACGATGGCGGCAAG CAAGCGCTCGAAACGGTGCAGCGGCTGTTGCCGGTGC TGTGCCAGGACCATGGCCTGACCCCGGACCAAGTGGT GGCTATCGCCAGCAACAATGGCGGCAAGCAAGCGCTC GAAACGGTGCAGCGGCTGTTGCCGGTGCTGTGCCAGG ACCATGGC-3’

ssOligo Donor Sequences:

Target Site	**Sequence (5’→3’)**
Actb Exon 2	AGTGGGCAGGGCGGCAGCGGCTGCTCTTGGCGGCCCCGAGG TGACTATAGCCTTCTTTTGTGTCTTGATAGTTCGCAATGGAAGA AGAAATCGCTGCGCGGTCATAGACAACGGATCCGGAATGTGC AAAGCCGGCTTCGCGGGCGACGATGCTCCCCGGGCTGTATTC CCCTCCATCGTGGGCCGCCCTAGGCACCAG

TALEN activity validation. TALEN RNA pairs (15µg each arm) were nucleofected (Amaxa® Cell Line Nucleofector® Kit R, Amaxa® Nucleofector® II) into 1x10^6 NIH3T3 fibroblasts. 3-days post nucleofection, gDNA was harvested from the cells with the PureLink® Genomic DNA Mini Kit, Invitrogen according to manufacture protocols. TALEN activity was assayed via the Surveyor Mutation Detection Kit (Transgenomic, Cat. #706020.) Primers: *Actb* Exon2 F 5’-GGTAATAATGCGGCCGGTCT-3’, *Actb* Exon2 R 5’-TACCCGGGATACTGACCTGG-3’. Additionally, *in-silico* off-target analysis using https://tale-nt.cac.cornell.edu with the most stringent cutoff showed that the most similar potential off-target sequences had a minimum of 7 nucleotides that differed between the on- and off-targets.

Figures

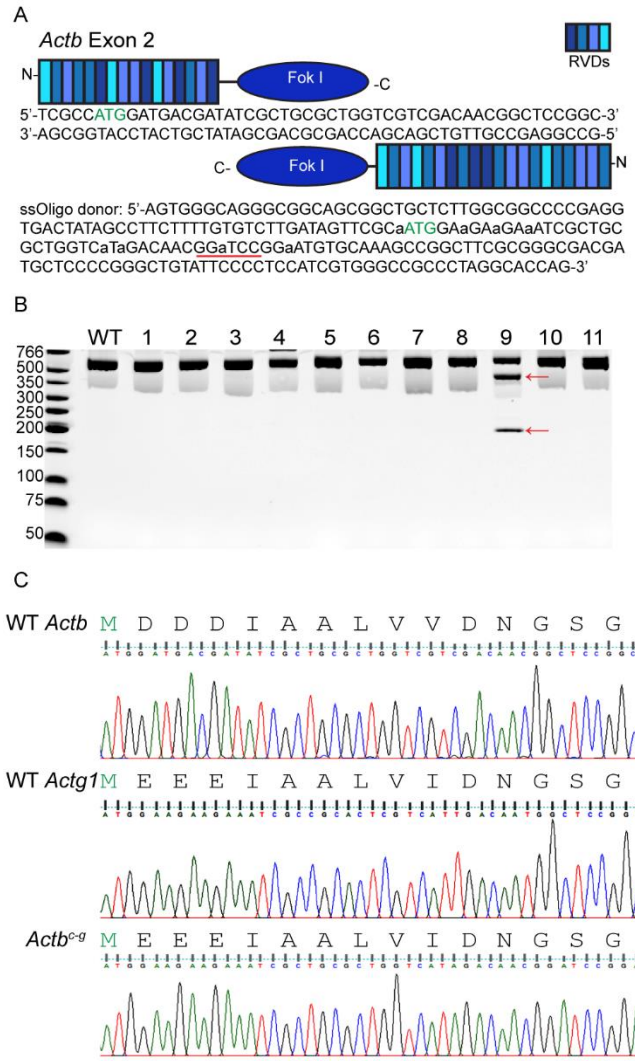

Figure 3-1 Genetically engineered *Actb*$^{c\text{-}g}$ mice via TALENs and a single-strand oligo donor. (A) Schematic of TALEN target sequence within WT mouse *Actb* exon 2 and the ssOligo homologous repair donor sequence. The start codon is labeled in green, BamHI restr enzyme site is underlined in red, edited nucleotides are denoted in lowercase letters. (B) RFLP results of WT and live born F0 pups using the BamHI restriction enzyme digestion. Red arrows indicate

the correct digested fragments. (C) Sanger sequence results for WT mouse pup number 9. Aspartic acids 2-4 and Valine 10 in WT β-actin have been changed to glutamic acids 2-4 and isoleucine 10 in the corresponding location in γ-actin.

A

	# of pups	Birth Ratio	Chi-Sq p=0.80
WT	33	26.61	
Actb$^{c\text{-}g/+}$	63	50.81	
Actb$^{c\text{-}g/c\text{-}g}$	28	22.58	
N=17 litters, Average litter size = 7.3			

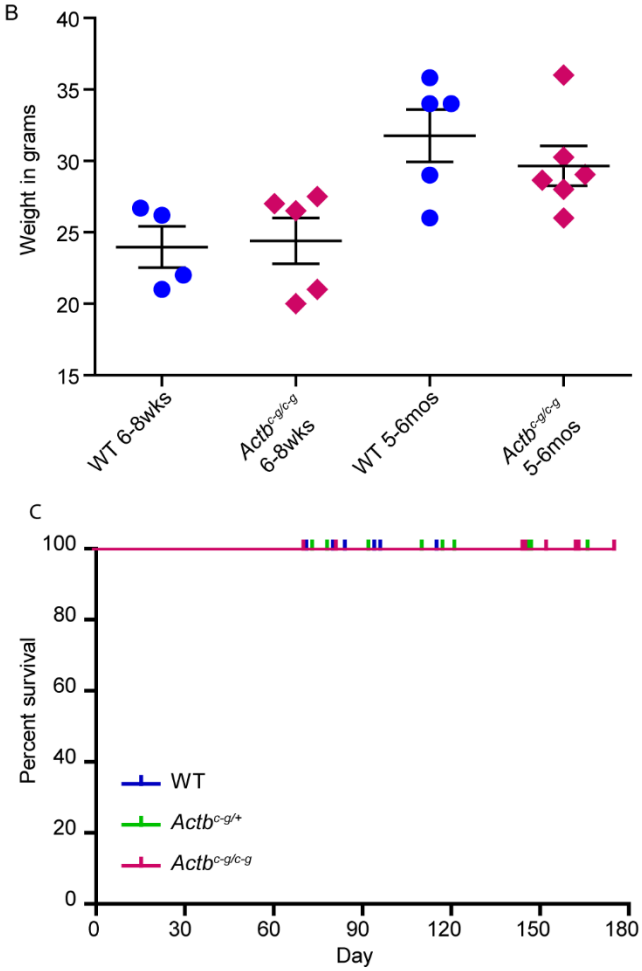

Figure 3-2 *Actb*$^{c\text{-}g}$ mice are born at Mendelian ratios and do not exhibit an early lethality phenotype. (A) Calculated Mendelian genetic ratio of WT, heterozygous and homozygous *Actb*$^{c\text{-}g}$ mice at weaning (21 days post birth). N=17 Het x Het crosses. B) WT and homozygous *Actb*$^{c\text{-}g}$ mice body mass at 6-8 weeks old and 5-6 months old. N≥4 mice per genotype for each age range. (C) Kaplan-Meier survival curve of wildtype, heterozygous and homozygous *Actb*$^{c\text{-}g}$

mice from 0-180 days post birth. Tick marks represent censored animals. N≥25 per genotype.

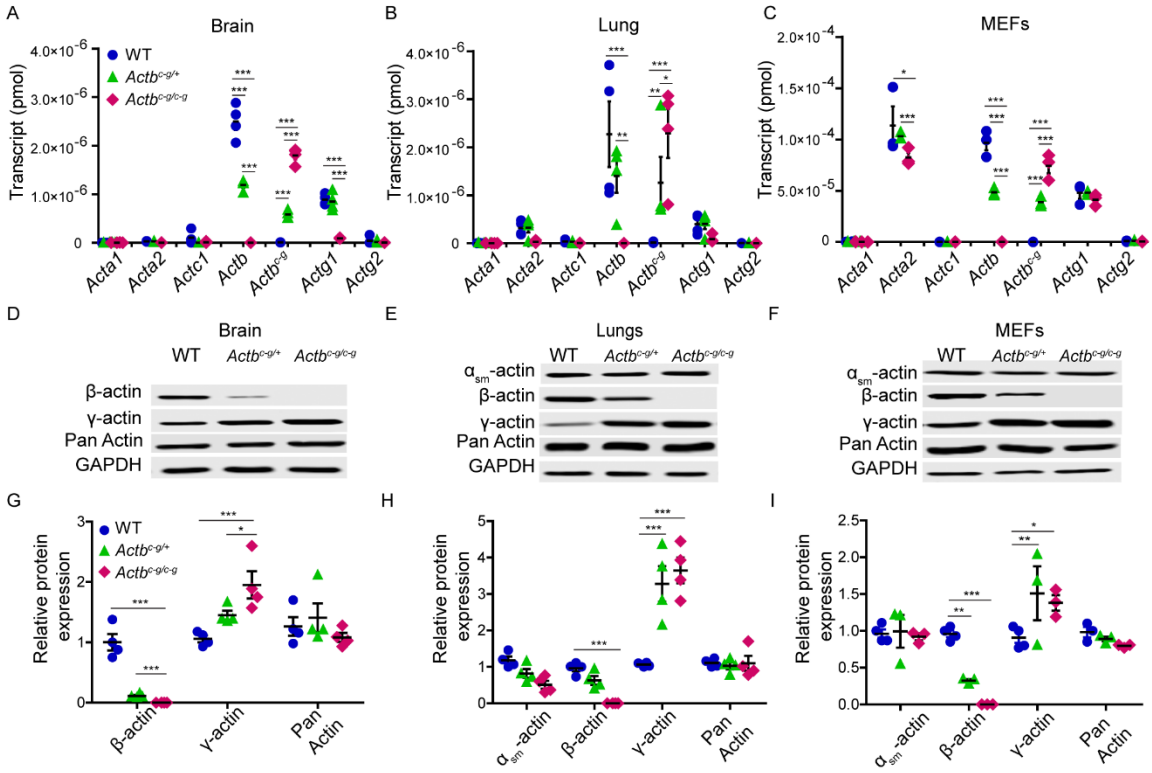

Figure 3-3 *Actb*$^{c\text{-}g}$ transcript is synthesized from the edited *Actb* locus and correlates with a 2-fold increase in γ-actin protein expression.

(A-C) Calculated quantity of isoactin transcript via qRT-PCRs in brain, lung tissues and MEFs. X-axis denotes actin isoform. Y-axis denotes Transcript in pmol. (D-F) Representative western blots in brain, lung and MEFs. (G-I) Calculated relative isoactin protein expression in WT, heterozygous and homozygous *Actb*$^{c\text{-}g}$ mice brain, lung and MEFs. X-axis denotes actin isoform. Y-axis denotes relative protein expression which were normalized to GAPDH and relative to a WT sample. Two-way ANOVA with Bonferroni post-test. Error bars are S.E.M. *p<0.05, **p<0.01, ***p<0.001

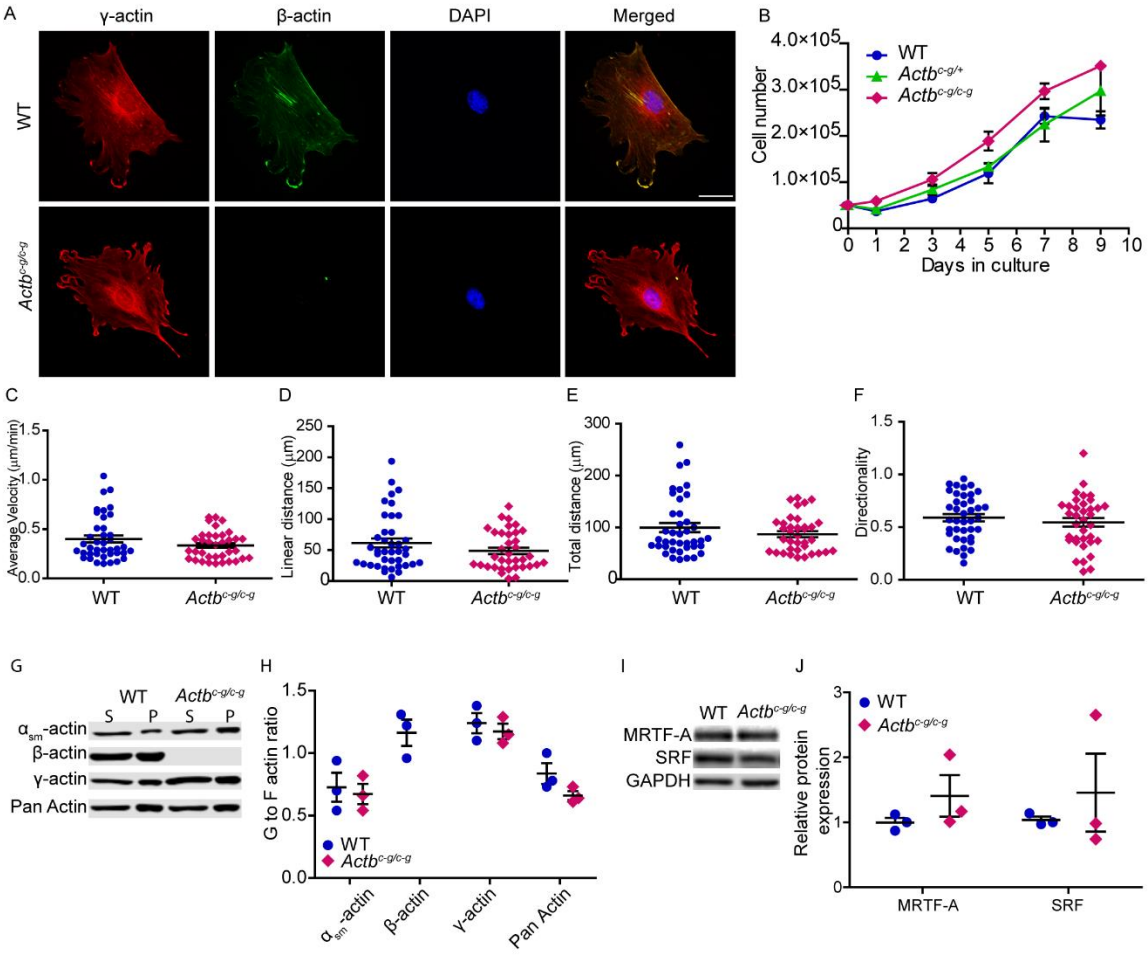

Figure 3-4 *Actb*$^{c\text{-}g}$ MEFs display cell proliferation and random migration rates not different than WT. (A) Representative immunofluorescence images of WT MEFs and *Actb*$^{c\text{-}g}$ MEFs. γ-actin is labeled in red, β-actin is labeled in green, nucleus is labeled in blue and the final merged image is on the right. Scare bar = 50μm. (B) MEFs growth curve analysis, cultured from 0-9 days. N=3 embryos. (C-F) Calculated average velocity, linear distance, total distance, and directionality from random migration assay. MEFs were live imaged for 4 hours, at 10-minute intervals. N≥4 embryos, n≥40 cells per genotype. (G-H) G- to F-Actin ratio in WT and *Actb*$^{c\text{-}g}$ MEFs. (I-J) Representative and calculated relative

isoactin protein expression in WT, homozygous *Actb*$^{c\text{-}g}$ MEFs for SRF and MRTF-A. X-axis denotes actin isoform. Y-axis denotes relative protein expression which were normalized to GAPDH and relative to a WT sample. Error bars are S.E.M.

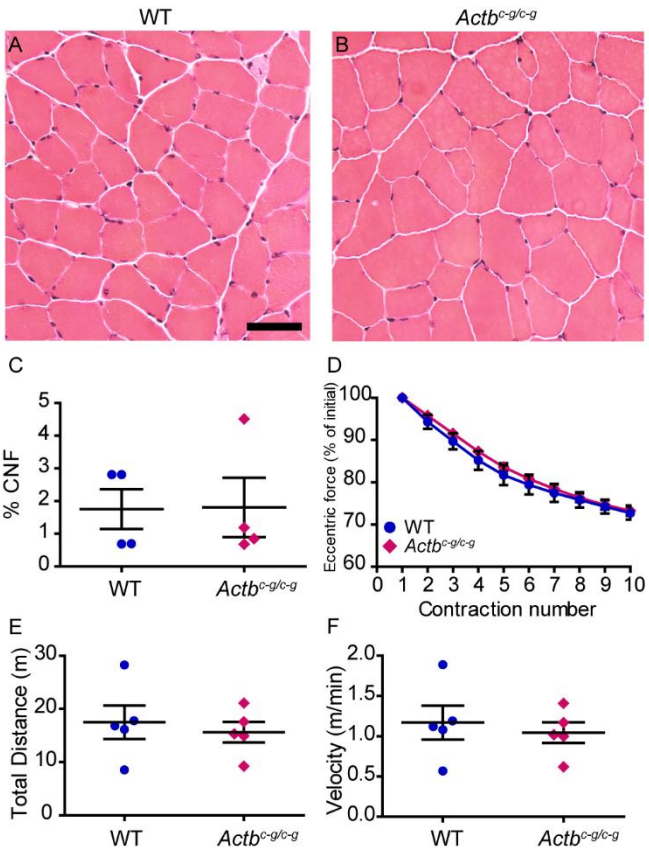

Figure 3-5 *Actb*$^{c\text{-}g}$ mice display CNF percentage and open field activity not different than WT. (A-B) Representative H&E images of WT and homozygous *Actb*$^{c\text{-}g}$ mice quadricep muscle. (C) Calculated CNF % of WT and homozygous *Actb*$^{c\text{-}g}$ mice quadricep. N=4 mice, n≥400 fibers per mouse. (D) Graph of eccentric force drop as a percentage of initial force. (E) Total distance traveled during an open field activity assay. (F) Average velocity of each mouse during an open field activity assay. N=4 for each genotype.

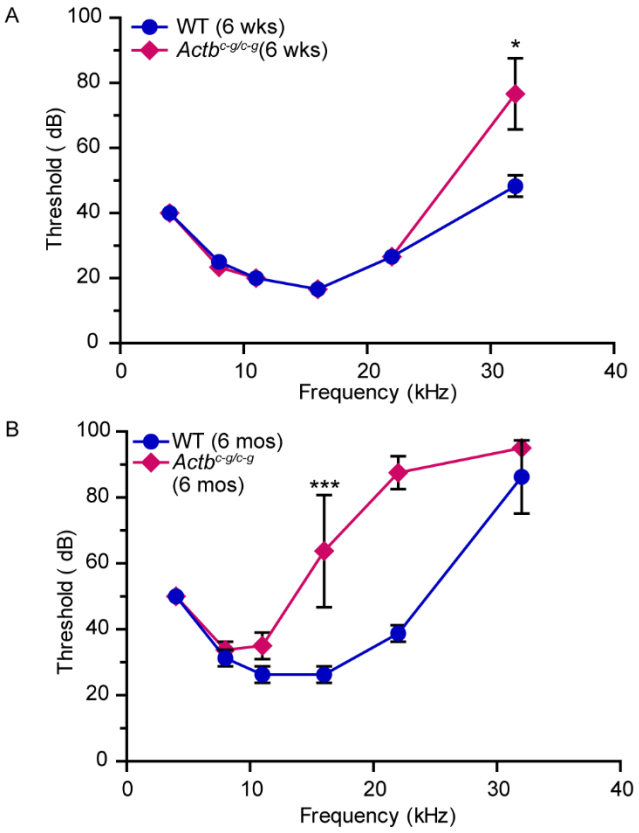

Figure 3-6 *Actb*$^{c\text{-}g}$ mice suffer from progressive hearing loss. (A) ABR of 6 weeks old WT and homozygous *Actb*$^{c\text{-}g}$ mice. (B). ABR of 6 months old WT and homozygous *Actb*$^{c\text{-}g}$ mice. X-axis denotes defined frequency in kHz, y-axis denotes threshold (dB) sound that elicit an ABR. N≥4 for each genotype. Student T-Test. *P<0.05, ***P<0.001. Error bars are S.E.M.

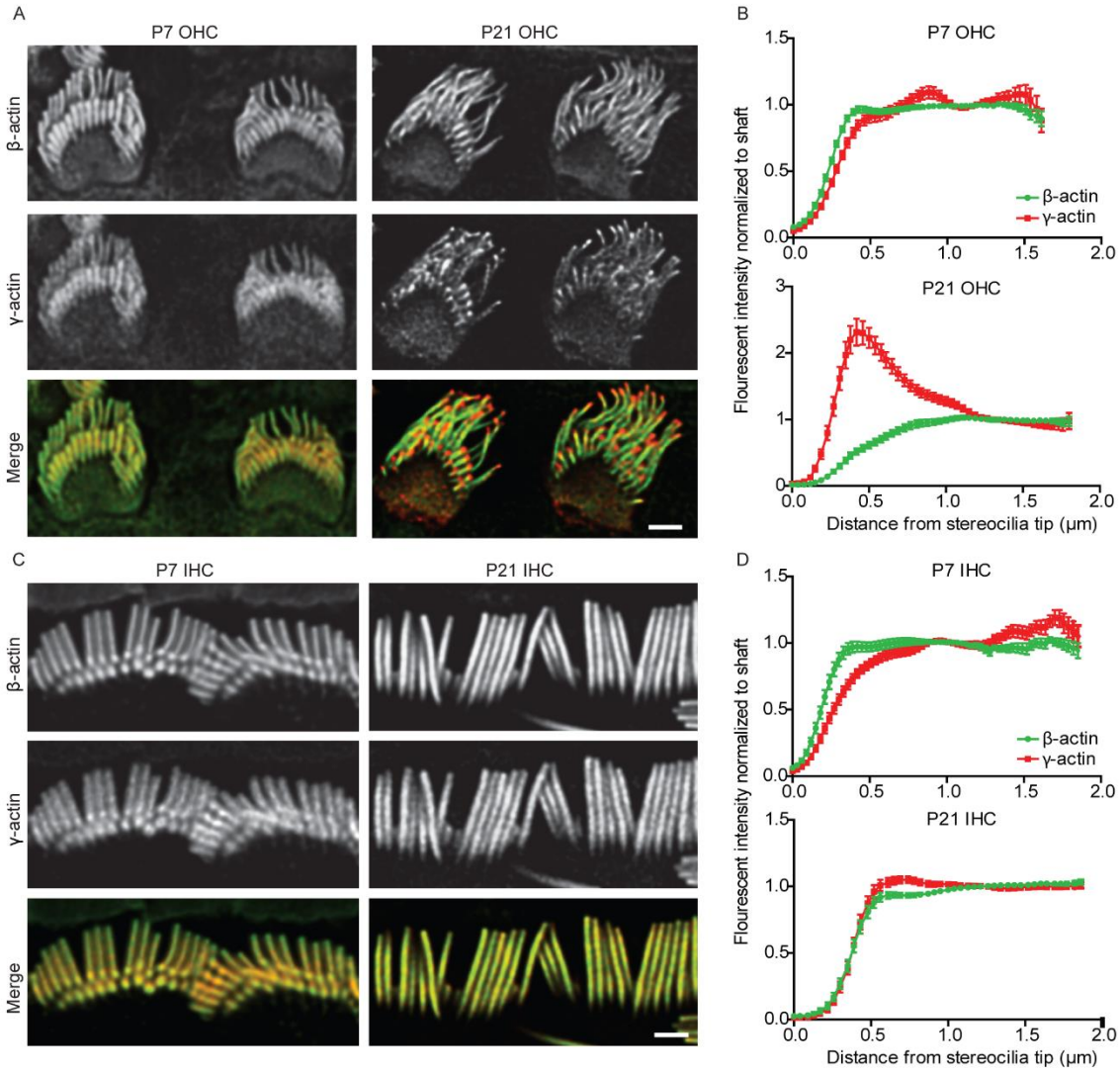

Figure 3-7 β-actin and γ-actin colocalized in developing OHC stereocilia. (A) Representative immunofluorescent images of the OHC in P7 and P21 C57BL/6 mice. β-actin is labeled in green, γ-actin is labeled in red. (B) Calculated fluorescent intensity of β- and γ-actin normalized to the shaft in the OHC. (C) Representative immunofluorescent images of the IHC in P7 and P21 C57BL/6 mice. β-actin is labeled in green, γ-actin is labeled in red. (D) Calculated

fluorescent intensity of β- and γ-actin normalized to the shaft in the IHC. Scare bar = 15μm. N=3 mice for each genotype.

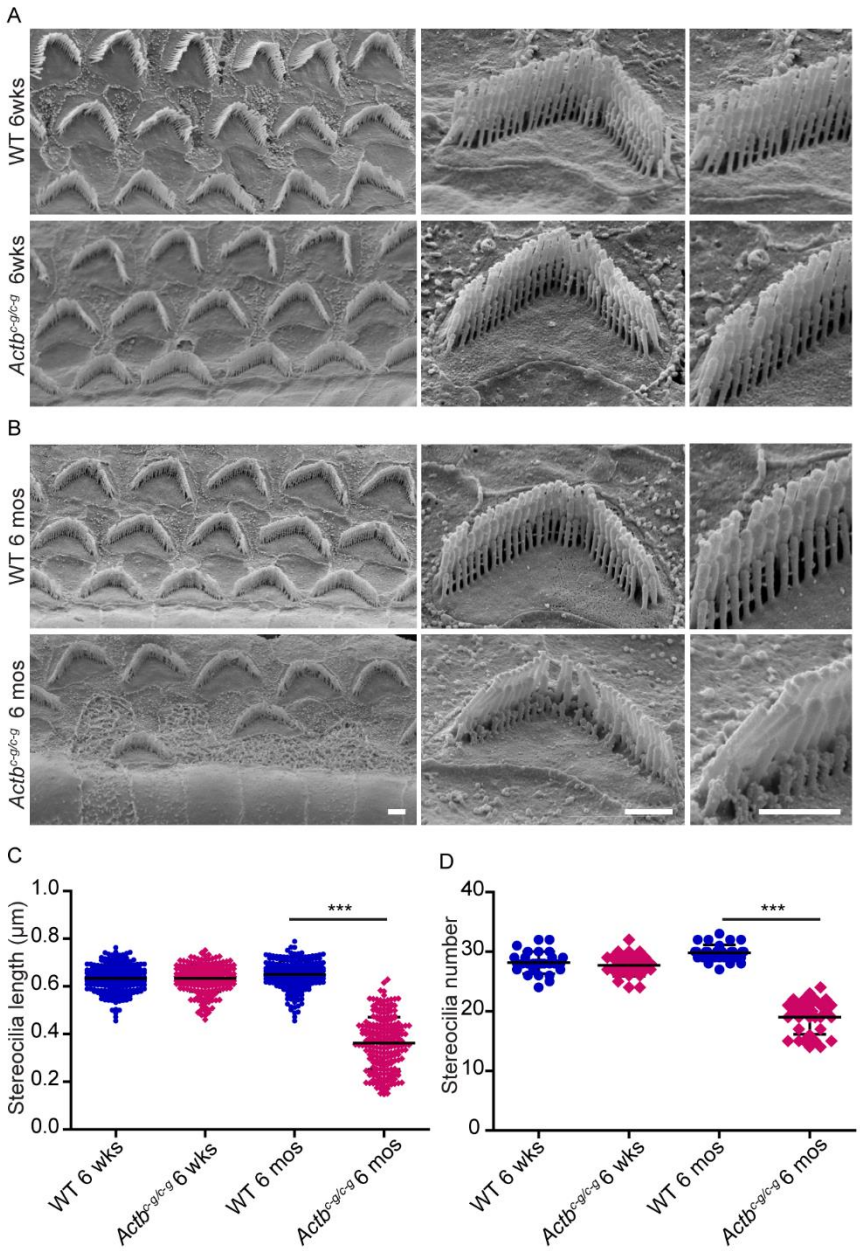

Figure 3-8 *Actb*$^{c\text{-}g}$ mice show evidence of stereocilia degeneration.

Representative images of scanning electron microcopy of (A) 6 weeks old, and (B) 6 months old of OHC stereocilia from the middle turn of the cochlea**.** Scare bar = 1 micron. (C) Third row stereocilia length (µm) of 6 weeks old and 6 months

old WT and homozygous *Actb*$^{c\text{-}g}$ mice**.** N≥4. (D) Third row stereocilia number of 6 weeks old and 6 months old WT and homozygous *Actb*$^{c\text{-}g}$ mice**.** N≥4. One-way ANOVA with Tukey's post-test. ***P<0.001. Error bars are S.E.M.

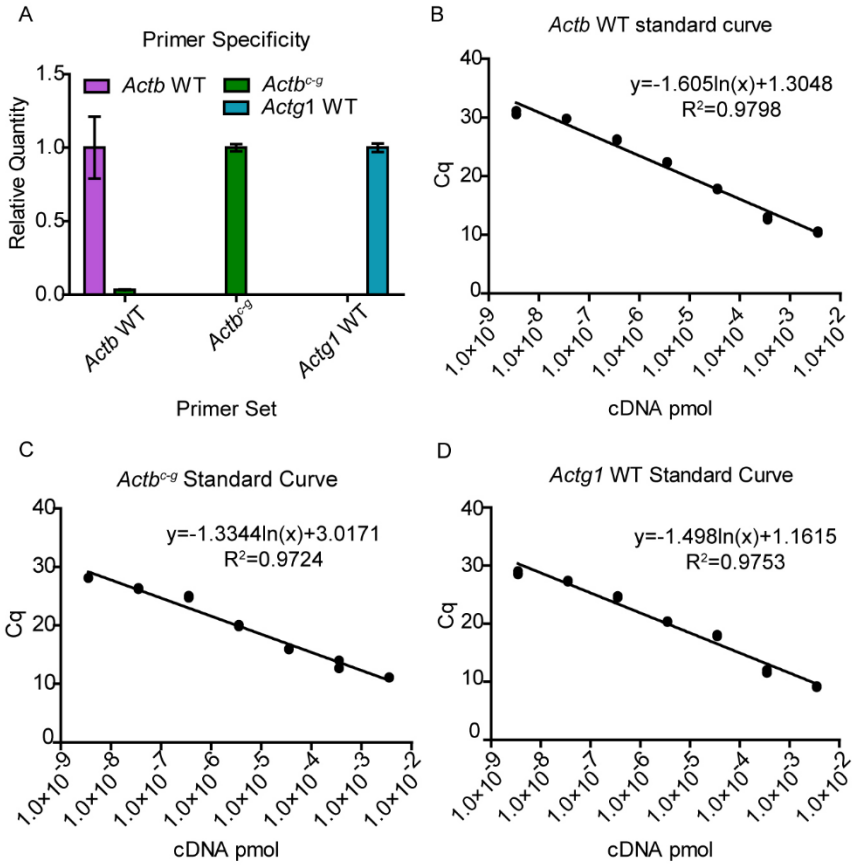

Figure 3-9 Mouse actin isoform standard curves and primer specificity analysis. (A) Representative graph of qRTPCR primer specificity. Two new primer sets were designed to specifically amplify WT *Actb* and *Actb*$^{c\text{-}g}$ edited transcript. Each primer set was used to amplify WT *Actb*, edited *Actb*$^{c\text{-}g}$, and WT *Actg1* control constructs to calculate relative quantity. Color bars represent individual actin isoform, y-axis denotes relative quantity, x-axis denotes primer set. (B-D) Representative standard curves generated using specific actin isoform primers with the corresponding control actin construct in a ten-fold dilution.

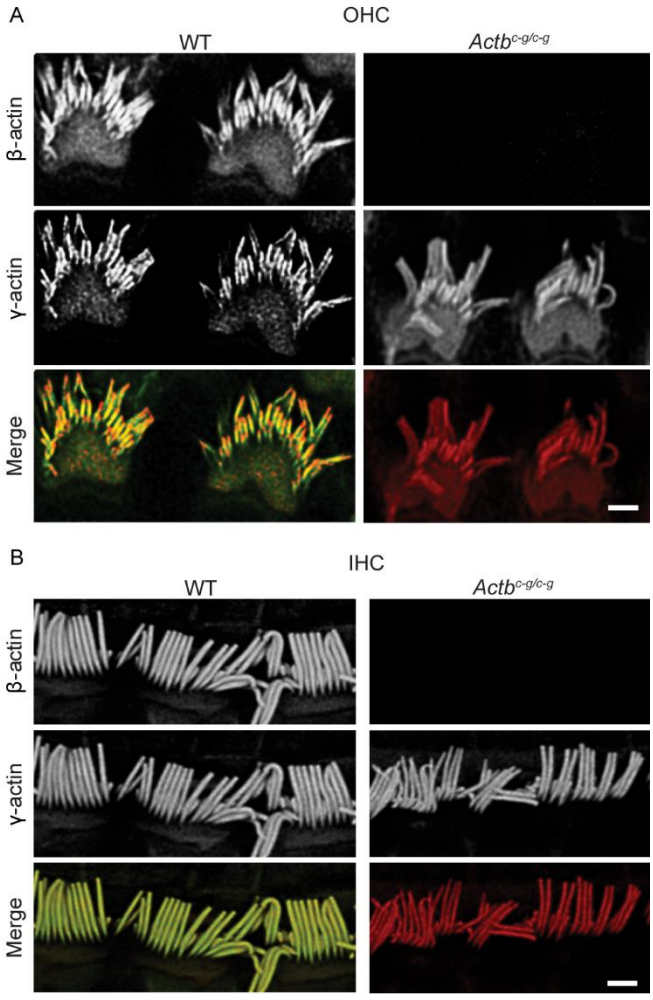

Figure 3-10 β-actin protein is not localized to stereocilia in *Actb*$^{c\text{-}g}$ mice. (A) Representative immunofluorescent images of β-actin (green), γ-actin (red) and merged image in the OHC between WT and homozygous *Actb*$^{c\text{-}g}$ mice. (B) Representative immunofluorescent images of β-actin (green), γ-actin (red) and merged image in the IHC between WT and homozygous *Actb*$^{c\text{-}g}$ mice. Scare bar = 5μm. N=3 mice for each genotype.

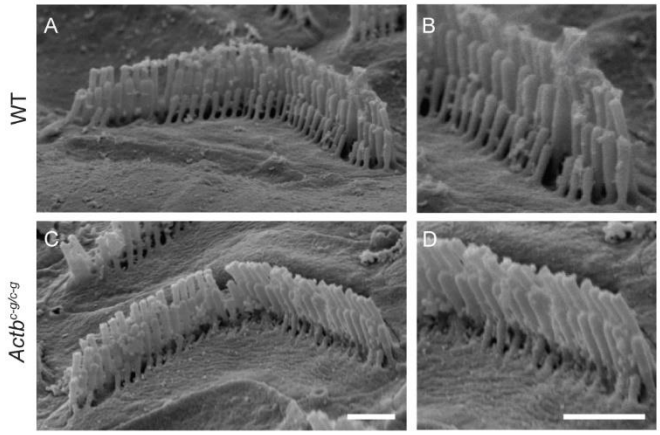

Figure 3-11 6 weeks old *Actb*$^{c-g}$ mice suffers from stereocilia degeneration.

(A-D) Representative scanning electron microscopy images of 6 weeks old OHC stereocilia from the base of the cochlea. Scare bars = 1μm. N≥4.

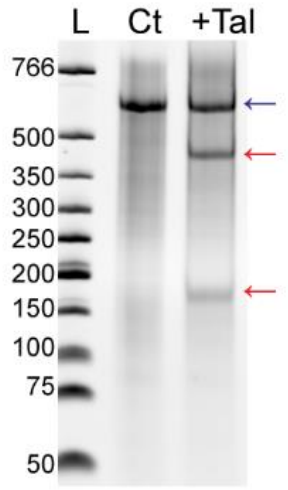

Figure 3-12 TALEN activity validation. TALEN RNA pairs (15µg each arm) were nucleofected (Amaxa® Cell Line Nucleofector® Kit R, Amaxa® Nucleofector® II) into $1x10^6$ NIH3T3 fibroblasts. 3-days post nucleofection, gDNA was harvested from the cells with the PureLink® Genomic DNA Mini Kit, Invitrogen according to manufacture protocols. TALEN activity was assayed via the Surveyor Mutation Detection Kit (Transgenomic, Cat. #706020.) Blue arrow denotes full length PCR fragment and the red arrows denote the digested fragments. Primers: *Actb* Exon2 F 5'-GGTAATAATGCGGCCGGTCT-3', *Actb* Exon2 R 5'-TACCCGGGATACTGACCTGG-3'.

Chapter 4

In vivo deletion of the *Actb* zipcode

Introduction

The central dogma states DNA encodes genetic information, which is transcribed into RNA that can then be translated into protein for cellular function. However, it is now clear that RNA is more than just a messenger between DNA and protein. RNA also serves as a regulatory point for gene expression. Classic RNA regulatory mechanisms such as RNA sequestration, localized expression, and RNA decay can regulate where, when and how much a gene is expressed. More recent discoveries of alternative polyadenylation signaling, micro-RNAs, and long non-coding RNAs provide additional mechanisms for fine-tuning regulation of gene expression.

The *Actb* transcript is a classic example of how regulation of RNA localization and translation affect protein function. The *Actb* 3'UTR contains a 54-nucleotide sequence called the zipcode that is negatively regulated by the RNA binding proteins (RBP) ZBP1 and ZBP2. ZBP2 first co-transcriptionally associates with the nascent *Actb* transcript and then facilitates the transfer of the *Actb* transcript to ZBP1 (Pan *et al.*, 2007). ZBP1 binds to the *Actb* zipcode through a bipartite binding motif consisting of a 5' -CGGAC- sequence and a more promiscuous 3' -C/A-CA-C/U-sequence with a 19 nucleotides linker region between the two motifs in mice. Both the binding site sequences and the correct linker region length are crucial for RNA-protein binding as the RNA physically loops around the protein to establish proper structural association (Chao *et al.*, 2010; Patel *et al.*, 2012). The ZBP1-RNA ribonucleoprotein complex is then shuttled out of the nucleus and transferred to the cell periphery on microtubules

via the Kif11 kinesin (Song *et al.*, 2015). At the cell periphery, Src phosphorylation of ZBP1 releases the *Actb* transcript, allowing for localized translation (Hüttelmaier *et al.*, 2005).

Numerous *in vitro* reports have shed light on the importance of the *Actb* zipcode for proper function. Antisense oligonucleotide masking of the endogenous *Actb* zipcode resulted in delocalized *Actb* mRNA, decreased cell motility in fibroblasts (Shestakova, Singer and Condeelis, 2001), and perturbed adherens junctions assembly in epithelial cells (Gutierrez *et al.*, 2014). siRNA mediated *Actb* KD reduced dynamic moments of growth cone filopodia and impaired presynaptic differentiation (Moradi *et al.*, 2017). Conversely, ZBP1 KD in primary neurons disrupted *Actb* localization and impaired dendritic filopodia growth (Eom *et al.*, 2003).

Although many studies have shown the importance of the zipcode sequence to proper *Actb* localization and translation, all the studies were carried out with *in vitro* systems. However, *in vitro* analyses do not always accurately reflect what occurs *in vivo* (Belanto *et al.*, 2014, 2016). To fully assess the importance of the zipcode sequence and its binding to ZBP1 in relationship to β-actin function, we used TALENs to mutate the zipcode bipartite motif to disrupt ZBP1-mRNA binding. While we succeeded to generate 1 correctly edited founder mouse, named $Actb^{MutZip}$, the mouse failed to propagate. We also generated a second mouse where only the 3' ZBP1 binding site was deleted. We name the mouse $Actb^{ZD25\text{-}39}$, which describes the 14 nucleotides deletion within the zipcode. $Actb^{ZD25\text{-}39}$ mice were born in Mendelian ratios, had litter size and life

spans not different than wildtypes. *Actb*$^{ZD25\text{-}39}$ mice and primary MEFs also expressed β-actin protein to similar levels as WTs. Finally, the *Actb*$^{ZD25\text{-}39}$ transcript retained ZBP1 binding activity, which we hypothesize was due to the presence of a pseudo 3' ZBP1 binding site sequence downstream to the deletion site. Overall the *Actb*$^{ZD25\text{-}39}$ mouse suggests that disruption of both ZBP1 binding sites will be necessary to assess the importance of the zipcode to β-actin function *in vivo*.

Results

Generation of the *Actb*$^{ZD25-39}$ mice.

We used transcription activator-like effector nucleases (TALENs) and a single-stranded oligo (ssOligo) donor template to edit the endogenous *Actb* 3'UTR within the mouse genome (Figure 4-1A). Of 23 live-born pups produced, restriction fragment length polymorphism (RFLP) analysis demonstrated that the ssOligo donor template was incorporated into one of the endogenous *Actb* loci of pup #1 (Figure 4-1B). Sanger sequencing confirmed that the 3'UTR in one allele of *Actb* in pup #1 was edited such that it altered the predicted ZBP1 binding sites to nonfunctional sequences (Figure 4-1C). Unfortunately, the founder female mouse, pup#1, only produced 1 litter which was filial cannibalized. The founder mouse did not produce any additional litters. Nonetheless, pup #2 had a 14 nucleotides deletion within the *Actb* 3'UTR, removing the 3' ZBP1 binding site. All subsequent experiments were performed on the *Actb*$^{ZD25-39}$ mouse line.

Actb$^{ZD25-39}$ mice are born at Mendelian ratios and do not exhibit early lethality

While no *Actb* zipcode edited mouse models exist, a ZBP1 KO mouse model resulted in high perinatal mortality, dwarfism and organ malformations (Hansen *et al.*, 2004). In contrast to the ZBP1 KO mice, crosses of heterozygous *Actb*$^{ZD25-39}$ mice yielded the expected Mendelian ratios with litter sizes typical of the C57BL/6 strain (Figure 4-2A) (Silver, 2001). Neither homozygous or

heterozygous *Actb*$^{ZD25\text{-}39}$ mice exhibited early lethality or survival rates that were distinguishable from WT to at least 6 months of age.

Actb$^{ZD25\text{-}39}$ β-actin protein expression is not different than wildtype

ZBP1 suppresses β-actin translation by physically inhibiting ribosomal complex formation on the *Actb* transcript (Hüttelmaier *et al.*, 2005). To assess if *Actb*$^{ZD25\text{-}39}$ mice exhibited altered β-actin protein expression, we immunoblotted tissue samples from the brain, lungs and the kidneys (Figure 4-3A). In all samples tested, homozygous and heterozygous *Actb*$^{ZD25\text{-}39}$ β-actin protein expression was not significantly different from WT (Figure 4-3B).

Actb$^{ZD25\text{-}39}$ primary MEFs express isoactin proteins to similar levels as wildtype.

Primary MEFs actin isoform composition is predominantly α_{sm}-, β- and γ-actin (Patrinostro *et al.*, 2017). We immunostained for all three actin isoforms in *Actb*$^{ZD25\text{-}39}$ primary MEFs and determined homozygous, heterozygous and wildtype primary MEFs expressed α_{sm}-, β- and γ-actin proteins to similar levels (Figure 4-4).

Both ZBP1 and ZBP2 can bind to the *Actb*$^{ZD25\text{-}39}$ transcript.

Both ZBP1 and ZBP2 have predicted binding sites within the deleted region (Pan *et al.*, 2007). To determine if the 3'UTR deletion disrupted protein-RNA binding, we performed RNA-immunoprecipitation (RNA-IP) assays on

lysates from primary MEFs using antibodies targeting either ZBP1 or ZBP2. We then used qRT-PCR to measure *Actb* transcript levels in the eluted mRNA from control, homozygous and heterozygous MEF samples. The amount of *Actb* transcript was calculated from a standard curve that was amplified in parallel. Based on our RNA-IP experiments, we conclude that the deleted 3'UTR did not inhibit *Actb* transcript binding to either ZBP1 or ZBP2.

Discussion

To assess the importance of *Actb* zipcode sequence in an *in vivo* system, we used TALENs to edit the endogenous *Actb* zipcode sequence. Two founder mice were generated, the first mouse was edited to encode the desired mutated zipcode sequence that disrupts the predicted ZBP1 binding sites (Chao *et al.*, 2010; Patel *et al.*, 2012), but unfortunately the mouse was unable to propagate. The second founder mouse had a 14 nucleotides deletion within the *Actb* zipcode sequence, which deleted the putative 3' ZBP1 binding site ($Actb^{ZD25\text{-}39}$).

$Actb^{ZD25\text{-}39}$ mice had litter size and life spans not different from WT and were born in Mendelian ratios suggesting the deletion does not affect viability. Additionally, heterozygous and homozygous $Actb^{ZD25\text{-}39}$ mice and MEFs expressed β-actin protein to WT levels, indicating the 14-nucleotide deletion within the *Actb* zipcode did not disrupt β-actin protein translation. Finally, we determined the edited mRNA was still able to bind to both ZBP1 and ZBP2, implying the 14-nucleotide deletion did not disrupt RNA-protein association. Upon closer inspection of the edited genome, we think it is likely that TALEN mediated double strand DNA breakage caused nonhomologous end joining (NHEJ), which resulted in the 14 nucleotides deletion. This deletion shifted a second downstream -ACA- sequence forward that may be able to substitute for the original 3' -C/A-CA-C/U- ZBP1 binding site. Additionally, the 19 nucleotides linker region is maintained post NHEJ. Since the 3' binding site is the more promiscuous binding motif (Chao *et al.*, 2010; Patel *et al.*, 2012), it is possible the

second –ACA- sequence was sufficiently similar to support ZBP1 binding (Figure 4-6).

Two independent and highly consistent studies, herein chapter 3 and Vedula *et al.*, 2017, demonstrated the 4 amino acid differences between β- and γ-actin proteins are dispensable for majority of actin functions. This striking result indicates regulatory elements within *Actb* nucleotides could be responsible for majority of *Actb* versus *Actg1* functional differences. One possibility is that a regulatory element resides within *Actb* intron 2, and its removal in gene-targeted KOs is responsible for the lethality phenotype. Another possibility is the resultant product from cre-mediated recombination produces a toxic transcript or truncated protein. Nonetheless, the zipcode sequence is still the most well studied regulatory element that could explain differential *Actb* and *Actg1* functions. Potentially, certain fundamental cellular processes require regulated and targeted expression of actin proteins. In order to do so, cells must maintain a high concentration of actin transcript pool, and cells can achieve this by regulating *Actb* via the zipcode and ZBP1. This hypothesis is strengthened by my data demonstrating that MEFs express 6-fold more *Actb* transcript than *Actg1* transcript even though their respective proteins are expressed to similar levels (Patrinostro *et al.*, 2017). Additionally, recent single molecule imaging in embryonic axons illustrated *Actb* mRNA translation occurs within 20 seconds of ligand stimulation, demonstrating growing axon terminals require rapid translation of β-actin protein in response to stimuli (Ströhl *et al.*, 2017). Finally, ZBP1 is predominantly expressed during embryonic development (Hansen *et al.*, 2004)

and localized β-actin expression is important for developing neurons (Zhang *et al.*, 2001; Eom *et al.*, 2003; Yao *et al.*, 2006) which suggest that developmental cellular processes may require zipcode function more than adult tissues. The developmental role is further strengthened by research illustrating the *Actb* mRNA zipcode regulates epithelial adherens junction assembly but not maintenance (Gutierrez *et al.*, 2014). Overall, the literature suggests that developmental processes employ the zipcode to regulate actin mRNA localization and translation, thereby allowing the cell to quickly translate protein for dynamic processes. To truly test this hypothesis, it remains necessary to generate and characterize a mouse line where zipcode function is completely abrogated.

Methods

Cell Culture: Primary MEFs were cultured from E13.5 WT, *Actb*$^{ZD25\text{-}39}$ heterozygous and homozygous mouse embryos as described previously (Bunnell and Ervasti, 2010). Cells were grown to 80% confluency on 10-cm plates and frozen down at passage 1 at 1x10^6 cells/mL in MEF freezing media (95% FBS and 5% dimethyl sulfoxide). Primary MEFs from individual embryos were thawed and cultured in MEF media (DMEM supplemented with 10% FBS, 1% Pen/Strep, 0.5ug/mL Fungizone), grown to 80% confluency.

TALEN construction and purification: TALEN constructs were generated in collaboration with the Voytas lab at the University of Minnesota Center for Genome Engineering using the Golden Gate TALEN assembly method (Cermak *et al.*, 2011) into RCIscript-GoldyTALEN backbone (Addgene #38142, Carlson *et al.*, 2012). TALEN DNA constructs were transformed into DH5α cells, miniprepped with Wizard ® *Plus* SV Minipreps DNA Purification System (Promega, Cat. #A1460), linearized with the BamHI restriction enzyme (New England Biolabs Inc. Cat. #R3136S), and then phenol/chloroform purified. TALEN RNAs were *in vitro* transcribed from purified linearized DNA using the mMESSAGE mMACHINE® T3 Transcription Kit. (Thermo Fisher Scientific, Cat. #AM1348) and then purified using the MEGAclear™ Kit. (Thermo Fisher Scientific, Cat. #AM1908M) following manufacture protocols. Purified RNAs were stored at -80°C until use. Please see supplemental methods for full TALEN RVDs sequences.

Generating genome engineered mice and validation:

TALEN RNA pairs (25ng/µL) and the corresponding *Actb* 3'UTR PAGE Ultramer ssOligo donor (15ng/µL) template (Integrated DNA Technologies) were sent to the Mouse Genetics Laboratory at The University of Minnesota for pronuclear microinjection into fertilized C57BL/6 zygotes, which were then implanted into pseudo-pregnant female mice. The donor template contained 14 nucleotide alterations to disrupt ZBP1 binding, TALEN re-binding to the edited locus, and to insert a BamHI site for restriction fragment length polymorphism (RFLP) analysis. Genomic DNA from all F0 mouse pup tail samples was purified (PureLink® Genomic DNA Mini Kit) and assessed by RFLP assay with the BamHI restriction enzyme (New England Biolabs Inc. Cat. #R3136S) and Sanger sequenced for donor template integration. Primers used for RFLP: *Actb* Zipcode F 5'-TCAGCAAGCAGGAGTACGATG-3', *Actb* Zipcode R 5'-CCTCAGACCTGGGCCATT-3'.

Western blotting

MEF and tissue protein was extracted with 1% SDS buffer in 1x PBS and a cocktail of protease inhibitors (100 µM aprotinin, 0.79 mg/ml benzamide, 10 nM E-64, 10 µM leupeptin, 0.1 mg/ml pepstatin, 1 mM phenylmethylsulfonyl fluoride), sonicated (Model 150V/T Ultrasonic homogenizer; BioLogics), boiled, and centrifuged to remove the insoluble fraction. Equal amounts of cleared total lysate protein (25 µg) were blotted with antibodies β-actin (AC-15; Sigma-Aldrich), γ-actin (mAb 117), α_{sm}-actin (A14; Sigma-Aldrich), Pan-actin (C4), with

glyceraldehyde 3-phosphate dehydrogenase (GAPDH; G9545 or G8795; Sigma-Aldrich) as loading control.

ZBP1-*Actb* mRNA Immunoprecipitation

RNA-IP assays were performed using the RIP-Assay Kit (MBL International, Cat# RN1001) according to manufacture protocols with antibodies anti-IGF2BP1/IMP1/ZBP1 (MBL International, Cat# RN007P), and anti-IGF2BP2/IMP2/ZBP1 (MBL International, Cat# RN008P). WT, *Actb*^{MutZip} heterozygous and homozygous primary MEF lysates were prepped according to RIP-Assay Kit protocols.

qRT-PCR

Generation of WT mouse β_{cyto}-actin control construct was previously described in Patrinostro *et al.*, 2017. RNA eluted from ZBP1 and ZBP2 RNA-IP were purified according to RIP-Assay Kit protocols. RNA concentration and purity (260/280 ratio) were determined using a NanoDrop spectrophotometer (Wilmington, DE). First-strand cDNA was synthesized with a Bio-Rad iScript Advanced cDNA Synthesis Kit for qRT-PCR using the same initial RNA amount (1 µg) for all samples. β_{cyto}-actin control construct was used in a 10-fold dilution to generate a standard curve, and RIP eluted samples were amplified in parallel with specific β_{cyto}-actin qRT-PCR primer set using Bio-Rad SsoAdvanced Universal SYBR polymerase on the Bio-Rad CFX96 Real Time System C1000 Touch Thermal Cycler to profile each actin isoform transcript amount (picomoles).

Animal care:

All mice were tail-clipped and genotyped at weaning (3 weeks) and kept alive until at least 6 months of age for Kaplan-Meier analysis. Heterozygous crosses were used to calculate Mendelian birth ratios. Animals were housed and treated in accordance with the standards set by the University of Minnesota Institutional Animal Care and Use Committee.

Supplemental Methods

Actb 3'UTR, left arm	**RVD:** NN NG NG NI HD NG NN NI NN HD NG NN HD NN NG NG NG NN NG NG NI HD NG NN NI NN HD **DNA sequence:** CTGACCCCGGACCAAGTGGTGGCTATCGCCAGCAACAATG GCGGCAAGCAAGCGCTCGAAACGGTGCAGCGGCTGTTGC CGGTGCTGTGCCAGGACCATGGCCTGACCCCGGACCAAG TGGTGGCTATCGCCAGCAACGGTGGCGGCAAGCAAGCGC TCGAAACGGTGCAGCGGCTGTTGCCGGTGCTGTGCCAGG ACCATGGCCTGACCCCGGACCAAGTGGTGGCTATCGCCA GCAACGGTGGCGGCAAGCAAGCGCTCGAAACGGTGCAGC GGCTGTTGCCGGTGCTGTGCCAGGACCATGGCCTGACCC CGGACCAAGTGGTGGCTATCGCCAGCAACATTGGCGGCA AGCAAGCGCTCGAAACGGTGCAGCGGCTGTTGCCGGTGC TGTGCCAGGACCATGGCCTGACTCCGGACCAAGTGGTGG CTATCGCCAGCCACGATGGCGGCAAGCAAGCGCTCGAAA CGGTGCAGCGGCTGTTGCCGGTGCTGTGCCAGGACCATG GCCTGACCCCGGACCAAGTGGTGGCTATCGCCAGCAACG GTGGCGGCAAGCAAGCGCTCGAAACGGTGCAGCGGCTGT TGCCGGTGCTGTGCCAGGACCATGGCCTGACCCCGGACC AAGTGGTGGCTATCGCCAGCAACAATGGCGGCAAGCAAG CGCTCGAAACGGTGCAGCGGCTGTTGCCGGTGCTGTGCC AGGACCATGGCCTGACCCCGGACCAAGTGGTGGCTATCG CCAGCAACATTGGCGGCAAGCAAGCGCTCGAAACGGTGC AGCGGCTGTTGCCGGTGCTGTGCCAGGACCATGGCCTGA CCCCGGACCAAGTGGTGGCTATCGCCAGCAACAATGGCG GCAAGCAAGCGCTCGAAACGGTGCAGCGGCTGTTGCCGG TGCTGTGCCAGGACCATGGCCTGACTCCGGACCAAGTGGT GGCTATCGCCAGCCACGATGGCGGCAAGCAAGCGCTCGA AACGGTGCAGCGGCTGTTGCCGGTGCTGTGCCAGGACCA

	TGGCCTGACCCCGGACCAAGTGGTGGCTATCGCCAGCAA CGGTGGCGGCAAGCAAGCGCTCGAAACGGTGCAGCGGCT GTTGCCGGTGCTGTGCCAGGACCATGGCCTGACCCCGGA CCAAGTGGTGGCTATCGCCAGCAACAATGGCGGCAAGCAA GCGCTCGAAACGGTGCAGCGGCTGTTGCCGGTGCTGTGC CAGGACCATGGCCTGACTCCGGACCAAGTGGTGGCTATC GCCAGCCACGATGGCGGCAAGCAAGCGCTCGAAACGGTG CAGCGGCTGTTGCCGGTGCTGTGCCAGGACCATGGCCTG ACCCCGGACCAAGTGGTGGCTATCGCCAGCAACAATGGC GGCAAGCAAGCGCTCGAAACGGTGCAGCGGCTGTTGCCG GTGCTGTGCCAGGACCATGGCCTGACCCCGGAC CAAGTGGTGGCTATCGCCAGCAACGGTGGCGGCAAGCAA GCGCTCGAAACGGTGCAGCGGCTGTTGCCGGTGCTGTGC CAGGACCATGGCCTGACCCCGGACCAAGTGGTGGCTATC GCCAGCAACGGTGGCGGCAAGCAAGCGCTCGAAACGGTG CAGCGGCTGTTGCCGGTGCTGTGCCAGGACCATGGC
Actb 3'UTR, right arm	**RVD:** NN HD NN HD NI NI NN NG NG NI NN NN NG NG NG NG NN NG HD NN HD NN HD NI NI NN NG NG NI **DNA sequence**: CTGACCCCGGACCAAGTGGTGGCTATCGCCAGCAACAATG GCGGCAAGCAAGCGCTCGAAACGGTGCAGCGGCTGTTGC CGGTGCTGTGCCAGGACCATGGCCTGACTCCGGACCAAG TGGTGGCTATCGCCAGCCACGATGGCGGCAAGCAAGCGC TCGAAACGGTGCAGCGGCTGTTGCCGGTGCTGTGCCAGG ACCATGGCCTGACCCCGGACCAAGTGGTGGCTATCGCCA GCAACAATGGCGGCAAGCAAGCGCTCGAAACGGTGCAGC GGCTGTTGCCGGTGCTGTGCCAGGACCATGGCCTGACTC CGGACCAAGTGGTGGCTATCGCCAGCCACGATGGCGGCA AGCAAGCGCTCGAAACGGTGCAGCGGCTGTTGCCGGTGC TGTGCCAGGACCATGGCCTGACCCCGGACCAAGTGGTGG CTATCGCCAGCAACATTGGCGGCAAGCAAGCGCTCGAAAC GGTGCAGCGGCTGTTGCCGGTGCTGTGCCAGGACCATGG CCTGACCCCGGACCAAGTGGTGGCTATCGCCAGCAACATT GGCGGCAAGCAAGCGCTCGAAACGGTGCAGCGGCTGTTG CCGGTGCTGTGCCAGGACCATGGCCTGACCCCGGACCAA GTGGTGGCTATCGCCAGCAACAATGGCGGCAAGCAAGCG CTCGAAACGGTGCAGCGGCTGTTGCCGGTGCTGTGCCAG GACCATGGCCTGACCCCGGACCAAGTGGTGGCTATCGCC AGCAACGGTGGCGGCAAGCAAGCGCTCGAAACGGTGCAG CGGCTGTTGCCGGTGCTGTGCCAGGACCATGGCCTGACC CCGGACCAAGTGGTGGCTATCGCCAGCAACGGTGGCGGC AAGCAAGCGCTCGAAACGGTGCAGCGGCTGTTGCCGGTG CTGTGCCAGGACCATGGCCTGACCCCGGACCAAGTGGTG GCTATCGCCAGCAACATTGGCGGCAAGCAAGCGCTCGAAA

	CGGTGCAGCGGCTGTTGCCGGTGCTGTGCCAGGACCATG GCCTGACCCCGGACCAAGTGGTGGCTATCGCCAGCAACA ATGGCGGCAAGCAAGCGCTCGAAACGGTGCAGCGGCTGT TGCCGGTGCTGTGCCAGGACCATGGCCTGACCCCGGACC AAGTGGTGGCTATCGCCAGCAACAATGGCGGCAAGCAAG CGCTCGAAACGGTGCAGCGGCTGTTGCCGGTGCTGTGCC AGGACCATGGCCTGACCCCGGACCAAGTGGTGGCTATCG CCAGCAACGGTGGCGGCAAGCAAGCGCTCGAAACGGTGC AGCGGCTGTTGCCGGTGCTGTGCCAGGACCATGGCCTGA CCCCGGACCAAGTGGTGGCTATCGCCAGCAACGGTGGCG GCAAGCAAGCGCTCGAAACGGTGCAGCGGCTGTTGCCGG TGCTGTGCCAGGACCATGGCCTGACCCCGGACCAAGTGG TGGCTATCGCCAGCAACGGTGGCGGCAAGCAAGCGCTCG AAACGGTGCAGCGGCTGTTGCCGGTGCTGTGCCAGGACC ATGGCCTGACCCCGGACCAAGTGGTGGCTATCGCCAGCA ACGGTGGCGGCAAGCAAGCGCTCGAAACGGTGCAGCGGC TGTTGCCGGTGCTGTGCCAGGACCATGGCCTGACCCCGG ACCAAGTGGTGGCTATCGCCAGCAACAATGGCGGCAAGCA AGCGCTCGAAACGGTGCAGCGGCTGTTGCCGGTGCTGTG CCAGGACCATGGCCTGACCCCGGACCAAGTGGTGGCTAT CGCCAGCAACGGTGGCGGCAAGCAAGCGCTCGAAACGGT GCAGCGGCTGTTGCCGGTGCTGTGCCAGGACCATGGC

ssOligo Donor Sequences:

Target Site	**Sequence (5'→3')**
Actb 3'UTR	ACTCTGTGTGGATCGGTGGCTCCATCCTGGCCTCACTGTCCAC CTTCCAGCAGATGTGGATCAGCAAGCAGGAGTACGATGAGTC CGGCCCCTCCATCGTGCACCGCAAGTGCTTCTAGGACCTATG CTCCTGAGCTGCATTTTACAGAGTTTCTTTGACGGATCCTAACT TGCACAGAAAAAAAAAAAATAAGAGACAA

Figures

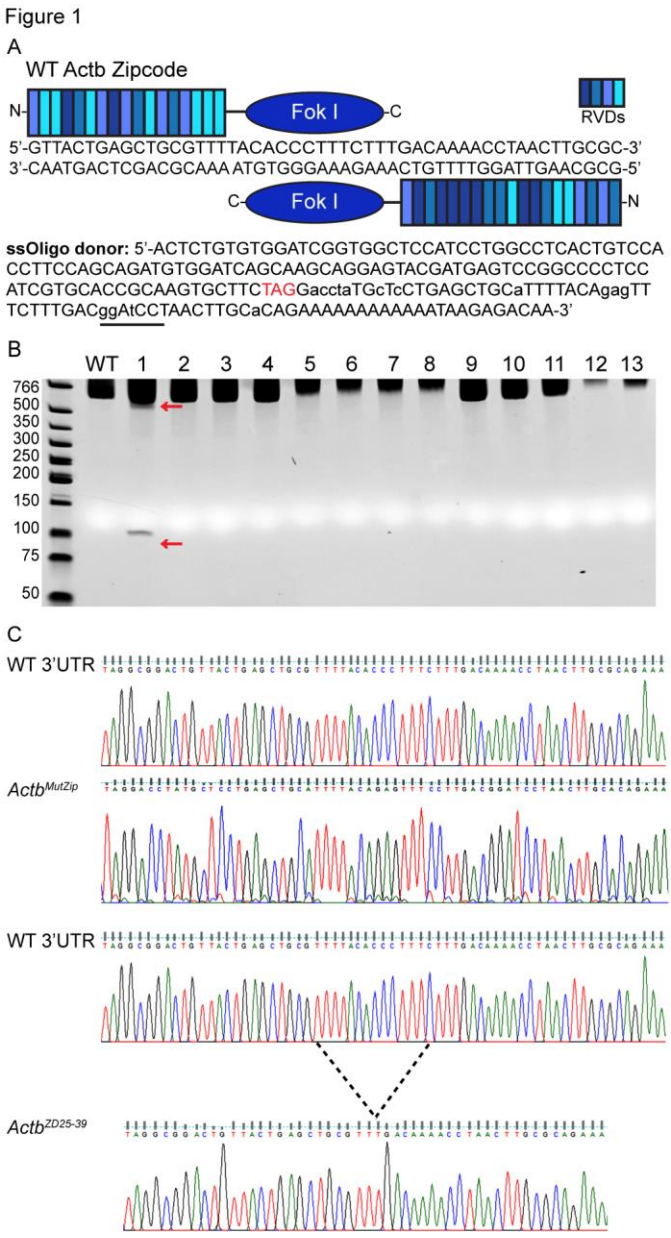

Figure 4-1 Genetically engineered *Actb*$^{ZD25-39}$ mice via TALENs and a single-strand oligo donor. (A) Schematic of TALEN target sequence within the WT mouse *Actb* exon 6 sequence and the ssOligo homologous repair donor sequence. The stop codon is labeled in red, BamHI restriction enzyme site is

underlined in black, edited nucleotides are denoted in lower case letters. (B) RFLP results of WT and live born F0 pups using the BamHI restriction enzyme digestion. Red arrows indicate the correct digested fragments. (C) Sanger sequence results for WT and pup number 1 and 2.

A

	# of pups	Birth Ratio	Chi-Sq p= 47.9
WT	29	25.9	
Het	59	52.68	
Hom	24	21.43	
N= litters 19, Average litter size = 5.89			

B

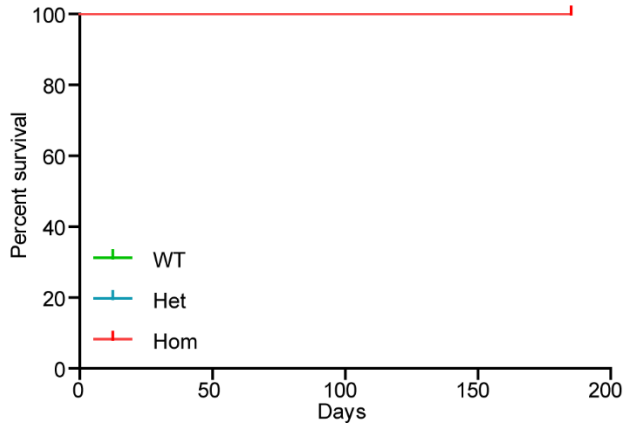

Figure 4-2 *Actb*$^{ZD25-39}$ mice are born at Mendelian ratios and do not exhibit an early lethality phenotype. (A) Calculated Mendelian genetic ratio of WT, heterozygous and homozygous *Actb*$^{ZD25-39}$ mice at weaning (21 days post birth). N=19 Het x Het crosses. (B) Kaplan-Meier survival curve of wildtype, heterozygous and homozygous *Actb*$^{ZD25-39}$ mice from 0-180 days post birth. N=30 per genotype.

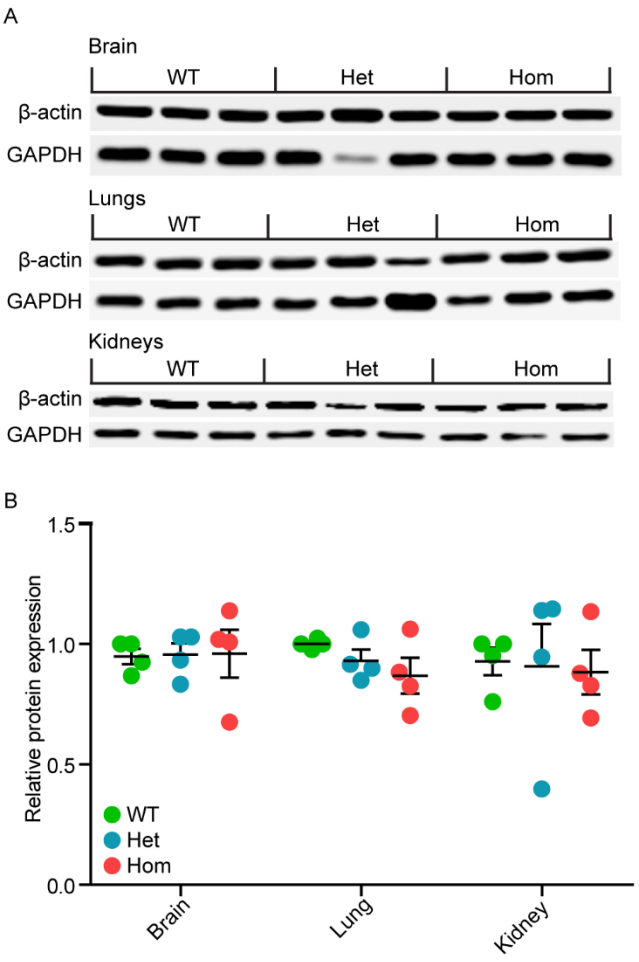

Figure 4-3 β_{cyto}-actin protein expression in *Actb*$^{ZD25-39}$ mice tissues. (A) Western blot images of WT, *Actb*$^{ZD25-39}$ heterozygous and homozygous brain, lung and kidney tissues blotted for β_{cyto}-actin and GAPDH. (B) Calculated relative β_{cyto}-actin protein expression in WT, heterozygous and homozygous *Actb*$^{ZD25-39}$ mice brain, lung and kidneys. X-axis denotes tissue. Y-axis denotes relative protein expression which were normalized to GAPDH and relative to a WT sample. Error bars are S.E.M.

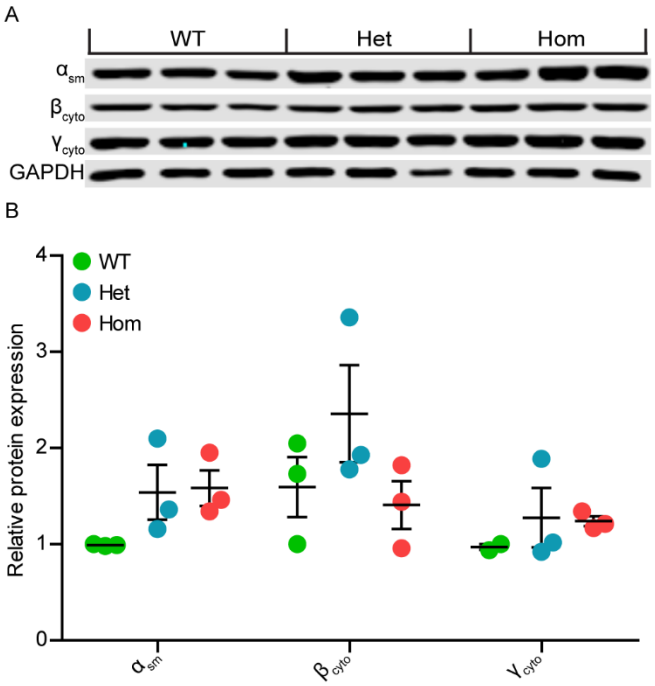

Figure 4-4 Actin isoform expression in *Actb*$^{ZD25-39}$ primary MEFs. (A) Western blot images of WT, heterozygous and homozygous *Actb*$^{ZD25-39}$ MEFs blotted for α_{sm}-, β_{cyto}-, γ_{cyto}-actin, and GAPDH. (B) Calculated relative isoactin protein expression in WT, heterozygous and homozygous *Actb*$^{ZD25-39}$ MEFs. X-axis denotes actin isoform. Y-axis denotes relative protein expression which were normalized to GAPDH and relative to a WT sample. Error bars are S.E.M.

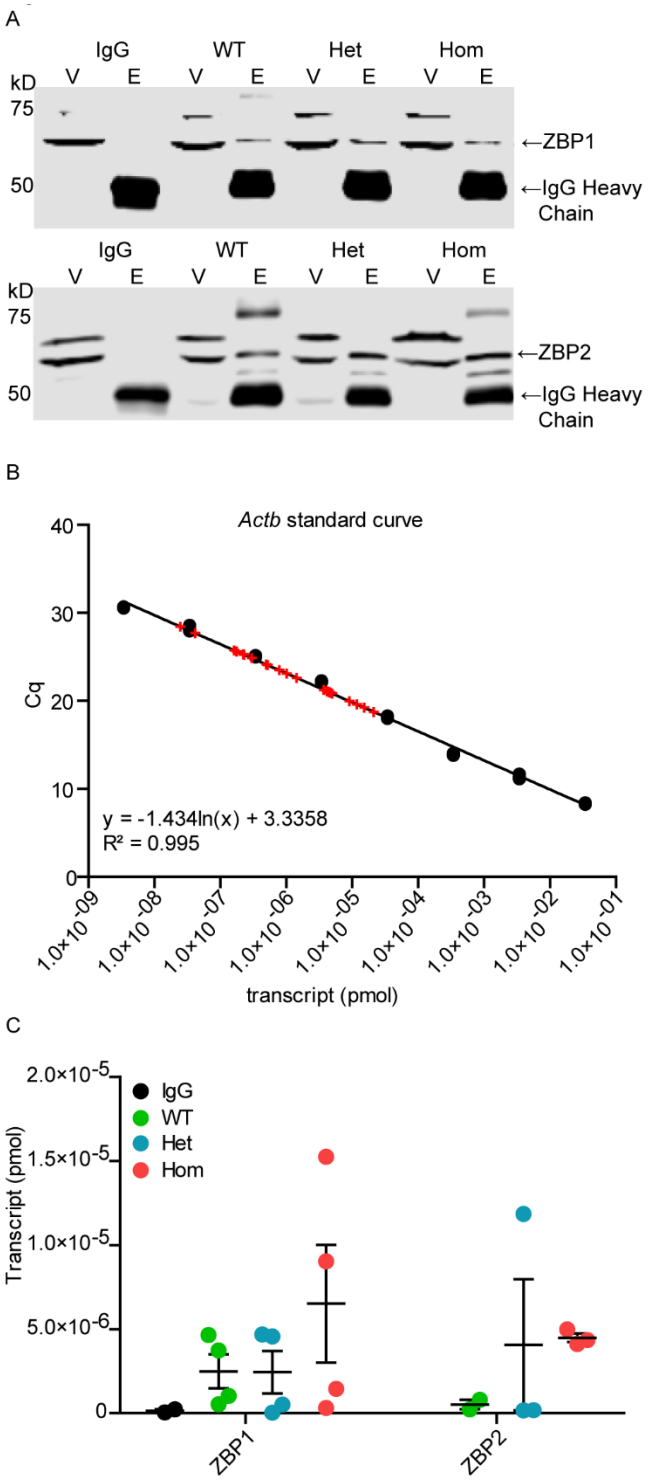

Figure 4-5 ZBP1 and ZBP2 RNA-IP in primary MEFs. (A) Representative RNA-IP images of ZBP1 and ZBP2 with primary MEF mRNA lysates. IgG is used

as negative control. V= void, E=elute. (B) Representative β_{cyto}-actin qRT-PCR of ZBP1 and ZBP2 RNA-IP eluted mRNA. (C) Calculated amount of β_{cyto}-actin transcript from ZBP1 and ZBP2 RNA-IP. X-axis denotes protein and Y-axis denotes transcript in pmol.

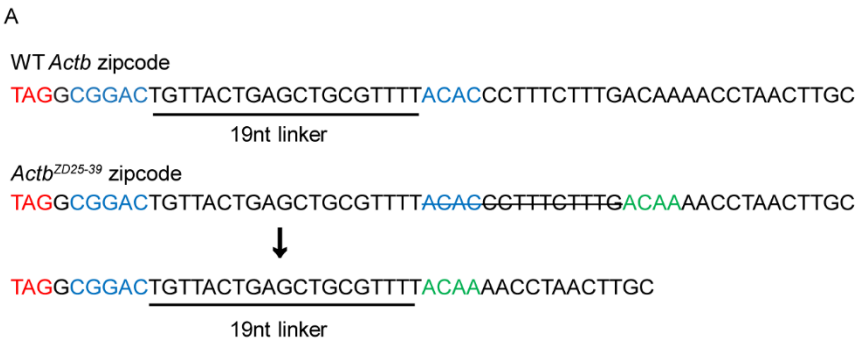

Figure 4-6 TALEN mediated *Actb* zipcode deletion synopsis. (A) WT *Actb* zipcode and the resultant *Actb*$^{ZD25\text{-}39}$ sequence. The stop codon is labeled in red, ZBP1 binding sites are labeled in blue, the possible pseudo 3' ZBP1 binding site is labeled in green.

Chapter 5

Conclusions and Future Directions

Thesis Findings

In addressing the questions proposed at the beginning of my thesis, my major findings are as follows:

Q1: How do different KO and KD methodologies affect β-actin function and biological findings?

A1: Both cre-mediated KO and siRNA mediated KD methodologies resulted in comparable and consistent data in primary MEFs demonstrating that the loss of *Actb* is more disruptive to cell function than is the loss of *Actg1*. However, SV40 largeT antigen transformed MEFs are able to support fibroblast proliferation in the absence of *Actb* through an unknown mechanism.

Q2: Do the four-amino acid differences between β- and γ-actin contribute to functional differences in cells or tissues?

A2: Genome edited mice, $Actb^{c\text{-}g}$, expressing γ-actin protein at the endogenous *Actb* locus are viable and lack the most severe phenotypes seen in previous *Actb* KO models, indicating β-actin protein is dispensable for most cellular functions. Nonetheless, $Actb^{c\text{-}g}$ mice displayed progressive hearing loss and degeneration of actin-based stereocilia indicating that amino acid sequence differences between isoforms are crucial for function in some specialized cell types.

Q3: How important is the *Actb* zipcode sequence and ZBP1 binding *in vivo*?

A3: The *Actb*$^{ZD25\text{-}39}$ mice were wildtype like in all categories tested, possibly due to a pseudo-ZBP1 binding site created post NHEJ. It is necessary to make another attempt to edit both ZBP1 binding sites in the *Actb* zipcode to assess its importance *in vivo*.

Conclusions

Cytoplasmic actins are highly homologous and conserved from birds to mammals. They differ by only 4 functionally similar amino acids on their N-terminus, and are ubiquitously expressed in all cells (Perrin and Ervasti, 2010). Recent research has demonstrated multiple mechanisms of transcriptional and translational regulation for the cytoplasmic actins. Additionally, individual gene targeted *Actb* and *Actg1* KO models indicated β- and γ-actins serve both unique and redundant functions, yet more questions remain. The combined work presented in this thesis elucidated important new aspects of actin regulation and provided us with a better understanding how two highly conserved genes are regulated both individually and collectively.

Multiple groups have described several specific *Actb* and *Actg1* cellular functions by using various KD and KO model systems. Previous whole body gene-targeted *Actb* and *Actg1* KO mouse models have consistently demonstrated that mice lacking β-actin are embryonically lethal (Shawlot *et al.*, 1998; Shmerling *et al.*, 2005; Bunnell *et al.*, 2011) leading scientists to believe that *Actb* is an essential gene. In contrast, *Actg1* KO mice are viable up to 2 years (Belyantseva *et al.*, 2009). Cell based assays have yielded conflicting results in terms of possible unique *Actb* and *Actg1* functions. Two *Actb* gene KO studies in MEFs both demonstrated cells lacking β-actin displayed cell migration defects and altered gene expression profiles leading to increased *Acta2* expression, but had conflicting reports on the effect of *Actb* ablation on cell proliferation (Bunnell *et al.*, 2011; Tondeleir *et al.*, 2012). Furthermore, others

using human derived cell lines show the same effects on cell motility and increased *Acta2* expression in *Actg1* KD (Dugina *et al.*, 2009; Shum *et al.*, 2011; Lechuga *et al.*, 2014) as we have seen in *Actb* KOs (Bunnell *et al.*, 2011).

Here, in chapter 2 and in Patrinostro *et al.*, 2017, we used both cre-mediated KO and siRNA mediated KD in the same cells to conclusively determine the effects of ablating either *Actb*, *Actg1* or both in both primary and immortalized MEFs. We illustrated in primary MEFs, the predominant actin isoform expressed are *Acta2*, *Actb* and *Actg1*. Even though *Actb* transcript was expressed 6-fold higher than *Actg1*, both cytoplasmic actin protein levels were expressed to similar levels. Ablation of *Actb* in primary MEFs resulted in drastic increase of *Acta2* expression, decreased cell proliferation, decreased cellular ATP concentration and increased fibroblast to myofibroblast transition related gene expression. Ablation of *Actg1* did not elicit the same dramatic cellular response in primary MEFs. Additionally, targeting by either cre-recombinase or siRNA did not alter the resultant data, indicating previously described data inconsistency between multiple groups could be due in part to cell type differences. Finally, we measured drastic defects in cell proliferation when *Actb* is ablated in primary cells, but SV40 LargeT antigen transformed MEFs rendered *Actb* nonessential for proliferation. As cell immortalization is associated with substantial changes in gene expression (Kuo, Burl and Hu, 2012; Gordon *et al.*, 2014), an altered cellular expression profile could explain this confounding difference between primary and immortalized cells. Overall, we conclude studies

using primary cells are a more appropriate model to analyze embryonic lethality associated with *Actb* KO mice.

Although gene-targeted ablation of either *Actb* or *Actg1* led to different phenotypes in both mice and cells, it was still unclear what caused these discrepancies. The two major differences between the cytoplasmic actins are mRNA regulation and the 4 amino acid variances on their N-terminus. A fundamental question of molecular biology is the importance of nucleotide sequence versus amino acid sequence and their implications on gene function. To distinguish the relative contributions of nucleotide and amino acid sequences to the unique functions of cytoplasmic actins, we used TALENs to engineer the endogenous *Actb* gene to express γ-actin instead of β-actin, while retaining all other regulatory elements in the gene (Chapter 3). Interestingly, the resulting mice, which lacked β-actin protein, had litter size and life spans similar to WTs. Additionally, the *Actb*$^{c\text{-}g}$ mice and MEFs also lacked all obvious phenotypes previously characterized in *Actb* KOs. These results demonstrated γ-actin protein can functionally replace β-actin in most cellular functions when expressed under the regulatory control of *Actb*. However, homozygous *Actb*$^{c\text{-}g}$ mice developed progressive hearing loss due to stereocilia degeneration, similar to hair-cell specific *Actb* KO mice (Perrin, Sonnemann and Ervasti, 2010; Perrin *et al.*, 2013), which may be due to the fact that β-actin protein is required for stereocilia maintenance. We observed β-actin enrichment at the stereocilia tips during development, and that β-actin is displaced by γ-actin in mature stereocilia. The preferential localization of β-actin to the growing tips and the progressive

degeneration of row 2 and 3 stereocilia in aging *Actb*$^{c\text{-}g}$ mice suggests β-actin is required for stereocilia regrowth, which is necessary to maintain stereocilia length and auditory function. Collectively, our data indicate that β-actin protein has functions in certain specialized cell types that cannot be compensated for by γ-actin.

Since amino acid differences are dispensable for some functions of β-actin, we next assessed the importance of the zipcode in an *in vivo* model. We used TALENs to edit the endogenous *Actb* zipcode sequence to disrupt *Actb* mRNA-ZBP1 association. Unfortunately, we were unable to generate a mouse model where both ZBP1 binding sites within the *Actb* zipcode were rendered nonfunctional. Instead, we were successful in generating the *Actb*$^{ZD25\text{-}39}$ mouse line, where the predicted 3' ZBP1 binding site was deleted. The *Actb*$^{ZD25\text{-}39}$ mice were wildtype like in all assessments and were still able to bind to ZBP1 *in vitro*. This initially suggested that *Actb* transcript can bind to ZBP1 without the 3' binding site. However, upon closer inspection, a downstream -ACA- sequence was shifted into the original binding site locus and allowed the retention of ZBP1 binding capabilities.

Future Directions

Although the work presented in this thesis answered and clarified several questions important to the field of actin biology, it also ignited new questions. The first question is why are *Actb*$^{c\text{-}g}$ mice viable but the cre-mediated *Actb* KO mice are embryonic lethal? One possibility is that some of the phenotypes observed following cre-mediated deletion of *Actb* exons 2-3 are independent of normal *Actb* function. It is possible that gene recombination produces a toxic transcript and/or truncated protein. Recently, the NCBI nucleotide database reported a novel predicted *Actg1* isoform (NM_001313923.1). The predicted transcript contains an alternative start codon in exon 4 to yield a truncated protein encoding only exons 4-6 of the *Actg1* gene. There are no known functions of the predicted truncated γ-actin protein and it has not been determined if *Actb* has a similar alternative start codon. Since *Actb* and *Actg1* are over 90% identical in their coding sequence, it is possible that a similar alternative start codon could exist for *Actb*.

In cre-mediated *Actb* and *Actg1* KO MEFs, expression of the recombined transcript lacking exons 2 and 3 is markedly elevated compared to WT transcript in control cells (Ervasti lab, unpublished data). Therefore, it is conceivable that a highly expressed recombined transcript causes a toxic effect in cells. A possible mechanism for this toxicity is that the highly expressed recombined transcript shunts ZBP1 from other crucial mRNAs. ZBP1 is known to also bind and regulate many other critical genes, such as Tau, c-myc and β-catenin (Yisraeli, 2005), therefore it is plausible the lethality phenotype we observe in *Actb* KOs is not due

to the loss of β-actin protein, but rather to delocalization of other essential mRNAs. Notably, in the *Actb* loss of function human patient population, two known point mutations are predicted to escape nonsense-mediated decay (Cuvertino *et al.*, 2017). Therefore, it is conceivable that a toxic *Actb* transcript is responsible for the some of the phenotypes we observe in the *Actb* KO models.

Any truncated protein produced from *Actb* or *Actg1* exons 4-6 will be identical and this truncated protein could disrupt filament formation. Although the truncated protein derived from exons 4-6 of *Actb* and *Actg1* will be identical, their respective transcripts will be regulated differently because of the *Actb* zipcode. Therefore, another hypothesis is that the truncated protein is more disruptive in the *Actb* KO because it will be enriched at the cell periphery inhibiting filament formation for critical functions such as cell migration. Even though *Actg1* KO cells could also express the truncated protein, since it is diluted throughout the cell, it is less detrimental. To test this theory, we will use a C-terminal pan actin antibody and blot for any truncated protein product in the *Actb* and *Actg1* KO cells. If a truncated protein is detected in cell lysates, we would next use immunofluorescent imaging to detect where the truncated proteins are located within cells. Finally, we would *in vitro* express the truncated protein and perform polymerization assays to determine possible mechanisms.

Finally, it is not well understood what specific changes between primary and the immortalized MEFs led to the divergent cell proliferation phenotypes seen in the perspective *Actb* KOs (Patrinostro *et al.*, 2017). However, it is known the immortalized cells have higher intracellular RNase activity (Personal

communications with Dr. Jeongsik Yong). Therefore, if immortalized cells can suppress the recombined transcript expression, it could explain why immortalized MEFs can tolerate *Actb* ablation while primary MEFs cannot. To assess if this is true, we quantitively determined the amount of aberrant transcript in both primary and immortalized *Actb* KO MEFs and found that aberrant transcript was significantly increased in only the primary MEFs and not in the immortalized MEFs (Figure 5-1). To further determine if the recombined transcript is truly toxic, we will next exogenously express the *Actb* transcript, without exons 2-3, into wildtype MEFs and measure cell proliferation. We can also express *Actg1*, without exons 2-3, as a control because *Actg1* KO MEFs do not present a proliferation defect. We hypothesize the exogenously expressed aberrant *Actb*Δ2-3 transcript would negatively affect WT MEF cell proliferation, in a similar manner as seen in *Actb* KO MEFs. Overall, we predict a combination of factors synergistically contribute to the distinct phenotypes we've observed between *Actb* KO and $Actb^{c\text{-}g}$ mice. We will analyze multiple avenues to determine the cause.

Another hypothesis is that all essential cytoplasmic actin function requires the zipcode, which is most important during development, when ZBP1 is also abundantly expressed (Hansen *et al.*, 2004). Any cellular processes that require precise spatial and temporal actin expression utilize the zipcode as the regulatory mechanism. Consistent with this hypothesis, *Actb* transcript is more abundant than *Actg1* transcript in primary MEFs even when β- and γ- actin protein levels are similarly expressed (Patrinostro *et al.*, 2017). Additionally, our findings in

chapter 3 and the recently published Vedula *et al.*, 2017 illustrated the 4 amino acid variances between β- and γ- actin protein are not critical to most cellular functions. It seems likely that transcript targeting and regulated translation via the zipcode is the essential feature of *Actb.*

Although we were unsuccessful in generating a mouse model where both *Actb* zipcode binding motifs were mutated to disrupt ZBP1-mRNA binding, in future studies it is pertinent to repeat pronuclear injection to generate the edited *Actb* zipcode mice again. To do so, we will first ensure the mutated zipcode does not bind to the zipcode *in vitro*. We will express the full *Actb* transcript with the mutated zipcode in fibroblast and then proceed to perform a RNA-IP with ZBP1 to assess protein-RNA interaction. Once we ensure the mutated zipcode cannot bind to ZBP1, we will then again perform pronuclear injection to generate the edited *Actb* zipcode mouse line. Once the mouse line is established, we will first assess mice viability and birth ratios to determine if the zipcode is essential for life. If the edited *Actb* zipcode mice are not viable, we will perform developmental assays to determine at what prenatal stage the pups perish, and compare it to the previous described *Actb* KO mice (Bunnell *et al.*, 2011). If the mice are viable, it will be interesting to perform biochemical assays to determine if the zipcode affect β-actin stability *in vivo*. It would also be of interest to form collaborations with neuroscientists to assess neuronal development as the *Actb* zipcode has classically been studied in neurite migration. Finally, *Actb* has been demonstrated to be polyadenylated (Ghosh *et al.*, 2008), but the significance this regulation is not well understood. It has not been demonstrated if ZBP1 binds

and regulates both *Actb* transcripts. Therefore, we will first test if ZBP1 binds to one or both *Actb* transcripts in WT samples and then possibly tease out if any phenotypes observed in the edited *Actb* zipcode mice is only associated with one of the *Actb* transcript. We hypothesize cells transition from an *Actb*-essential state to an *Actb*-important state as development and differentiation progress *in vivo* and the zipcode is required for this process.

Figures

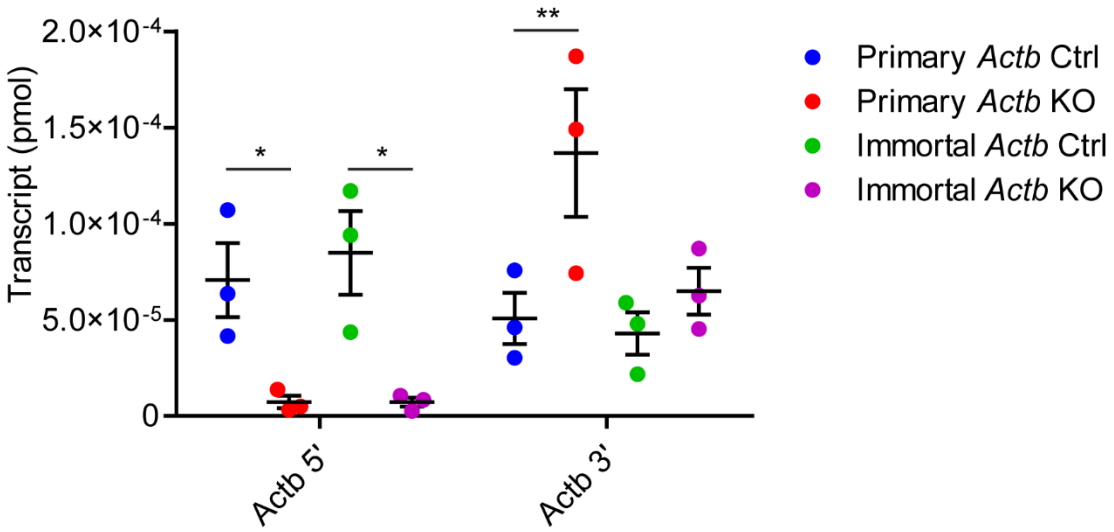

Figure 5-1 Transcript analysis in primary and immortalized MEFs. X-axis denotes the location of the primer set and the y-axis denotes amount of transcript in pmol. *Actb* 5' primers are located within *Actb* exon 2 and the *Actb* 3' primers are located in exon 6.

References

Almuzzaini, B., Sarshad, A. A., Rahmanto, A. S., Hansson, M. L., Von Euler, A., Sangfelt, O., Visa, N., Farrants, A. K. O. and Percipalle, P. (2016) 'In b-actin knockouts, epigenetic reprogramming and rDNA transcription inactivation lead to growth and proliferation defects', *The FASEB Journal*, 1(8), pp. 2860–73. doi: 10.1096/fj.201600280R.

Ampe, C. and Troys, M. Van (2017) *The Actin Cytoskeleton*. doi: 10.1007/978-3-319-46371-1.

Artman, L., Dormoy-Raclet, V., Von Roretz, C. and Gallouzi, I. E. (2014) 'Planning Your Every Move: The Role of Beta Actin and its Post-Transcriptional Regulation in Cell Motility', *Seminars in Cell & Developmental Biology*. Elsevier Ltd, pp. 1–11. doi: 10.1016/j.semcdb.2014.05.012.

Belanto, J. J., Mader, T. L., Eckhoff, M. D., Strandjord, D. M., Banks, G. B., Gardner, M. K., Lowe, D. A. and Ervasti, J. M. (2014) 'Microtubule binding distinguishes dystrophin from utrophin', *Proceedings of the National Academy of Sciences of the United States of America*, 111(15), pp. 5723–5728. doi: 10.1073/pnas.1323842111.

Belanto, J. J., Olthoff, J. T., Mader, T. L., Chamberlain, C. M., Nelson, D. M., McCourt, P. M., Talsness, D. M., Gundersen, G. G., Lowe, D. A. and Ervasti, J. M. (2016) 'Independent variability of microtubule perturbations associated with dystrophinopathy', *Human Molecular Genetics*, 25(22), pp. 4951–4961. doi: 10.1093/hmg/ddw318.

Belyantseva, I. A., Perrin, B. J., Sonnemann, K. J., Zhu, M., Stepanyan, R., McGee, J., Frolenkov, G. I., Walsh, E. J., Friderici, K. H., Friedman, T. B. and Ervasti, J. M. (2009) 'Gamma-actin is required for cytoskeletal maintenance but not development.', *Proceedings of the National Academy of Sciences of the United States of America*, 106(24), pp. 9703–8. doi: 10.1073/pnas.0900221106.

Bergeron, S. E., Zhu, M., Thiem, S. M., Friderici, K. H. and Rubenstein, P. A. (2010) 'Ion-dependent polymerization differences between mammalian beta- and gamma-nonmuscle actin isoforms.', *The Journal of biological chemistry*, 285(21), pp. 16087–95. doi: 10.1074/jbc.M110.110130.

Bunnell, T. M., Burbach, B. J., Shimizu, Y. and Ervasti, J. M. (2011) 'β-Actin specifically controls cell growth, migration, and the G-actin pool.', *Molecular biology of the cell*, 22(21), pp. 4047–58. doi: 10.1091/mbc.E11-06-0582.

Bunnell, T. M. and Ervasti, J. M. (2010) 'Delayed embryonic development and impaired cell growth and survival in Actg1 null mice.', *Cytoskeleton*, 67(9), pp.

564–72. doi: 10.1002/cm.20467.

Bunnell, T. M. and Ervasti, J. M. (2011) ‘Structural and functional properties of the actin gene family.’, *Critical reviews in eukaryotic gene expression*, 21(3), pp. 255–66.

Carlson, D. F., Tan, W., Lillico, S. G., Stverakova, D., Proudfoot, C., Christian, M., Voytas, D. F., Long, C. R., Whitelaw, C. B. A. and Fahrenkrug, S. C. (2012) ‘Efficient TALEN-mediated gene knockout in livestock’, *Proceedings of the National Academy of Sciences*, 109(43), pp. 17382–17387. doi: 10.1073/pnas.1211446109.

Cermak, T., Doyle, E. L., Christian, M., Wang, L., Zhang, Y., Schmidt, C., Baller, J. a, Somia, N. V, Bogdanove, A. J. and Voytas, D. F. (2011) ‘Efficient design and assembly of custom TALEN and other TAL effector-based constructs for DNA targeting.’, *Nucleic acids research*, 39(12), p. e82. doi: 10.1093/nar/gkr218.

Chao, J. A., Patskovsky, Y., Patel, V., Levy, M., Almo, S. C. and Singer, R. H. (2010) ‘ZBP1 recognition of beta-actin zipcode induces RNA looping.’, *Genes & development*, 24(2), pp. 148–58. doi: 10.1101/gad.1862910.

Cheever, T. R., Li, B. and Ervasti, J. M. (2012) ‘Restricted morphological and behavioral abnormalities following ablation of beta-actin in the brain’, *PLoS ONE*, 7(3). doi: 10.1371/journal.pone.0032970.

Cheever, T. R., Li, B. and Ervasti, J. M. (2012) ‘Restricted morphological and behavioral abnormalities following ablation of β-actin in the brain.’, *PloS one*, 7(3), p. e32970.

Cheever, T. R., Olson, E. A. and Ervasti, J. M. (2011) ‘Axonal regeneration and neuronal function are preserved in motor neurons lacking beta-actin In Vivo’, *PLoS ONE*, 6(3), pp. 1–13. doi: 10.1371/journal.pone.0017768.

Condeelis, J. and Singer, R. H. (2005) ‘How and why does beta-actin mRNA target?’, *Biology of the cell*, 97(1), pp. 97–110. doi: 10.1042/BC20040063.

Cordes, K. R., Sheehy, N. T., White, M. P., Berry, E. C., Morton, S. U., Muth, A. N., Lee, T. H., Miano, J. M., Ivey, K. N. and Srivastava, D. (2009) ‘miR-145 and miR-143 regulate smooth muscle cell fate and plasticity.’, *Nature*. Nature Publishing Group, 460(7256), pp. 1–7. doi: 10.1038/nature08195.

Cuvertino, S., Stuart, H. M., Chandler, K. E., Roberts, N. A., Armstrong, R., Bernardini, L., Bhaskar, S., Callewaert, B., Clayton-Smith, J., Davalillo, C. H., Deshpande, C., Devriendt, K., Digilio, M. C. and Banka, S. (2017) ‘ACTB Loss-of-Function Mutations Result in a Pleiotropic Developmental Disorder’, 13(13), pp. 1021–1033. doi: 10.1016/j.ajhg.2017.11.006.

Davis, J. and Molkentin, J. D. (2013) ‘Myofibroblasts: Trust your heart and let fate decide.’, *Journal of molecular and cellular cardiology*. Elsevier B.V., 70, pp. 9–18. doi: 10.1016/j.yjmcc.2013.10.019.

Di Donato, N., Rump, A., Koenig, R., Der Kaloustian, V. M., Halal, F., Sonntag, K., Krause, C., Hackmann, K., Hahn, G., Schrock, E. and Verloes, A. (2014) ‘Severe forms of Baraitser-Winter syndrome are caused by ACTB mutations rather than ACTG1 mutations’, *European Journal of Human Genetics*. Nature Publishing Group, 22(2), pp. 179–183. doi: 10.1038/ejhg.2013.130.

Dopie, J., Skarp, K. P., Rajakylä, E. K., Tanhuanpää, K. and Vartiainen, M. K. (2012) ‘Active maintenance of nuclear actin by importin 9 supports transcription.’, *Proceedings of the National Academy of Sciences of the United States of America*, 109(9), pp. E544-52. doi: 10.1073/pnas.1118880109.

Doyle, M. and Kiebler, M. A. (2012) ‘A zipcode unzipped.’, *Genes & development*, 26(2), pp. 110–3. doi: 10.1101/gad.184945.111.

Dugina, V., Zwaenepoel, I., Gabbiani, G., Clément, S. and Chaponnier, C. (2009) ‘Beta and gamma-cytoplasmic actins display distinct distribution and functional diversity.’, *Journal of cell science*, 122(Pt 16), pp. 2980–8. doi: 10.1242/jcs.041970.

Eom, T., Antar, L. N., Singer, R. H. and Bassell, G. J. (2003) ‘Localization of a beta-actin messenger ribonucleoprotein complex with zipcode-binding protein modulates the density of dendritic filopodia and filopodial synapses.’, *The Journal of neuroscience : the official journal of the Society for Neuroscience*, 23(32), pp. 10433–44.

Frid, M. G., Shekhonin, B. V, Koteliansky, V. E. and Glukhova, M. A. (1992) ‘Phenotypic changes of human smooth muscle cells during development: late expression of heavy caldesmon and calponin.’, *Developmental biology*, 153(2), pp. 185–93. doi: 0012-1606(92)90104-O [pii].

Gautier, C. A., Kitada, T. and Shen, J. (2008) ‘Loss of PINK1 causes mitochondrial functional defects and increased sensitivity to oxidative stress’, *Proceedings of the National Academy of Sciences*, 105(32), pp. 11364–11369. doi: 10.1073/pnas.0802076105.

Ghosh, T., Soni, K., Scaria, V., Halimani, M., Bhattacharjee, C. and Pillai, B. (2008) ‘MicroRNA-mediated up-regulation of an alternatively polyadenylated variant of the mouse cytoplasmic {beta}-actin gene.’, *Nucleic acids research*, 36(19), pp. 6318–32. doi: 10.1093/nar/gkn624.

Giaime, E., Yamaguchi, H., Gautier, C. A., Kitada, T. and Shen, J. (2012) ‘Loss of DJ-1 does not affect mitochondrial respiration but increases ROS production

and mitochondrial permeability transition pore opening', *PLoS ONE*, 7(7). doi: 10.1371/journal.pone.0040501.

Gordon, K., Clouaire, T., Bao, X. X., Kemp, S. E., Xenophontos, M., De Las Heras, J. I. and Stancheva, I. (2014) 'Immortality, but not oncogenic transformation, of primary human cells leads to epigenetic reprogramming of DNA methylation and gene expression', *Nucleic Acids Research*, 42(6), pp. 3529–3541. doi: 10.1093/nar/gkt1351.

Gordon, T. and Stein, R. B. (1988) 'Comparison of force and stiffness in normal and dystrophic mouse muscles', *Muscle & Nerve*, 11(8), pp. 819–827. doi: 10.1002/mus.880110804.

Gunning, P., Ponte, P., Okayama, H., Engel, J., Blau, H. and Kedes, L. (1983) 'Isolation and characterization of full-length cDNA clones for human alpha-, beta-, and gamma-actin mRNAs: skeletal but not cytoplasmic actins have an amino-terminal cysteine that is subsequently removed.', *Molecular and cellular biology*, 3(5), pp. 787–95. doi: 10.1128/MCB.3.5.787.Updated.

Gunning, P. W., Ghoshdastider, U., Whitaker, S., Popp, D. and Robinson, R. C. (2015) 'The evolution of compositionally and functionally distinct actin filaments.', *Journal of cell science*, 128(11), pp. 2009–2019. doi: 10.1242/jcs.165563.

Gutierrez, N., Eromobor, I., Petrie, R. J., Vedula, P., Cruz, L. and Rodriguez, A. J. (2014) 'The β-actin mRNA zipcode regulates epithelial adherens junction assembly but not maintenance', *Rna*, 20(5), pp. 689–701. doi: 10.1261/rna.043208.113.

Hansen, T. V. O., Hammer, N. A., Nielsen, J., Madsen, M., Dalbaeck, C., Wewer, U. M., Christiansen, J. and Nielsen, F. C. (2004) 'Dwarfism and Impaired Gut Development in Insulin-Like Growth Factor II mRNA-Binding Protein 1-Deficient Mice', *Molecular and Cellular Biology*, 24(10), pp. 4448–4464. doi: 10.1128/MCB.24.10.4448-4464.2004.

Hofmann, W. A., Stojiljkovic, L., Fuchsova, B., Vargas, G. M., Mavrommatis, E., Philimonenko, V., Kysela, K., Goodrich, J. a, Lessard, J. L., Hope, T. J., Hozak, P. and de Lanerolle, P. (2004) 'Actin is part of pre-initiation complexes and is necessary for transcription by RNA polymerase II.', *Nature cell biology*, 6(11), pp. 1094–101. doi: 10.1038/ncb1182.

Hu, P., Wu, S. and Hernandez, N. (2004) 'A role for beta-actin in RNA polymerase III transcription.', *Genes & development*, 18(24), pp. 3010–5. doi: 10.1101/gad.1250804.

Hudson, R. S., Yi, M., Esposito, D., Watkins, S. K., Hurwitz, A. A., Yfantis, H. G., Lee, D. H., Borin, J. F., Naslund, M. J., Alexander, R. B., Dorsey, T. H.,

Stephens, R. M., Croce, C. M. and Ambs, S. (2012) 'MicroRNA-1 is a candidate tumor suppressor and prognostic marker in human prostate cancer', *Nucleic Acids Research*, 40(8), pp. 3689–3703. doi: 10.1093/nar/gkr1222.

Hüttelmaier, S., Zenklusen, D., Lederer, M., Dictenberg, J., Lorenz, M., Meng, X., Bassell, G. J., Condeelis, J. and Singer, R. H. (2005) 'Spatial regulation of beta-actin translation by Src-dependent phosphorylation of ZBP1.', *Nature*, 438(7067), pp. 512–5. doi: 10.1038/nature04115.

Jalali, S., Ramanathan, G. K., Parthasarathy, P. T., Aljubran, S., Galam, L., Yunus, A., Garcia, S., Cox, R. R., Lockey, R. F. and Kolliputi, N. (2012) 'Mir-206 regulates pulmonary artery smooth muscle cell proliferation and differentiation.', *PloS one*, 7(10), p. e46808. doi: 10.1371/journal.pone.0046808.

Jepsen, L., Kruth, K. A., Rubenstein, P. A. and Sept, D. (2016) 'Two Deafness-Causing Actin Mutations (DFNA20/26) Have Allosteric Effects on the Actin Structure', *Biophysical Journal*. Biophysical Society, 111(2), pp. 323–332. doi: 10.1016/j.bpj.2016.06.012.

Kapoor, P. and Shen, X. (2013) 'Mechanisms of nuclear actin in chromatin-remodeling complexes.', *Trends in cell biology*. Elsevier Ltd, pp. 1–9. doi: 10.1016/j.tcb.2013.10.007.

Kapustina, M., Read, T. and Vitriol, E. A. (2016) 'Simultaneous quantification of actin monomer and filament dynamics with modeling-assisted analysis of photoactivation', pp. 4633–4643. doi: 10.1242/jcs.194670.

Karakozova, M., Kozak, M., Wong, C. C. L., Bailey, A. O., Yates, J. R., Mogilner, A., Zebroski, H. and Kashina, A. (2006) 'Arginylation of beta-actin regulates actin cytoskeleton and cell motility.', *Science (New York, N.Y.)*, 313(5784), pp. 192–6. doi: 10.1126/science.1129344.

Khaitlina, S. Y. (2001) 'Functional specificity of actin isoforms', *International Review of Cytology*, 202(February 2001), pp. 35–98. doi: 10.1016/S0074-7696(01)02003-4.

Kislauskis, E. H., Li, Z., Singer, R. H. and Taneja, K. L. (1993) 'Isoform-specific 3'-untranslated sequences sort alpha-cardiac and beta-cytoplasmic actin messenger RNAs to different cytoplasmic compartments.', *The Journal of cell biology*, 123(1), pp. 165–72.

Kuo, S. M., Burl, L. R. and Hu, Z. (2012) 'Cellular phenotype-dependent and -independent effects of vitamin C on the renewal and gene expression of mouse embryonic fibroblasts.', *PloS one*, 7(3), p. e32957. doi: 10.1371/journal.pone.0032957.

Lechuga, S., Baranwal, S., Li, C., Naydenov, N. G., Kuemmerle, J. F., Dugina, V., Chaponnier, C. and Ivanov, A. I. (2014) 'Loss of γ-cytoplasmic actin triggers myofibroblast transition of human epithelial cells', *Molecular Biology of the Cell*, 25(20), pp. 3133–3146. doi: 10.1091/mbc.E14-03-0815.

Leung, K. M., Van Horck, F. P., Lin, A. C., Allison, R., Standart, N. and Holt, C. E. (2006) 'Asymmetrical beta-actin mRNA translation in growth cones mediates attractive turning to netrin-1', *Nat.Neurosci.*, 9(10), pp. 1247–1256.

Liu, S., Tetzlaff, M. T., Liu, A., Liegl-Atzwanger, B., Guo, J. and Xu, X. (2012) 'Loss of microRNA-205 expression is associated with melanoma progression.', *Laboratory investigation; a journal of technical methods and pathology*, 92(7), pp. 1084–96. doi: 10.1038/labinvest.2012.62.

Miralles, F. and Visa, N. (2006) 'Actin in transcription and transcription regulation.', *Current opinion in cell biology*, 18(3), pp. 261–6. doi: 10.1016/j.ceb.2006.04.009.

Moradi, M., Sivadasan, R., Saal, L., Lüningschrör, P., Dombert, B., Rathod, R. J., Dieterich, D. C., Blum, R. and Sendtner, M. (2017) 'Differential roles of α-, β-, and γ-actin in axon growth and collateral branch formation in motoneurons.', *The Journal of cell biology*, 216(3), pp. 793–814. doi: 10.1083/jcb.201604117.

Müller, M., Diensthuber, R. P., Chizhov, I., Claus, P., Heissler, S. M., Preller, M., Taft, M. H. and Manstein, D. J. (2013) 'Distinct Functional Interactions between Actin Isoforms and Nonsarcomeric Myosins.', *PloS one*, 8(7), p. e70636. doi: 10.1371/journal.pone.0070636.

Narayanan, P., Chatterton, P., Ikeda, A., Ikeda, S., Corey, D. P., Ervasti, J. M. and Perrin, B. J. (2015) 'Length regulation of mechanosensitive stereocilia depends on very slow actin dynamics and filament-severing proteins', *Nature Communications*. Nature Publishing Group, 6, pp. 1–8. doi: 10.1038/ncomms7855.

O'Rourke, A. R., Lindsay, A., Tarpey, M. D., Perrin, B. J., Spangenburg, E. J., Lowe, D. A. and Ervasti, J. M. (2017) 'Impaired muscle relaxation and mitochondrial fission associated with genetic ablation of cyoplasmic isoforms', *The FEBS Journal - In Review*. doi: 10.1111/febs.14367.

Olson, E. N. and Nordheim, A. (2010) 'Linking actin dynamics and gene transcription to drive cellular motile functions.', *Nature reviews. Molecular cell biology*. Nature Publishing Group, 11(5), pp. 353–65. doi: 10.1038/nrm2890.

Pan, F., Hüttelmaier, S., Singer, R. H. and Gu, W. (2007) 'ZBP2 facilitates binding of ZBP1 to beta-actin mRNA during transcription.', *Molecular and cellular biology*, 27(23), pp. 8340–51. doi: 10.1128/MCB.00972-07.

Parisis, N., Krasinska, L., Harker, B., Urbach, S., Rossignol, M., Camasses, A., Dewar, J., Morin, N. and Fisher, D. (2017) 'Initiation of DNA replication requires actin dynamics and formin activity', pp. 1–20. doi: 10.15252/embj.201796585.

Patel, V. L., Mitra, S., Harris, R., Buxbaum, A. R., Lionnet, T., Brenowitz, M., Girvin, M., Levy, M., Almo, S. C., Singer, R. H. and Chao, J. a (2012) 'Spatial arrangement of an RNA zipcode identifies mRNAs under post-transcriptional control.', *Genes & development*, 26(1), pp. 43–53. doi: 10.1101/gad.177428.111.

Patrinostro, X., Rourke, A. R. O., Chamberlain, C. M., Moriarity, B. S., Perrin, B. J. and Ervasti, J. M. (2017) 'Relative importance of β cyto - and γ cyto -actin in primary mouse embryonic fibroblasts', *Molecular biology of the cell*, 28. doi: 10.1091/mbc.E16-07-0503.

Pavlyk, I., Leu, N. A., Vedula, P., Kurosaka, S. and Kashina, A. (2018) 'Rapid and dynamic arginylation of the leading edge β- actin is required for cell migration', *Traffic*, pp. 0–2. doi: 10.1111/tra.12551.

Perrin, B. J. and Ervasti, J. M. (2010) 'The actin gene family: function follows isoform.', *Cytoskeleton (Hoboken, N.J.)*, 67(10), pp. 630–4. doi: 10.1002/cm.20475.

Perrin, B. J., Sonnemann, K. J. and Ervasti, J. M. (2010) 'β-actin and γ-actin are each dispensable for auditory hair cell development but required for Stereocilia maintenance.', *PLoS genetics*, 6(10), p. e1001158. doi: 10.1371/journal.pgen.1001158.

Perrin, B. J., Strandjord, D. M., Narayanan, P., Henderson, D. M., Johnson, K. R. and Ervasti, J. M. (2013) 'β-Actin and fascin-2 cooperate to maintain stereocilia length.', *The Journal of neuroscience : the official journal of the Society for Neuroscience*, 33(19), pp. 8114–21. doi: 10.1523/JNEUROSCI.0238-13.2013.

Philimonenko, V. V, Zhao, J., Iben, S., Dingová, H., Kyselá, K., Kahle, M., Zentgraf, H., Hofmann, W. a, de Lanerolle, P., Hozák, P. and Grummt, I. (2004) 'Nuclear actin and myosin I are required for RNA polymerase I transcription.', *Nature cell biology*, 6(12), pp. 1165–72. doi: 10.1038/ncb1190.

Pollard, T. D. (2015) 'What we know and do not know about actin', *Handbook of Experimental Pharmacology*, (January), pp. 251–263. doi: 10.1007/164.

Pollard, T. D. and Borisy, G. G. (2003) 'Cellular motility driven by assembly and disassembly of actin filaments.', *Cell*, 112(4), pp. 453–65.

Pollard, T. D. and Cooper, J. a (2009) 'Actin, a central player in cell shape and movement.', *Science (New York, N.Y.)*, 326(5957), pp. 1208–12. doi: 10.1126/science.1175862.

Posern, G. and Treisman, R. (2006) ‘Actin’ together: serum response factor, its cofactors and the link to signal transduction.’, *Trends in cell biology*, 16(11), pp. 588–96. doi: 10.1016/j.tcb.2006.09.008.

Prins, K. W., Call, J. A., Lowe, D. A. and Ervasti, J. M. (2011) ‘Quadriceps myopathy caused by skeletal muscle-specific ablation of β(cyto)-actin.’, *Journal of cell science*, 124(Pt 6), pp. 951–7. doi: 10.1242/jcs.079848.

Rivière, J., van Bon, B. W. M., Hoischen, A., Kholmanskikh, S. S., O’Roak, B. J., Gilissen, C., Gijsen, S., Sullivan, C. T., Christian, S. L., Abdul-Rahman, O. a, Atkin, J. F., Chassaing, N., Drouin-Garraud, V., Fry, A. E., Fryns, J.-P., Gripp, K. W., Kempers, M., Kleefstra, T., Mancini, G. M. S., Nowaczyk, M. J. M., van Ravenswaaij-Arts, C. M. a, Roscioli, T., Marble, M., Rosenfeld, J. a, Siu, V. M., de Vries, B. B. a, Shendure, J., Verloes, A., Veltman, J. a, Brunner, H. G., Ross, M. E., Pilz, D. T. and Dobyns, W. B. (2012) ‘De novo mutations in the actin genes ACTB and ACTG1 cause Baraitser-Winter syndrome.’, *Nature genetics*. Nature Publishing Group, 44(4), pp. 440–4, S1-2. doi: 10.1038/ng.1091.

Ross, A. F., Oleynikov, Y., Kislauskis, E. H. and Taneja, K. L. (1997) ‘Characterization of a beta-actin mRNA zipcode-binding protein .’, *Molecular and cellular biology*, 17(4), pp. 2158–2165.

Rossi, A., Kontarakis, Z., Gerri, C., Nolte, H., Hölper, S., Krüger, M. and Stainier, D. Y. R. (2015) ‘Genetic compensation induced by deleterious mutations but not gene knockdowns.’, *Nature*, 524(7564), pp. 230–3. doi: 10.1038/nature14580.

Rubenstein, P. A. (1990) ‘The Functional Importance of Multiple Actin Isoforms’, *BioEssays*, 12(7), pp. 309–315.

Rubenstein, P. A. and Wen, K. K. (2014) ‘Insights into the effects of disease-causing mutations in human actins’, *Cytoskeleton*, 71(4), pp. 211–229. doi: 10.1002/cm.21169.

Rubenstein, P. A. and Wen, K. K. (2018) ‘NATure of actin amino-terminal acetylation’, *PNAS*, pp. 3–5. doi: 10.1073/pnas.1803804115.

Sasaki, Y., Welshhans, K., Wen, Z., Yao, J., Xu, M., Goshima, Y., Zheng, J. Q. and Bassell, G. J. (2010) ‘Phosphorylation of zipcode binding protein 1 is required for brain-derived neurotrophic factor signaling of local beta-actin synthesis and growth cone turning.’, *The Journal of neuroscience : the official journal of the Society for Neuroscience*, 30(28), pp. 9349–58. doi: 10.1523/JNEUROSCI.0499-10.2010.

Schmidt, L. J., Duncan, K., Yadav, N., Regan, K. M., Verone, A. R., Lohse, C. M., Pop, E. a, Attwood, K., Wilding, G., Mohler, J. L., Sebo, T. J., Tindall, D. J. and Heemers, H. V (2012) ‘RhoA as a mediator of clinically relevant androgen action

in prostate cancer cells.', *Molecular endocrinology (Baltimore, Md.)*, 26(5), pp. 716–35. doi: 10.1210/me.2011-1130.

Serebryannyy, L. A., Cruz, C. M. and De Lanerolle, P. (2016) 'A role for nuclear actin in HDAC 1 and 2 regulation', *Scientific Reports*. Nature Publishing Group, 6(May), pp. 1–10. doi: 10.1038/srep28460.

Shawlot, W., Deng, J. M., Fohn, L. E. and Behringer, R. R. (1998) 'Restricted beta-galactosidase expression of a hygromycin-lacZ gene targeted to the beta-actin locus and embryonic lethality of beta-actin mutant mice', *Transgenic Res.*, 7(2), pp. 95–103.

Shestakova, E. A, Singer, R. H. and Condeelis, J. (2001) 'The physiological significance of beta -actin mRNA localization in determining cell polarity and directional motility.', *Proceedings of the National Academy of Sciences of the United States of America*, 98(13), pp. 7045–50. doi: 10.1073/pnas.121146098.

Shmerling, D., Danzer, C. P., Mao, X., Boisclair, J., Haffner, M., Lemaistre, M., Schuler, V., Kaeslin, E., Korn, R., Bürki, K., Ledermann, B., Kinzel, B. and Müller, M. (2005) 'Strong and ubiquitous expression of transgenes targeted into the beta-actin locus by Cre/lox cassette replacement.', *Genesis (New York, N.Y. : 2000)*, 42(4), pp. 229–35. doi: 10.1002/gene.20135.

Shum, M. S. Y., Pasquier, E., Po'uha, S. T., O'Neill, G. M., Chaponnier, C., Gunning, P. W. and Kavallaris, M. (2011) 'gamma-Actin regulates cell migration and modulates the ROCK signaling pathway', *The FASEB Journal*, 25(12), pp. 4423–4433. doi: 10.1096/fj.11-185447.

Silver, L. M. (2001) *Reproductive characteristics of some important inbred strains*, *Mouse Genome Informatics, The Jackson Laboratory*. Available at: http://www.informatics.jax.org/silver/tables/table4-1.shtml.

Singhal, P. K., Sassi, S., Lan, L., Au, P., Halvorsen, S. C., Fukumura, D., Jain, R. K. and Seed, B. (2016) 'Mouse embryonic fibroblasts exhibit extensive developmental and phenotypic diversity.', *Proceedings of the National Academy of Sciences of the United States of America*, 113(1), pp. 122–7. doi: 10.1073/pnas.1522401112.

Small, E. M. (2012) 'The actin-MRTF-SRF gene regulatory axis and myofibroblast differentiation.', *Journal of cardiovascular translational research*, 5(6), pp. 794–804. doi: 10.1007/s12265-012-9397-0.

Song, T., Zheng, Y., Wang, Y., Katz, Z., Liu, X., Chen, S. and Singer, R. H. (2015) 'Specific interaction of KIF11 with ZBP1 regulates the transport of b -actin mRNA and cell motility', pp. 1001–1010. doi: 10.1242/jcs.161679.

Sonnemann, K. J., Fitzsimons, D. P., Patel, J. R., Liu, Y., Schneider, M. F., Moss, R. L. and Ervasti, J. M. (2006) 'Cytoplasmic gamma-actin is not required for skeletal muscle development but its absence leads to a progressive myopathy.', *Developmental cell*, 11(3), pp. 387–97. doi: 10.1016/j.devcel.2006.07.001.

Spiess, C., Meyer, A. S., Reissmann, S. and Frydman, J. (2004) 'Mechanism of the eukaryotic chaperonin: Protein folding in the chamber of secrets', *Trends in Cell Biology*, 14(11), pp. 598–604. doi: 10.1016/j.tcb.2004.09.015.

Stein, R. B. and Gordon, T. (1986) 'Nonlinear stiffness--force relationships in whole mammalian skeletal muscles.', *Canadian journal of physiology and pharmacology*, 64(9), pp. 1236–44.

Ströhl, F., Lin, J. Q., Laine, R. F., Wong, H. H. W., Urbančič, V., Cagnetta, R., Holt, C. E. and Kaminski, C. F. (2017) 'Single Molecule Translation Imaging Visualizes the Dynamics of Local β-Actin Synthesis in Retinal Axons', *Scientific Reports*, 7(1), p. 709. doi: 10.1038/s41598-017-00695-7.

Stüven, T., Hartmann, E. and Görlich, D. (2003) 'Exportin 6: A novel nuclear export receptor that is specific for profilin-actin complexes', *EMBO Journal*, 22(21), pp. 5928–5940. doi: 10.1093/emboj/cdg565.

Terman, J. R. and Kashina, A. (2013) 'Post-translational modification and regulation of actin.', *Current opinion in cell biology*. Elsevier Ltd, 25(1), pp. 30–8. doi: 10.1016/j.ceb.2012.10.009.

Tondeleir, D., Lambrechts, A., Müller, M., Jonckheere, V., Doll, T., Vandamme, D., Bakkali, K., Waterschoot, D., Lemaistre, M., Debeir, O., Decaestecker, C., Hinz, B., Staes, A., Timmerman, E., Colaert, N., Gevaert, K., Vandekerckhove, J. and Ampe, C. (2012) 'Cells lacking β-actin are genetically reprogrammed and maintain conditional migratory capacity.', *Molecular & cellular proteomics : MCP*, 11(8), pp. 255–71. doi: 10.1074/mcp.M111.015099.

Troys, C. A. and M. Van (2015) 'Mammalian Actins: Isoform-Specific Functions and Diseases', *Handbook of Experimental Pharmacology*, (January), pp. 251–263. doi: 10.1007/164.

Ueki, N., Sobue, K., Kanda, K., Hada, T. and Higashino, K. (1987) 'Expression of high and low molecular weight caldesmons during phenotypic modulation of smooth muscle cells.', *Proceedings of the National Academy of Sciences of the United States of America*, 84(24), pp. 9049–9053.

Vasioukhin, V., Bauer, C., Yin, M. and Fuchs, E. (2000) 'Directed actin polymerization is the driving force for epithelial cell-cell adhesion.', *Cell*, 100(2), pp. 209–219. doi: 10.1016/S0092-8674(00)81559-7.

Vedula, P., Kurosaka, S., Leu, N., Wolf, Y., Shabalina, S., Wang, J., Sterling, S., Dong, D. and Kashina, A. (2017) 'Diverse functions of closely homologous actin isoforms are defined by their nucleotide, rather than their amino acid sequence.', *eLife*, p. 227546. doi: 10.1101/227546.

Virtanen, J. A. and Vartiainen, M. K. (2017) 'Diverse functions for different forms of nuclear actin', *Current Opinion in Cell Biology*. Elsevier Ltd, 46(Figure 1), pp. 33–38. doi: 10.1016/j.ceb.2016.12.004.

Wade, W. N., Willingham, M. C., Koumenis, C. and Cramer, S. D. (2002) 'p27Kip1 is essential for the antiproliferative action of 1,25-dihydroxyvitamin D3 in primary, but not immortalized, mouse embryonic fibroblasts', *Journal of Biological Chemistry*, 277(40), pp. 37301–37306. doi: 10.1074/jbc.M204162200.

Wang, J., Pavlyk, I., Vedula, P., Sterling, S., Leu, N. A., Dong, D. W. and Kashina, A. (2017) 'Arginyltransferase ATE1 is targeted to the neuronal growth cones and regulates neurite outgrowth during brain development', *Developmental Biology*. Elsevier Inc., 430(1), pp. 41–51. doi: 10.1016/j.ydbio.2017.08.027.

Wang, N., Zhang, W., Cui, J., Zhang, H., Chen, X., Li, R., Wu, N., Chen, X., Wen, S., Zhang, J., Yin, L., Deng, F., Liao, Z., Zhang, Z., Zhang, Q., Yan, Z., Liu, W., Ye, J., Deng, Y., Wang, Z., Qiao, M., Luu, H. H., Haydon, R. C., Shi, L. L., Liang, H. and He, T.-C. (2014) 'The piggyBac transposon-mediated expression of SV40 T antigen efficiently immortalizes mouse embryonic fibroblasts (MEFs).', *PloS one*, 9(5), p. e97316. doi: 10.1371/journal.pone.0097316.

Yao, J., Sasaki, Y., Wen, Z., Bassell, G. J. and Zheng, J. Q. (2006) 'An essential role for beta-actin mRNA localization and translation in Ca2+-dependent growth cone guidance', *Nat.Neurosci.*, 9(10), pp. 1265–1273. doi: 10.1038/nn1773.

Yisraeli, J. K. (2005) 'VICKZ proteins: a multi-talented family of regulatory RNA-binding proteins.', *Biology of the cell / under the auspices of the European Cell Biology Organization*, 97(1), pp. 87–96. doi: 10.1042/BC20040151.

Zhang, F., Saha, S., Shabalina, S. A. and Kashina, A. (2010) 'Differential arginylation of actin isoforms is regulated by coding sequence-dependent degradation.', *Science (New York, N.Y.)*, 329(5998), pp. 1534–7. doi: 10.1126/science.1191701.

Zhang, H. L., Eom, T., Oleynikov, Y., Shenoy, S. M., Liebelt, D. A., Dictenberg, J. B., Singer, R. H. and Bassell, G. J. (2001) 'Neurotrophin-induced transport of a β-actin mRNP complex increases β-actin levels and stimulates growth cone motility', *Neuron*, 31(2), pp. 261–275. doi: 10.1016/S0896-6273(01)00357-9.

Zhao, K., Wang, W., Rando, O. J., Xue, Y., Swiderek, K., Kuo, A. and Crabtree,

G. R. (1998) ‘Rapid and phosphoinositol-dependent binding of the SWI/SNF-like BAF complex to chromatin after T lymphocyte receptor signaling’, *Cell*, 95(5), pp. 625–636.